Kalle Salmenhaara

Impact of refractive surgery to the biomechanical properties of the cornea – a finite element analysis

School of electrical engineering

Thesis submitted for examination for the degree of Master of Science in Technology

Espoo 30.11.2015

Thesis supervisor

Prof. Mervi Paulasto-Kröckel

Thesis advisors

D.Med.Sci. Juhani Pietilä
D.Sc. (tech) Jue Li

Aalto University
School of Electrical Engineering

Aalto University
School of electrical engineering

Abstract
of the master's thesis

Author: Kalle Salmenhaara
Title: Impact of refractive surgery to the biomechanical properties of the cornea – a finite element analysis

Date: 30.11.2015 Language: English Number of pages: 8 + 67

Department of electronics

Supervisor: Prof. Mervi Paulasto-Kröckel

Advisors: D.Med.Sci Juhani Pietilä
D.Sc. (tech) Jue Li

Refractive surgery is used to remove tissue from the outermost layer of the eye, cornea, in order to change the curvature of the anterior surface, thus focusing the image to the correct location in the retina. In Finland, mainly two techniques of refractive surgery are used. FemtoLASIK, where a thin flap is formed in surface of the cornea and underneath the flap, a refractive correction is made with laser ablation. SMILE, which is a flapless technique, a lenticule is created inside the cornea and extracted through a small incision. When a part of a tissue is removed, in addition to optical changes in cornea, the biomechanical properties are changed. Currently SMILE is considered as a safer technique for high refractive corrections since the stiffer anterior layers of the cornea remain intact.

In this thesis the current knowledge of the structure and biomechanical properties of the cornea are reviewed. Based on the review, a model of the cornea is built using the finite element method (FEM). With the model, the previously mentioned refractive surgery techniques are simulated. The results of the simulations are compared to previous research and the applicability to the physiological conditions is discussed.

The results of the simulations agree with the current view, which suggests that SMILE is safer procedure when correcting high refractive errors. However measurements from patients would indicate different kind of corneal behavior than the simulations, which would suggest that the current models of the cornea are not applicable in physiological conditions. A new theory of corneal biomechanics is proposed to explain the corneal deformation after refractive surgery.

Keywords: Cornea, Refractive surgery, SMILE, FemtoLASIK, finite element method, FEM

Aalto Yliopisto
Sähkötekniikan korkeakoulu

Diplomityön
Tiivistelmä

Tekijä: Kalle Salmenhaara
Työn nimi: Refraktiivisen kirurgian vaikutus sarveiskalvon biomekaanisiin ominaisuuksiin – elementtimenetelmä-analyysi

Päivämäärä: 30.11.2015 Kieli: Englanti Sivumäärä: 8 + 67

Elektroniikan laitos

Valvoja: Prof. Mervi Paulasto-Kröckel

Työn ohjaajat: LT Juhani Pietilä
TkT Jue Li

Refraktiivisessa kirurgiassa sarveiskalvosta, eli silmän uloimmasta kerroksesta, poistetaan kudosta, jotta sarveiskalvon pinnan kaarevuus muuttuu, jolloin kuva kohdistuisi oikealle kohdalle verkkokalvossa. Suomessa tehdään pääasiassa taittovirheleikkauksia kahdella tekniikalla. FemtoLASIK:issa sarveiskalvon pintaan tehdään ohut läppä, joka siirretään syrjään, sen alta laserilla muokataan sarveiskalvoa halutun muotoiseksi. SMILE:ssä sarveiskalvon sisälle muodostetaan laserin avulla lentikkeli, joka poistetaan pienestä avauksesta. Poistettaessa osa kudoksesta, vaikutetaan optisten ominaisuuksien lisäksi biomekaanisiin ominaisuuksiin. Vallitsevan käsityksen mukaan syvemmälle sarveiskalvoon tehty lentikkeli säästää enemmän mekaanisesti jäykempiä pintakerroksia sarveiskalvosta kuin läppäleikkaukset, jolloin suurissa taittovirheen korjauksissa SMILE olisi tekniikkana turvallisempi kuin femtoLASIK.

Tässä työssä selvitetään tämänhetkinen tieto sarveiskalvon rakenteesta ja biomekaanisista ominaisuuksista. Selvityksen perusteella mallinnetaan sarveiskalvoa elementtimenetelmän (FEM) avulla. Mallin avulla simuloidaan edellä mainittuja refraktiivisen kirurgian tekniikoita. Saatuja tuloksia verrataan aiempaan tutkimukseen sekä pohditaan saatujen tulosten soveltuvuutta sarveiskalvoon fysiologisissa olosuhteissa.

Elementtimenetelmä-analyysin tulokset viittaavat vallitsevaan käsitykseen, joka puoltaa SMILE:n käyttöä suurien taittovirheiden korjauksessa. Toisaalta potilasmittausten tulokset ovat ristiriitaiset elementtimenetelmä-analyysin kanssa, joka viittaisi siihen että vallitseva teoria sarveiskalvon biomekaniikasta ei kuvasta hyvin sarveiskalvon käyttäytymistä fysiologisissa olosuhteissa. Lopuksi esitetään uusi teoria sarveiskalvon biomekaniikasta, joka selittäisi sarveiskalvon muodonmuutokset taittovirheleikkauksen jälkeen

Avainsanat: Sarveiskalvo, Refraktiivinen kirurgia, SMILE, FemtoLASIK, elementtimenetelmä, FEM

Preface

I want to thank my supervisor Mervi Paulasto-Kröckel and my advisors Juhani Pietilä and Jue Li for their instructions, guidance and interesting conversations. Also I want to thank Jarno Ylitalo, Jukka Häkämies, Kimmo Rantakurtakko, Teppo Rajala and others with whom I have had interesting discussions about the topics presented in this thesis. Additionally I want to thank CSC – IT Center for Science for providing the license for Abaqus CAE 6.13.

Otaniemi 30.11.2015

Kalle Salmenhaara

Table of contents

Dictionary

Abbe number	Variation of refractive index with wavelength, the higher the value the lower the dispersion in lens and better optical quality
Anastomosis	Reconnection of a branched streams or fibers, in this case a reconnection of branched collagen fibers
Astigmatism	Asymmetric myopia or hyperopia. *Hajataitteisuus*
CH	Corneal hysteresis
Chromatic aberration	Inability of the lens to focus different colors to the same point
Collagen fiber	Bundle of collagen fibrils that forms the lamellae in the cornea
Collagen fibril	Assembly of collagen molecules, diameter of 50 nm to 500 nm
Corneal vertex or apex	The highest point of the cornea, usually in the center
CRF	Corneal resistance factor
Defocus	Wave aberration of myopia and hyperopia
Dispersion	Refractive index of a material depends on the wavelength of the light
Emmetropia	State of sight when distant object is in focus when lens is relaxed.
femtoLASIK	Femtosecond laser in situ keratomileusis
Floater	Small particle of cellular debris in vitreous humour that can be seen in ones field of view as floating. *Lasiaissamentuma*
High order aberrations	Coma, trefoil and spherical aberration etc.
Hyperopia	Far sightedness, focus point of the image is behind the retina. *Kaukonäköisyys*
IOP	Intraocular pressure, typically 15 mmHg or ~2 kPa
IOPcc	Cornea compensated intraocular pressure
LASEK	Laser sub-epithelial keratectomy
LASIK	Laser in situ keratomileusis
Liou-Brennan model	Finite model of the eye with aspheric refractive surfaces based on experimental research
Low order aberrations	Defocus, astigmatism, x- & y-tilt
Myopia	Near sightedness, focus point of the image is in front of the retina. *Likinäköisyys*
Optical axis	Straight line passing through the center of cornea and crystalline lens
Presbyopia	Diminished ability of accommodation, i.e. to focus on nearby objects due aging. *Ikänäkö*
Prism	Decentration of optical path
PRK	Photorefractive keratectomy
Secant modulus	A chord between two points in stress-strain curve

SMILE	Small incision lenticule extraction
Stiffness	Highest resistance to deformation. Stiffness is used instead of Young's modulus to describe the material properties of different parts of the eye
Strabismus	When the eyes are not properly aligned with each other. *Karsastus*
Tangential modulus	Instantaneous slope of stress-strain curve
Visual axis	Straight line passing through center of crystalline lens and fovea centralis

List of symbols

D	Diopters (m^{-1})
E	Young's modulus, elastic modulus
f	Focal length (m)
G	Shear modulus
n	Refractive index
P_{lens}	Lens power $P_{lens} = \frac{1}{f}$ (D)
v	Poisson's ratio
V_D	Abbe number or V-Number $V_D = \frac{n_D - 1}{n_F - n_C}$
κ	Dispersion parameter $0 \leq \kappa \leq ⅓$
μ	Shear modulus
Ψ	Strain energy potential

1 Introduction

Poor vision is usually caused by mismatch with the eye length and the focal length of the cornea and the lens. To correct the refractive errors in the eye, refractive surgery is used to modify the corneal curvature in order to change the lens power of the cornea thus changing the focal point to the retina. A contact lens, for a myopic eye, is thin in the center and thick in the periphery, resulting to a flatter surface of the eye. Refractive surgery, for a myopic eye, removes more tissue in the center and less in the periphery, leading to a similar result as with a contact lens.

Between 10 000 to 16 000 corneal refractive surgeries are performed each year in Finland [1] and since the early 1990's over 34 million eyes worldwide have undergone an excimer laser based (LASIK, PRK, LASEK) refractive surgery. Between 2009 and 2013 over 80 000 eyes have been treated with SMILE [2], which is the newest generation of refractive surgery. Several different types of techniques are used today, and different styles, as many as there are surgeons, performing these procedures. The accuracy of the lasers and predictability of the procedures have increased and nowadays the level of patient specific customization has increased as well. There is an ongoing debate of the limits of a safe procedure and with different types of techniques, the effects to the cornea are different. Sections 2.1 to 2.3 describe the structure of the eye, what are the main refractive errors and how the refractive errors can be corrected with refractive surgery.

With soft tissues, such as the cornea, the biomechanical properties are difficult to determine, especially *in vivo*. The complexity, the high level of anisotropy and nonlinearity, viscoelasticity and the variation between the individuals, lead to difficulties in prediction and modeling of the eye. Mechanical measurements of the cornea have a high variation of results and only few studies have considered a wide range of biomechanical properties. Mainly the research has focused on finding only few parameters to describe the cornea. For example many studies tried to measure the Young's modulus of the cornea, but in nonlinear, viscoelastic materials the Young's modulus varies for different strains and strain rates, since the stress-strain curve is nonlinear and rate dependent. The cornea is a layered structure and the biomechanical properties depend on the depth, location and orientation. Sections 2.4 to 2.7 describe the structure of the cornea, how the biomechanical properties are measured and the current state of the research. In this thesis the focus is on the relative differences between the different layers, locations and orientations.

Predicting the mechanical response in a complex structure, such as the cornea, is nearly impossible with traditional methods. Numerical analysis can be used to analyze the mechanical response of a material. The most popular technique is the finite element method (FEM), in which a structure is divided to small subparts, finite elements. Division of the structure allows the model to have finite number of nodes and degrees of freedom [3]. A few publications have used the finite element method to model the corneal behavior, but the models are mainly based on the corneal microstructure i.e. the collagen fibril distribution, which does not explain all the biomechanical properties of the cornea (see section 2.6). In this thesis FEM is used for modeling the cornea and its mechanical response to different types of refractive surgeries. In chapter 3 a simplified model of the cornea is built and the mechanical properties are assigned based on the relative differences between the different layers, locations and orientations. With non-linear materials the stress-

strain curves do not follow the same path and the relative differences are assumed to be valid in certain strains i.e. in this thesis the relative difference in stiffness is assumed to occur with 10% strain. Viscoelastic behavior is left out of the simulations and the results are interpreted to apply in equilibrium. Dynamic simulations would require more complex material properties and more accurate knowledge of the stress distribution in the cornea to provide useful results.

The model is used to compare the biomechanical response of the cornea to the different techniques of refractive surgery. Chapter 4 presents the results of the simulations and Chapter 5 discuss about the implications to clinical work and how well the current theory explains the behavior of the cornea in physiological conditions.

2 Background, image formation & the structure of the eye

Sections 2.1 and 2.2 describe the structure of the eye, how the image is formed in the retina and what the refractive errors in the eye are. Section 2.3 presents a brief introduction to the refractive surgery and what are the main techniques used clinically today. Sections 2.4 and 2.5 describe the structure of the cornea and how the biomechanical properties of the cornea have been measured in the previous research. Sections 2.6 and 2.7 review what the current knowledge of the biomechanical properties of the cornea is and what are the effects of the different techniques of refractive surgery to the biomechanical properties.

Determining the Young's modulus of the cornea has been the main focus in the research of the biomechanical properties of the cornea. For a nonlinear material, the Young's modulus is not an accurate description of the material, especially when it is not known whether it is the tangential or secant modulus from the stress-strain curve and from which part of the curve it is measured.

2.1 Anatomy of the eye

Eyeball is an almost spherical globe of approximately 24 mm [4] in diameter. The eye can be described as a positive lens system that refracts light to form the image in the rear surface of the eye, the retina. Following the optical path of light rays, the biological components are: cornea, anterior chamber, iris, lens, posterior chamber and retina, Figure 1. [5]

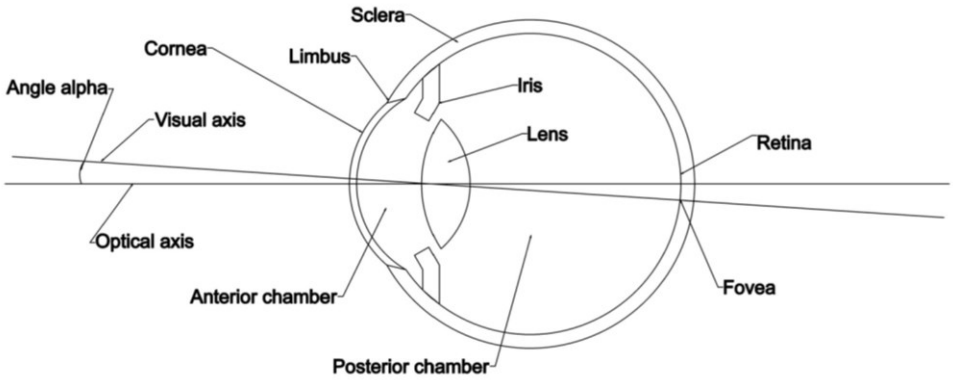

Figure 1. The eye

H. Liou and N. Brennan [4] described an anatomically accurate, finite model eye for optical modeling that is still used in the literature [6-9]. In this thesis the Liou-Brennan model will be used when describing non-patient specific eye. The model was built from previous studies made between 1948 and 1996 the model is an accurate description of an emmetropic (no refractive errors) eye. Advantage in using an emmetropic eye model is that it disregards the cause of the refractive error, meaning that simulations of the biomechanical changes in the cornea are considering a typical cornea of a healthy eye. Refractive indices presented later in this chapter, are taken for the wavelength of 555 nm (green), which is the peak of the photopic curve, meaning the wavelength that is perceived as the brightest. Refractive index changes with the wavelength and that causes chromatic aberration, see section 2.2.

Cornea

Cornea is the outermost layer of the eye that provides the most of the refractive power of the eye ~78 %. Cornea is an elliptic structure with a larger radius in the nasal-temporal (NT) direction. Thickness is approximately 600 µm, thinner in the central area and thicker in the periphery. Average central corneal thickness for a Finn having a refractive surgery is 549 µm [10] and in Liou-Brennan model it is 500 µm [4]. Refractive index of the cornea is 1.376 [4, 5] and approximately 95 % of the light in the visible spectrum is transmitted [11]. One way to describe an aspheric surface, that represents the cornea, is to use a conicoid in the form of equation 1 [4].

$$x^2 + y^2 + (1 + Q)z^2 - 2zR = 0 \quad (1)$$

Where the origin is at the surface apex (center of the cornea), x and y are the nasal-temporal and superior-inferior (SI) meridians respectively. Z is the axis of revolution and the R is the radius at the apex and Q represents the asphericity parameter that specifies the type of the conicoid. This model is rotationally symmetric and does not allow regional variations of the values R and Q, which exist in normal corneas. When assuming an emmetropic eye, the differences in the value R are insignificant. British study in 1960 [12] showed that 80 % of the eyes of young men have less than ±0.5 D of astigmatism. Astigmatism is an asymmetric defocus in the lens system, see section 2.2. In the model, corneal radius for the anterior surface is set to 7.77 mm and posterior surface to 6.4 mm [4]. The ratio of anterior and posterior surface radius is 1:0.823 [4]. The Q value (asphericity) in the model is set to -0.18 and -0.60 for anterior and posterior surfaces of the cornea, respectively [4].

Other way to describe cornea mathematically is an ellipsoid from equation 2. [13]

$$(1 - e^2)z^2 + x^2 + y^2 = R^2 \quad (2)$$

Where e is the eccentricity, which relates to the maximum radius of the cornea in x- and y-direction (R) and z-direction (R_z) and the asphericity parameter Q in equations 3 and 4.

$$\mathrm{e} = \sqrt{1 - \frac{R^2}{R_z^2}} \quad (3)$$

$$\mathrm{Q} = -e^2 \quad (4)$$

Cornea and sclera forms a corneoscleral shell that encloses and protects the intraocular tissues.

Anterior chamber

Anterior chamber is a small space filled with watery fluid that provides nutrients for the cornea. The fluid has a refractive index of 1.336, which is close to that of water 1.333 [4, 5]. The depth of the anterior chamber decreases by age, 3.86 mm for 20-29 year-olds to 3.58 mm for 40-49 year-olds [4].

Iris

Iris is the diaphragm that controls the amount of light rays that goes to the eye. The iris has two sets of muscles that change the size of the pupil. The aperture of the pupil affects the depth of focus of the eye, which is why the refractive errors are easier to detect in low light conditions. The diameter of the pupil varies from 2

mm to 8 mm depending on the lighting conditions. [5] Pupil is not exactly centered with the eye. On average it is displaced nasally by 0.5 mm and the decentration changes when the pupil size changes, i.e. when the illumination conditions change [4]. The shift of center of the pupil can be up to 0.6 mm (mean shift is 0.19 mm) [4] and that can cause problems with refractive surgery techniques that use eye tracking technology, which means that the laser beams are aligned in respect to the center of the pupil. If the pupil dilates during the operation the centration also moves, which means that the laser ablation does not have the same centration respectively to the cornea.

Crystalline lens

After passing through the pupil, light enters the crystalline lens, the last refractive structure. Ciliary muscles are controlling the shape of the lens. In its relaxed (flat) state the eye is focused on distant objects and in tensed (curved) state it is focused on nearby objects. The lens is layered mass of tissue held together by an elastic membrane. Its refractive index is not homogenous, at the center it is 1.41 and in periphery it sets to about 1.38 [5]. The curvature and the thickness of the lens increase (steepens) with age but those do not increase the refractive power of the lens. The phenomenon is called the lens paradox and it is hypothesized that it is caused by the changes of the refractive indices of the crystalline lens. Instead of increasing the refractive power, the refractive power of the lens decreases on average by 2 D between the ages 30 to 60 years. Other possibility is that the length of the eye decreases with age but it has not been confirmed. [14] The decreased length could be a result of the age related increase of stiffness of the cornea and sclera.

For the model eye the lens has anterior (front) central radius of 12.3 mm and anterior peripheral radius of 13.3 mm. The posterior (back) central radius is 8.1 mm and posterior peripheral radius is 7.1 mm [4].

Posterior chamber

Posterior chamber or *the vitreous humour* is behind the lens. It is a transparent, jellylike, substance with refractive index same as in anterior chamber, 1.336.

Retina

Retina is composed of over 100 million photoreceptive cells. It is in contact and weakly attached to the vitreous humour. There are two different types of photoreceptive cells, rods and cones. Rods are concentrated more on the periphery of the retina and are more sensitive for dim light and do not react to different colors compared to the cones. Cones are near the center of the retina in a 3 mm wide region called *macula*. Cones are sensitive to colors and bright light and are able to perceive finer detail and faster changes in image than the rods. *Fovea centralis* is the center pit of the macula and the area of the sharp central vision. Optical nerve that takes the information from retina to the brain starts from the retina, which creates a blind spot in the field of vision (FOV).[5]

Optical axis of the eye is the axis that is created by the center of the cornea, pupil and lens. Visual axis, which differs from the optical axis by approximately 5° nasally, is the axis that coincides with the actual light that enters the eye and focuses on the fovea centralis. The angle between the optical and visual axis is called angle alpha.

Table 1. Properties of the ocular components of the eye.[4, 15]

Ocular component	Mean	Range
Anterior corneal radius	7.77 mm	7-8.65 mm
Anterior corneal power	43.4 D	
Anterior corneal asphericity (Q)	-0.18	
Posterior corneal radius	6.4 mm	6.2 – 6.6 mm
Posterior corneal asphericity (Q)	-0.6	
Anterior chamber depth	3.68 mm	2.8 – 4.6 mm
Crystalline lens power	20.35 D	15.0 – 27.0 D
Crystalline lens thickness	4.0 mm	
Anterior lens radius	12.4 mm	8.8 – 11.9 mm
Anterior lens asphericity (Q)	-0.94	
Posterior lens radius	-8.1 mm	
Posterior lens asphericity (Q)	+0.96	
Axial length	24.0 mm	20.0 – 29.5 mm
Ocular power	60.35 D	54.0 – 65.0 D

Abbe number (or *constringence*) V_D (equation 5) describes the chromatic dispersion of a transparent material. Terms n_D, n_F and n_C are the refractive indices for the wavelengths: 587 nm, 486 nm, 656 nm respectively, which are the Fraunhofer D, F and C lines. The lower the Abbe number, the higher the chromatic aberration. [16] Flint glass has Abbe number of 29 [17], which makes it a good material for prism.

$$V_D = \frac{n_D - 1}{n_F - n_C} \tag{5}$$

Table 2. Refractive indices at 555 nm and Abbe numbers of optical components [4, 15]

Material	Index	Abbe number
Cornea	1.376	57.1
Aqueous humour	1.336	61.3
Crystalline lens	1.36 – 1.41	47.7
Vitreous humour	1.336	61.1

2.2 Refractive errors

The optical elements of the eye are cornea, pupil, and lens. Light rays going through those elements create the image to the retina. Since no optical system is perfect, there are always errors in the image formation. At perfectly focused point the area would be infinitesimal, leading to infinite irradiance, which is not physically possible [18]. Errors caused by the optical system are called optical aberrations.

One way to characterize optical aberrations is to quantify the difference of the generated wavefront of the system and the spherical reference wavefront. These are called wavefront aberrations. [19]

Wavefront analysis is a way to determine the optical aberrations in the eye. Wavefront is a surface joining all points of equal phase [18]. In an ideal situation

when a point light source is centered *in the middle of the fovea centralis in the middle of the optical axis*, the optical elements of the eye would refract a perfect spherical wavefront outside the cornea.

Optical aberrations can be described by using mono- or polychromatic light. Optical aberrations have an effect to the image quality. Optical aberrations for monochromatic light are divided to low order aberrations and high order aberrations. Low order aberrations causes ~90 % of the wave aberrations [20]. Zernike polynomials can be used to describe and define the optical aberrations. Individual polynomials are orthogonal, meaning they are independent. When polychromatic light enters the eye, the difference of refractive indices for different wavelengths causes longitudal chromatic aberration (LCA), which is the difference of focal lengths in different wavelengths, meaning that the focus point is not the same for the whole spectrum. Transverse chromatic aberration (TCA) moves the position of focus point for different wavelengths. The effect of TCA can be estimated by eq. 6 where φ is TCA in radians, h is the pupil decentration and ΔRx is the LCA in diopters. The longer the wavelength, the lower the refractive index [21].

$$\varphi = h\Delta Rx \tag{6}$$

The magnitude of foveal TCA can vary from 0.05 to 2.67 arc minutes (0.0008 to 0.0445 degrees) for 605 nm and 497 nm wavelengths of red and blue light respectively.

A wavefront profile of optical aberrations can be mathematically modeled with a set of Zernike polynomials. Zernike polynomials are a series of polynomials that models a circular wavefront profile. Wavefront aberrations are the difference of ideal wavefront to the actual wavefront. Zernike polynomials are the building blocks when describing any circular wavefront, the same way as sine and cosine terms in Fourier series are when describing any periodic signal [19]. Table 3 and Figure 2 shows the first Zernike polynomials and their names. N is the radial degree and m is the azimuthal degree.

Table 3. The first 12 Zernike polynomials

j	**n**	**m**	**$Z_j(\rho,\theta)$**	**Aberration name**
1	0	0	1	Piston
2	1	1	$2\rho\cos\theta$	x-tilt
3	1	1	$2\rho\sin\theta$	y-tilt
4	2	0	$\sqrt{3}\,(2\rho^2-1)$	defocus
5	2	2	$\sqrt{6}\,\rho^2\sin 2\theta$	45° astigmatism
6	2	2	$\sqrt{6}\,\rho^2\cos 2\theta$	0° astigmatism
7	3	1	$\sqrt{8}\,(3\rho^3-2\rho)\sin\theta$	y-coma
8	3	1	$\sqrt{8}\,(3\rho^3-2\rho)\cos\theta$	x-coma
9	3	3	$\sqrt{8}\,\rho^3\sin 3\theta$	45° trefoil
10	3	3	$\sqrt{8}\,\rho^3\cos 3\theta$	0° trefoil
11	4	0	$\sqrt{5}\,(6\rho^4-6\rho^2+1)$	spherical aberration

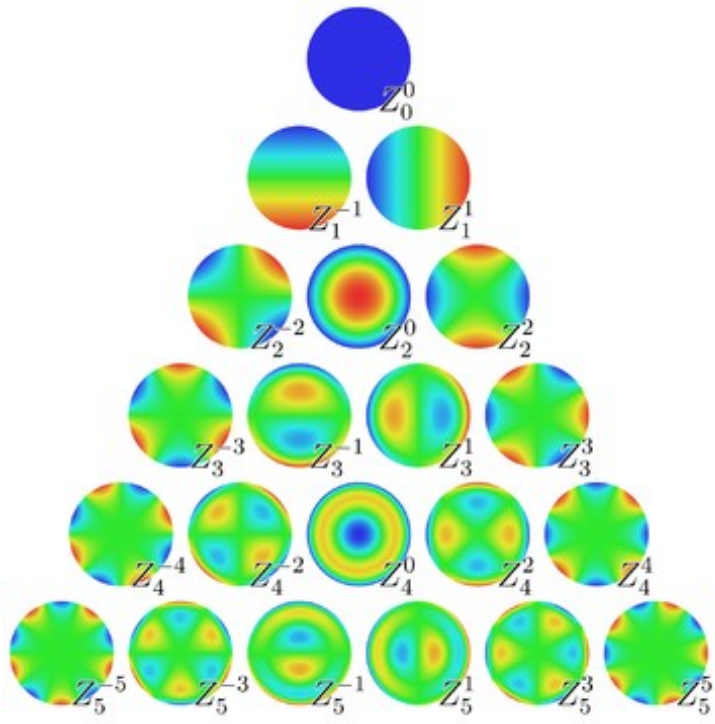

Figure 2. The first 21 Zernike polynomials [22]

When describing the refractive errors in the eye, we are assuming, if not otherwise stated, a single wavelength point light source at infinity, so that the light rays are parallel when coming to the eye.

Piston is the ideal situation when there are no optical aberrations.

Tilt –y & -x (prism) is the decentration of light rays from fovea centralis and it is caused by strabismus, which means that the visual axis of the eyes are not properly aligned with each other leading eventually to a doubled image.

Defocus describes the error of the focal length from the desired focal point in the lens system, i.e. the eye. *Emmetropia* is when the focus point is in the retina, Figure 3. In an emmetropic eye when the lens is relaxed the focus point for distant objects is in the retina. When the object comes closer to the eye the focus point starts to move behind the retina. The ciliary muscles contracts so that the tension to the lens is decreased, thus becoming more curved and moving the focus point closer to the retina. The lenses ability to accommodate diminishes due aging.

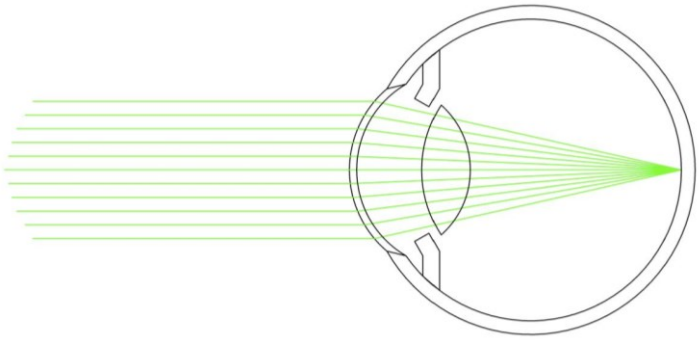

Figure 3. Emmetropic eye

When the focus point of the light rays is in front of the retina it is called *myopia*, Figure 4. The eye is too long (from cornea to retina) or the lens system

(cornea and lens) has too much refractive power. Depending on the refractive error the myopic eye focuses on objects between infinity and corneal vertex (apex).

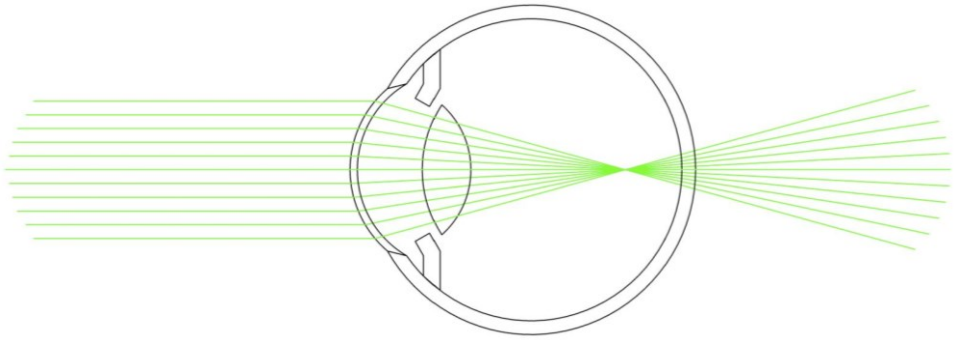

Figure 4. Myopic eye with a focus point in front of the retina

Hyperopia is when the focus point is behind the retina, Figure 5. Depending on the refractive error the hyperopic eye may be able to focus at infinity and some near point due to accommodation. [15]

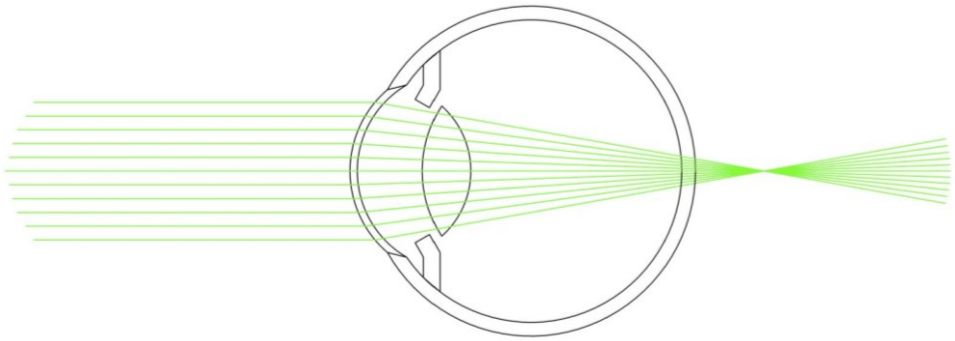

Figure 5. Hyperopic eye with a focus point behind the retina

The diminished ability to focus on close object is called presbyopia. The amplitude of accommodation for a 10 year-old is around 14 D and decreases to somewhere from 0 to 1 D for a 60 year-old and then stabilizes. The loss of accommodation starts as early as 10 years of age but becomes a problem when a person is not able to focus on reading distance, which is at +30 years of age. The lens grows throughout the lifetime and becomes larger and stiffer leading to a decreased tension from the ciliary muscles. [15]

For an unaccommodated eye, Figure 6, when bringing the light source closer to the eye the focus point shifts further behind from the retina. To correct that, the lens accommodates, Figure 7, meaning that the ciliary muscles contract, which in turn relaxes the lens itself and increases the curvature of the lens.

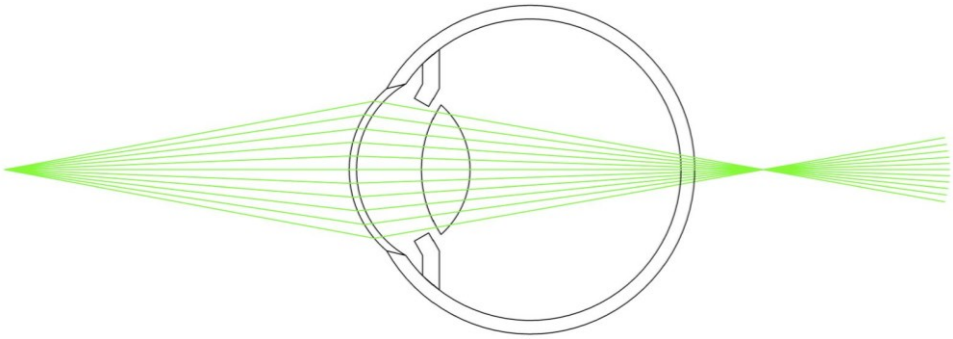

Figure 6. Unaccommodated eye with a focus for close object point behind the retina

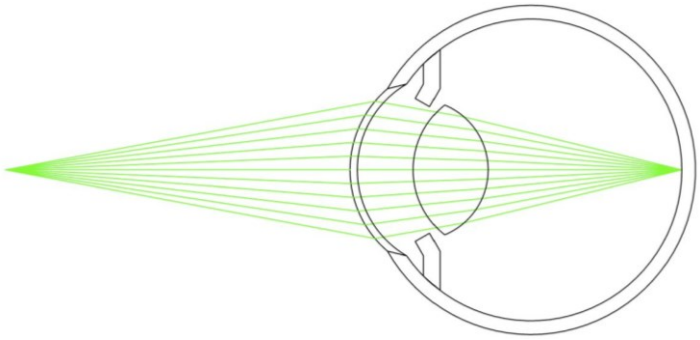

Figure 7. Accommodated eye

With myopic eye, when bringing the object closer to the eye, the image is focused first in front of the retina but starts to move closer to the retina and finally reaches the retina. Added the accommodation of the lens, myopic eyes can focus on objects that are closer to the eye as compared to the emmetropic and hyperopic eyes.

With hyperopic eyes the accommodation of the lens moves the focus point from behind the retina closer to retina. With low hyperopia one does not usually need glasses but on average needs reading glasses at younger age than emmetropic or myopic eyes.

Astigmatism is when the focal length of the lens system is different for different axes. For example eye glass prescription -2.0 D -1.0 D 90° means that the horizontal power of the lens is -2.0 D and vertical power of the lens is -3.0 D.

Spherical aberration, Figure 8, causes the focus point to be different for light rays entering different parts of the lens. For a spherical lens the refraction of light is not the same in the center and periphery, meaning that the focus point is different for the peripheral light rays than for the central. Theoretically if the spherical aberration is increased in presbyopic eye, the depth of focus is increased, thus minimizing presbyopia.

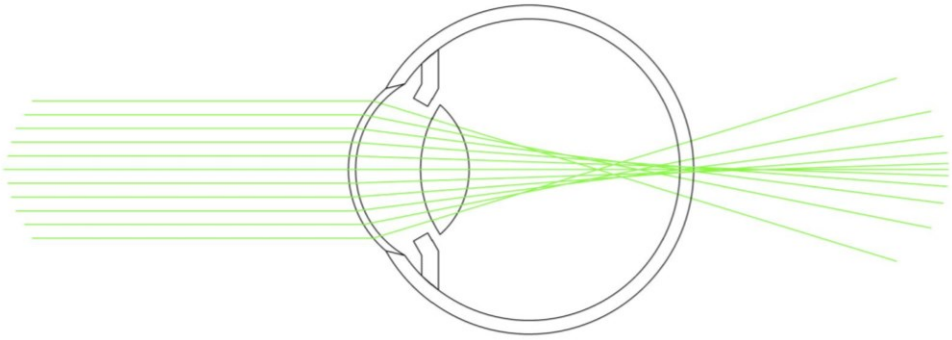

Figure 8. Spherical aberration

In chromatic aberration, Figure 9, the different wavelengths focus on different distances due to the difference in refractive indices for different wavelengths. For blue light the refractive index, in the cornea and the lens, is higher than for the green and red light.

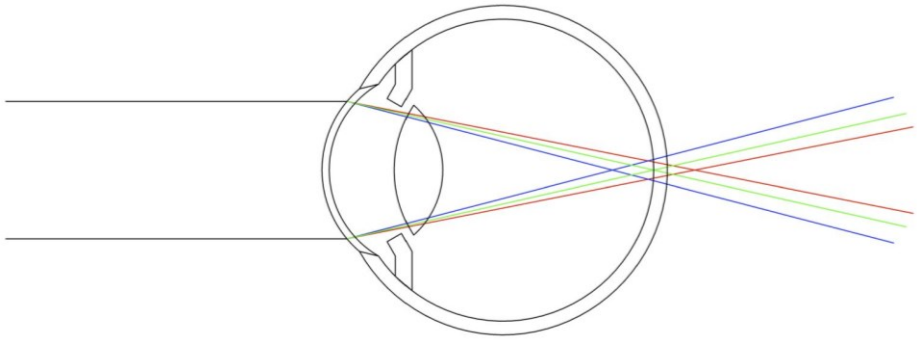

Figure 9. Chromatic aberration

When the pupil contracts, the beam that enters to the lens, and eventually the retina, is narrower than the beam that enters through dilated pupil. The refractive error does not affect so much when the pupil is contracted since the image is perceived less blurry in the retina, because the peripheral light rays, that are more bent, than the central light rays, stops at the iris, Figure 10.

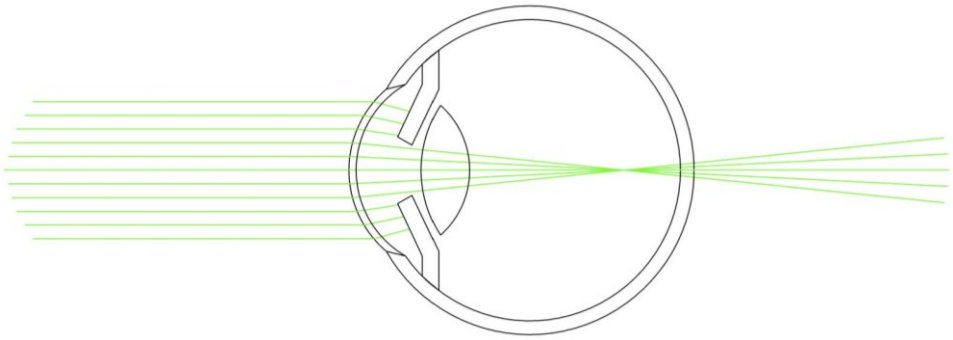

Figure 10. Myopic eye with contracted pupil

Actual vision is a combination of multiple aberrations, the low order aberrations can be corrected with eyeglasses. Prism lens tilts the path of the light to the correct position in retina, the fovea centralis, which is the area of sharp central vision. Myopia is corrected with concave lenses and hyperopia with convex lenses. Astigmatism can be corrected with regional differences in concavity/convexity in

the lens. Higher order aberrations are not possible to correct with eyeglasses, but contact lenses can be modeled to reduce the effects of spherical aberration. Theoretically refractive surgery can be used to correct low- and high-order optical aberrations of the eye but for the higher order aberrations the limiting factors are the accuracy of diagnostic devices and the lasers used in refractive surgery.

2.3 Introduction to refractive surgery

Keratomileusis, *keratos* meaning cornea and *mileusi* meaning carving, is a surgical procedure aiming to modify the refractive power of the cornea. Colombian doctor José Barraquer started to develop it in 1949. The idea was to use lamellar keratoplasty to correct the spherical refractive errors. Lamellar keratoplasty is the procedure to treat abnormal corneas by corneal transplants from donors. A slice of cornea is dissected from the patient and a matching donor cornea is transplanted to the eye. The procedure was developed to dissect approximately half of the cornea and then process, "*carve"*, it to increase or decrease the curvature of the dissection and finally placed back to the eye. At first the dissection was made manually but in the 1960s the microkeratome was developed to perform a more precise cut. Since the cornea is soft tissue, there were problems with the processing and fixating the lamellae of the cornea. Freezing of the corneal lamellae was used to ease the procedure. [23]

In the early 1950s, especially in the former Soviet Union, radial keratectomies (RK), where radial incisions are cut to the cornea, were used to modify the corneal curvature. Radial incisions relax the tensions of the cornea, thus flattening the surface. Radial keratectomy was used to treat myopia and astigmatism and in early 1990s RK reached relatively high levels of success but at the same time laser systems were producing more reliable results and the amount of RK procedures started to decline. [13, 23]

Excimer lasers were the first lasers for corneal refractive surgery. Excimer lasers used in refractive surgery are in the ultraviolet region of the spectrum. Argon-Fluoride gas produces a laser with a wavelength of 193 nm. Argon is an inert noble gas that usually does not form compounds but when excited it can form a molecule (*excited dimer,* excimer) with fluoride, which only exists when excited. The emission disassociates the excimer, and emits the photon with a wavelength of 193 nm. [24]

The frequency of laser pulses with the modern machines is from 500 Hz to 1050 Hz. Even though the pulse rates varies quite much the ablation speeds are close to each other from Schwind Amaris 1050 and Zeiss MEL 90, 1,3 s/diopter to WaveLight EX 500 1,4 s/diopter.

In excimer lasers the laser pulse ablates a small piece of corneal tissue and the ablation of thousands of pulses is used to modify the curvature of the cornea. Main methods used today are LASIK or femtoLASIK, PRK and SMILE. *Laser-assisted in situ keratomileusis* (LASIK) is a method where a thin flap is created on the anterior surface of the cornea and with an excimer laser the ablation is made under the flap. The flap is either created with a *microkeratome,* which is a small blade that dissects the tissue at certain depth, when the flap is made with a microkeratome the procedure is called LASIK. *FemtoLASIK* is a variation of LASIK, the flap is created with a femtosecond laser that emits low energy pulses with high frequency (50 kHz to 20 MHz). The pulses are focused at the wanted depth of the cornea and the optical breakdown, which is in the focus point, creates a small

plasma bubble that dissects the tissue when expanding rapidly. Tissue loss with the femtosecond lasers is only few micrometers. When millions of cavities are created, it is possible to lift the flap manually and make the wanted refractive correction under the flap.

PRK, *photorefractive keratectomy* is a method where the posterior most layer of the cornea, epithelium, is removed, either manually or by laser, and the refractive correction is made to the Bowman's membrane and stroma. PRK where the epithelium is removed with laser is sometimes called advanced surface ablation ASA. When the epithelium is softened with an alcohol solution and slid away before the refractive correction, the method is called *laser-assisted sub-epithelial keratectomy*, LASEK, after the refractive correction it is possible to place back the epithelium above the ablation zone.

The energy per pulse in excimer lasers is in the millijoule region, in femtosecond lasers it is somewhere in the micro- or nanojoule region. The high energy per pulse in excimer lasers limits their use to surface ablations only, focusing high energy pulse inside the tissue would severe the tissue in a larger area than intended since the excess energy would diffuse to surrounding tissue, damaging it. The small energy per pulse in femtosecond lasers makes it possible to use them in dissecting tissue below the surface.

The amount of tissue ablated can be calculated from the Munnerlyn equation [25], equation 7. The depth of central ablation d (μm) divided with the intended refractive correction D (diopters) equals the optical zone z (mm) squared divided by 3. For example 1 diopter correction with 6.5 mm optical zone ablates ~14 μm of tissue.

$$\frac{d}{D} = \frac{z^2}{3} \tag{7}$$

Small incision lenticule extraction, SMILE, Figure 11, is a femtosecond laser based method where a small lenticule is made inside the cornea, through a small opening on the side, the lenticule is removed. The anterior, stiffer, parts of the cornea are mainly untouched and the refractive correction is made to the deeper layers of the cornea. The amount of tissue removed with SMILE procedure differs from the excimer based methods; 15 μm slice is added to the refractive correction to ease the removal of the lenticule, otherwise the side of the lenticule could easily break when removed.

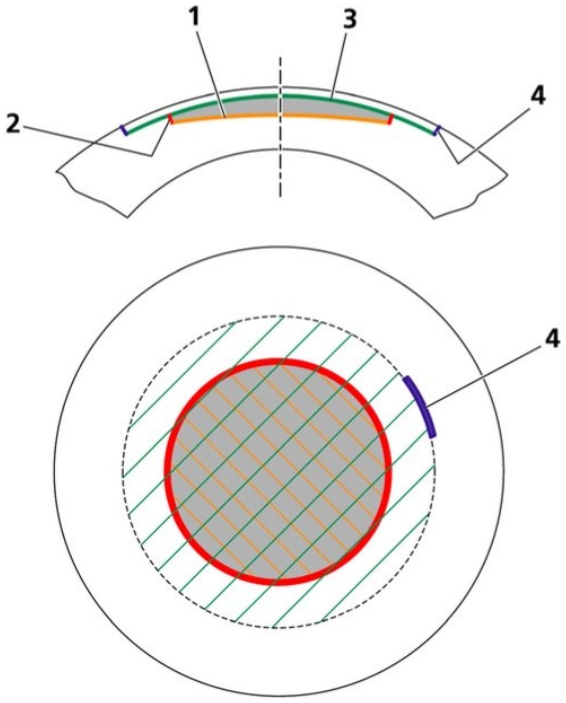

1 Lenticule cut (underside of lenticule)
2 Lenticule side cut
3 Cap cut (concurrently upper side of lenticule)
4 Cap opening incision

Figure 11. SMILE procedure [26]

2.4 Structure of the cornea

Cornea is an elliptic structure, the nasal-temporal (NT) diameter is approximately 10-12 mm and the superior-inferior (SI) diameter is slightly smaller. The central thickness of the cornea varies from under 500 µm to over 600 µm [10], normally roughly 520 µm centrally and 650 µm peripherally [27]. The peripheral cornea is thicker than the center and the thinnest part is in the central region. Healthy pre-presbyopic Caucasian eyes have been shown to have an average central thickness of 552 µm, with the thickness increasing by 22 % and 32 % at 4 mm temporally and nasally, respectively [28].

Figure 12 shows nasal-temporal cross-sectional Scheimpflug image of the cornea. Figure 13 shows topography images of corneal thickness and keratometric values (in diopters). The topography images are built from series of Scheimpflug images. Astigmatism of ~1.8 D at ~100° is clearly visible in the image. Figure 14 shows the mean corneal thickness values at different distances from the thinnest location.

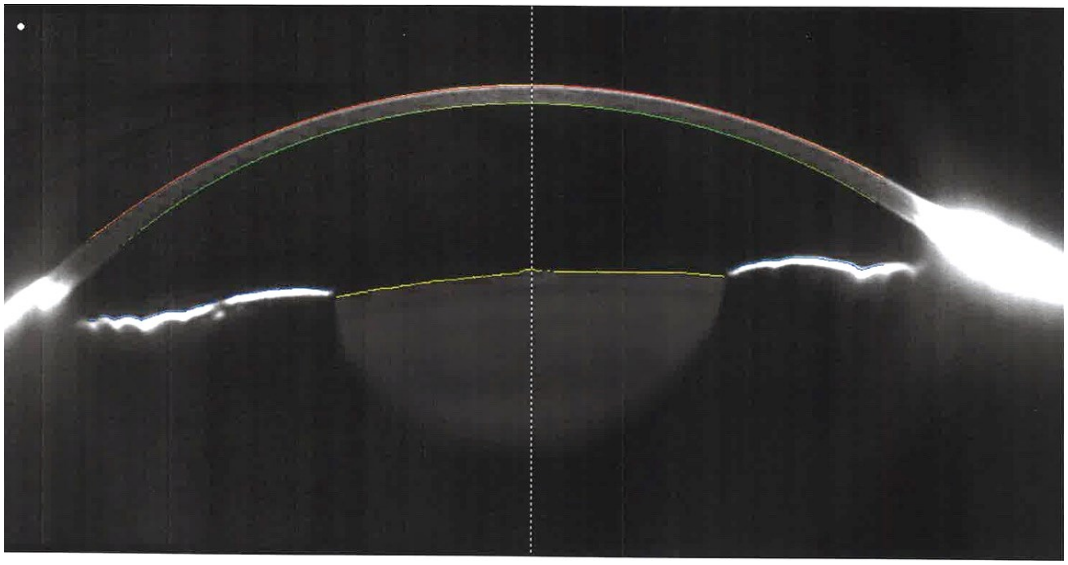

Figure 12. Scheimpflug image of central nasal-temporal (NT) cornea

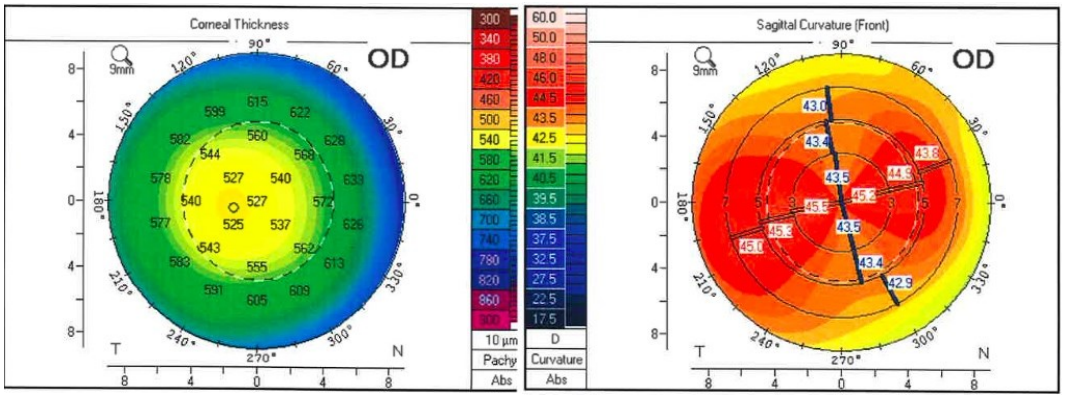

Figure 13. Topographic image of corneal thickness (µm) and keratometric values in diopters (D)

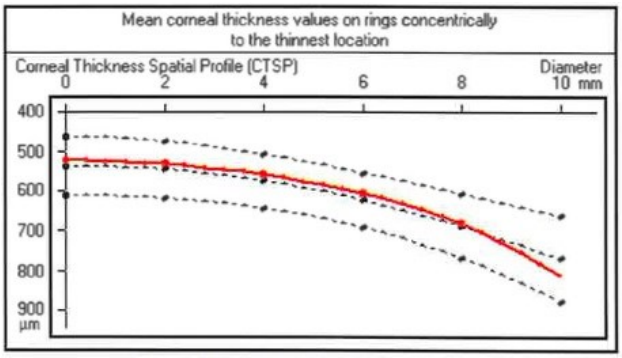

Figure 14. Mean corneal thickness values compared to the thinnest location

The keratometric K-values (in diopters) in Figure 13 can be converted to radius values with equation 8, r is radius in mm.

$$r = \frac{337.5}{K} \tag{8}$$

The cornea is highly structured and relatively acellular, transparent and collagenous tissue [27] consisting of five to seven layers (Figure 15), which are parallel to the external surfaces: external epithelium*, (anterior basement membrane),* Bowman's membrane, stroma, Descemet's membrane and endothelium (or internal epithelium) [13]. In two studies by Dua et al a sixth layer was identified, the pre-Descemet layer called Dua's layer but other research has reported that the data provided is not sufficient to determine a new anatomical layer in the cornea [29-32]. The identified layer is approximately 10 µm thick and stronger than the adjacent layers [31]. However, this has not been supported by numerical data, since measurements of the cornea have tended to focus on the entire cornea, rather than on identifying the distinct layers. Moreover the resolution of these measurements have limited detection of such a thin layer, the proposed Dua's layer could also lie outside the range of measurements. Jester et al [29] suggests that using the proposed terminology is not justified and would only confuse the literature.

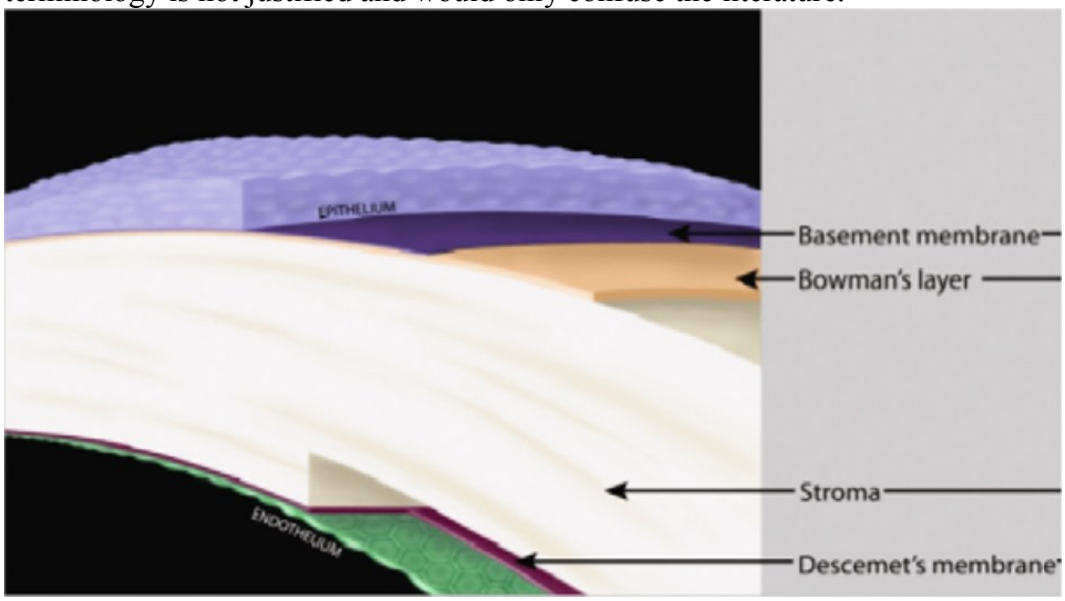

Figure 15. Corneal layers [33]

External epithelium

The external epithelium is the protective anterior surface of the cornea, which consists of 5 to 7 layers of cells with a total thickness of about 50 μm to 52 μm [27, 34]. The most posterior cell layer is the only layer of epithelium capable of undergoing mitosis [27]. The cells in more anterior layers are constantly pushed forward during the epithelial desquamation [27]. Continual desquamation of epithelial cells is possible due to a stable supply of stem cells from the limbal niches, thus creating a protective chemical and antigen barrier in the cornea [27]. A complete turnover of epithelium occurs in 5 to 7 days. Despite the high activity of the epithelial cells, the epithelium must maintain the same thickness profile to maintain the same corneal power, which is on average, in the central 2 mm diameter zone, approximately 1.03 diopters [34]. The refractive power of the epithelium comes from the difference between refractive indices in the epithelium and stroma, which are 1.401 and 1.377 respectively. Poor formation of the epithelium can be a result of denervation [27], which is not a problem with refractive surgery in which the nerves regenerate in the epithelium. The epithelium is slightly thicker inferiorly than superiorly and thicker nasally than temporally with the thinnest point having a distance of 0.33 mm temporally and 0.9 mm and superiorly from the corneal vertex [34]. Since the epithelium contains no collagen fibers, the effect on the mechanical stability remains negligible [35].

Bowman's membrane

Bowman's membrane is approximately a 15-μm (or 0.5 μm [36]) thick layer of randomly oriented and strongly interwoven collagen fibers [37]. An extracellular matrix, where the epithelial cells are attached, is between the epithelium and the Bowman's membrane. The extracellular matrix is called the anterior basement membrane, which is formed in honeycomb pattern. There are pores where the nerves can penetrate from the deeper layers to the epithelium. The Young's modulus for the anterior basement membrane is 9.6 kPa.[33, 38]

Stroma

Stroma is a relatively acellular, non-linear, inhomogeneous, anisotropic, viscoelastic material [27, 39] of a series of layered lamellae (Figure 16) at various orientations that stretches from limbus to limbus [40]. Each lamella is from 0.2 μm to 2.5 μm thick and 0.5 μm to 250 μm wide [38] that consists of parallel uniform diameter 31 nm to 32 nm fibrils [27, 41]. The width and the thickness of the lamellae tend to increase toward the posterior region of the stroma. The anterior region has a flat, tape-like shape 0.2 – 1.2 μm thick and 0.5 – 20 μm wide. Toward the posterior regions, the lamellae change to broadsheet like structure 1 – 2.5 μm thick and 100 – 200 μm wide. [38]The posteriormost layer of the stroma has randomly arranged collagen fibrils in very thin sheet [38], which lies in the same location that Dua et al [31] described as a distinct layer.

Collagen molecules, about 1.7 nm apart from each other, compose the fibril [41]. The orientation of the fibrils in the adjacent lamellae is at approximately right angle [41, 42]. All the collagen fibrils lie in the plane of the cornea but do not cross the cornea from front to back [41]. 3 % to 10 % of the volume of the stroma consists of inactive keratocytes [27]. Only 15 % of the weight is collagen fibrils, 78 % is water and 7 % is non-collagenous proteins, proteoglycans and salts [43].

In the central (optical) region of the cornea 66 % of the collagen fibers are oriented in two-directions, nasal-temporal (NT) and superior-inferior (SI). The orientations of the collagen fibers in those lamellae differ from the orthogonal NT and SI axes less than 22.5°. The remaining 33 % are randomly oriented. [13, 41] In total 4 sectors of 45° add up to 180° where 66 % of collagen fibers are oriented. Another way to say same thing is, 83 % of the collagen fibers are randomly oriented and the orientation of the remaining 16 % is nasal-temporal and superior-inferior. Since the x-ray scattering measurements by Aghamohammadzadeh [41] only give the orientation of the collagen fibrils in all the layers of cornea, it is not known, what are the proportions of randomly oriented layers and highly oriented layers from all the layers. Significant variations of preferred directions between the samples were also observed, e.g. one sample had almost 25 % more fibrils oriented SI than NT, and some samples vice versa. Other study by Abahussin et al [44] found that in the posterior stroma 42 % of the lamellae are preferentially aligned in the superior-inferior and nasal-temporal directions, the remaining 58 % are randomly orientated. In the anterior stroma the proportion of the preferentially aligned collagen fibrils drops down to 11 %. The orthogonal arrangement in the posterior two thirds of the cornea may help the cornea to withstand the pull from the extraocular muscles. The isotropic organization of the anterior one third may help the cornea to maintain the spherical curvature under intraocular pressure.

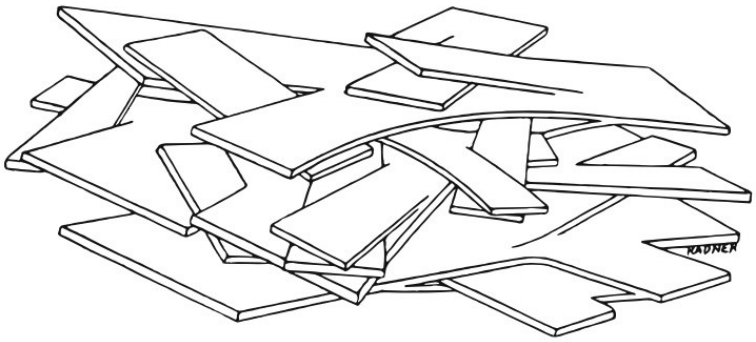

Figure 16. Possible organization of lamellae in the cornea [45]

The stroma consists of between 200 and 400 (*or 300-500* [27]*, or 250-400* [46] *or ~200* [47]*or 200-250* [44]*or 200-500*[48]) lamellae, thinnest part at the apex of the cornea has the least amount of lamellae and more in the periphery near the limbus [49]. Peripheral collagen fibers tend to be oriented circumferentially [13, 42, 50] and parallel to the surface. The stiffness of the cornea is not uniform, in the nasal-temporal and superior-inferior directions, the ratio sets up to approximately 3:1, and the diagonal meridian is the weakest [13, 51]. One study states that the superior-inferior meridian is 10 % to 20 % stiffer than the nasal-temporal meridian [52]. Both articles [51, 52] agree that the diagonal meridians are the least stiff. Tensile strength in the stroma is measured to be 10 % - 20 % higher in superior-inferior direction than nasal-temporal [52], or 1 MPa in NT direction, 3 MPa SI and 13.0 MPa circumferentially in the periphery [27]. The literature does not show consistency in radial differences.

Figure 17 shows two possible collagen fibril orientations in the cornea and limbus by Aghamohammadzadeh et al [41] and Meek & Boote[53]. It is possible that there are lamellae from sclera to cornea that anchors the cornea to the sclera, if the arrangement is as Aghamohammadzadeh et al predict, the orthogonal SI and NT

forces, maintaining the structure of corneoscleral shell, would be highest in the nasal-temporal and superior-inferior directions. On the other hand if the Meek & Boote model is correct, the force distribution would be more even, though the muscles that move the eye create stresses in SI and NT direction.

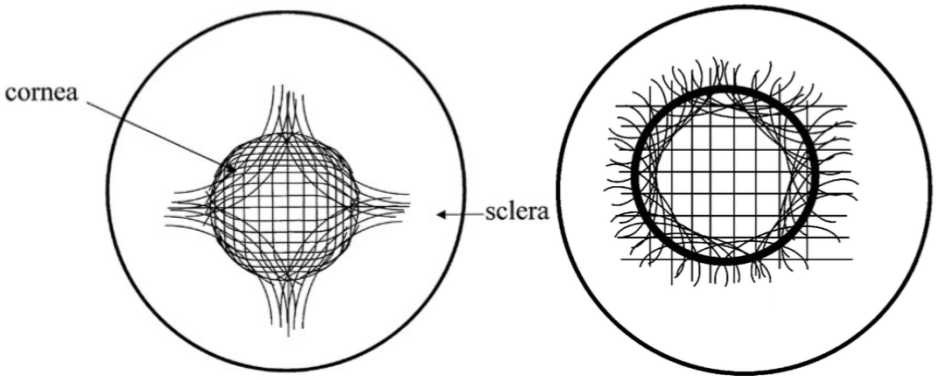

Figure 17. Possible collagen arrangements of cornea and limbus, left [41] right [53]

Figure 18 [41] shows the preferred orientations of collagen fibrils in human eyes related to the location. The image shows a montage of polar plots of the preferred orientations of the collagen fibrils, where each plot represents the orientation and the proportion of oriented fibrils. Since the corneal thickness increases towards the periphery the amount of collagen lamellae increases as well. The peripheral plots have been scaled down to fit in the image. The scaling factors for different colors are: green 1, pink 2, red 3, blue 4 and black 5. [41]

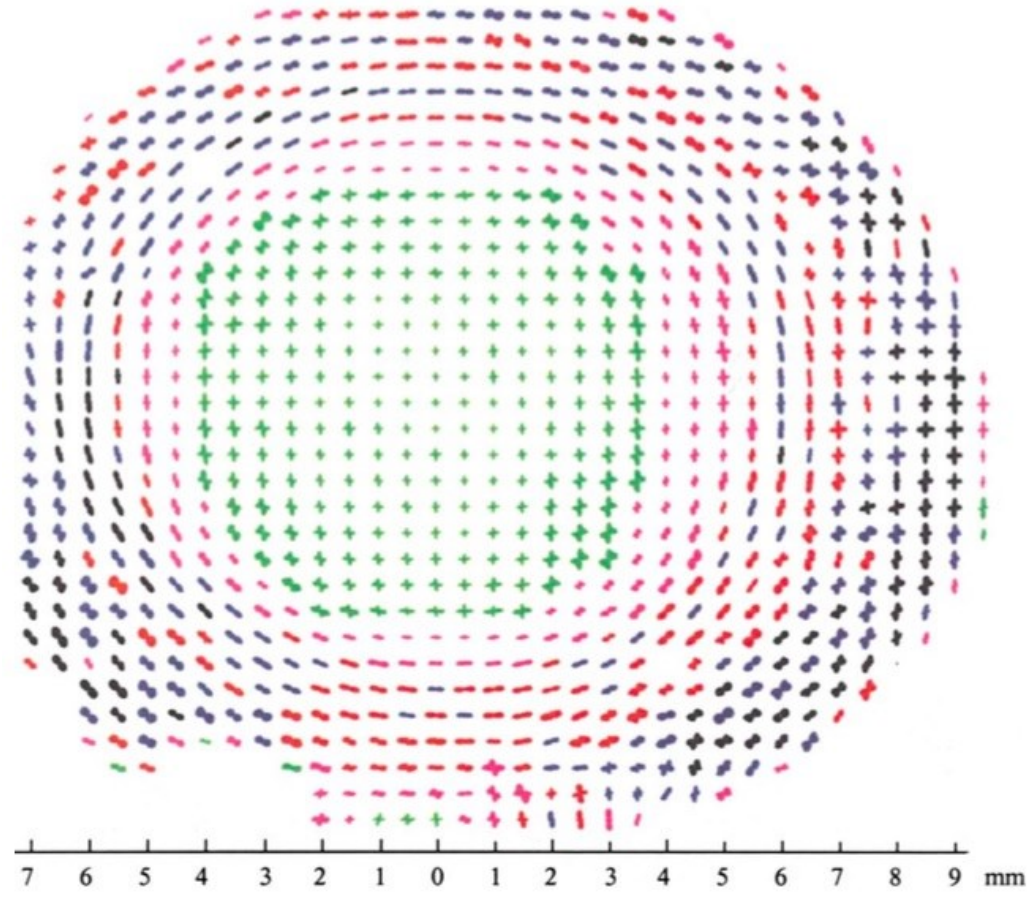

Figure 18. Preferred orientation of collagen fibers [41]

Cornea is radially strongest at the central region and circumferentially strongest at the limbus [54], and mechanical properties depend on the radial direction [41].

In a study by Randleman et al [55] the depth-dependent corneal cohesive tensile strength was measured from lamellar strips that were dissected from nasal-temporal meridian of the cornea. Samples were from the stroma, so the cohesive tensile strength of the external epithelium, Bowman's membrane, Descemet's membrane and endothelium were not measured. From the measurements of Randleman et al [55] Reinstein et al [56] derived a polynomial (equation 9), using regression analysis, which represents the percentage of the maximum depth-dependent cohesive tensile strength of the stromal cornea.

$$\mathrm{y} = -4 * 10^{-6}x^4 + 0.0009x^3 - 0.0745x^2 + 2.6709\mathrm{x} + 9.2996 \quad (9)$$

Due to rounding of Excel, the 4th and 3rd order terms should be approximately -3.6 and 0.00093 respectively, so the plot would represent the actual curve. The mathematical model by Reinstein et al assumes that the cohesive tensile strength is directly proportional to the tensile strength, i.e. the intertwining and branching between the stacks of lamellae in different depths is directly proportional to the tensile strength of the whole lamellar structure of the cornea.

The depth-dependent differences of mechanical properties are thought to be a result of the intertwining and branching of the collagen fibers. The collagen fibers are not only interwoven and interlaced but the structure is more complicated. The individual fibers have branches and anastomoses independently to multiple fibers. Effectively the entire stroma can be seen as one interlinked structure, where the relative stiffness is related to the density of intertwining at the different areas, which changes from anterior to posterior stroma and central to peripheral stroma [29]. The density of collagen fiber intertwining is logarithmically declining from anterior to posterior stroma [29, 57]and the superficial one third of the lamellae are more irregularly interwoven than those in the posterior two thirds[38]. Peripheral lamellae are more branched than the central lamellae [43]. Small bundles of collagen fibrils extend from one lamella to other [38]. Collagen fibers have physical insertions into Bowman's and Descemet's membranes that keep the endothelium and epithelium attached to the cornea. [29] Not only the arrangement of lamellae affects the mechanical properties but also the structure, branching, anastomosis and proteoglycan connections in the collagen fibrils have important roles.

If the organization of the collagen fibrils in distinct lamellae is disrupted the stiff anisotropic structure of the stromal layer is lost and the tissue appears isotropic, which reduces the mechanical properties of the cornea, leading to corneal diseases, e.g. keratoconus.[13] Keratoconus is a disorder of the eye where the cornea becomes thinner and changes to a more conical shape, leading to a distorted vision that can be difficult to correct with glasses. Effects on the cornea by keratoconus are irreversible but the symptoms can be delayed or even stopped by corneal collagen crosslinking (CCL), which is a treatment where riboflavin (vitamin B_2) solution is applied to the cornea and with UVA radiation, collagen cross-links are formed to the stromal cornea, resulting to an increased stiffness. [58]

Descemet's membrane (or posterior basement membrane)

Young's modulus for the Descemet's membrane is approximately 38.9 kPa. Endothelial cells attach to the Descemet's membrane, which is similar to the anterior basement membrane where the epithelial cells attach. [33]

Endothelium

The most posterior layer, endothelium, is a 4 μm to 6 μm thick monolayer of about 400 000 hexagonal cells, diameter of 20 μm. Endothelium is responsible of corneal dehydration that prevents the cornea to imbibe too much liquid, which would lead to swelling, opacity and reduced optical performance.[27]

Corneoscleral shell

The corneoscleral shell has a high Young's modulus, from 5 MPa to 13 MPa, and high shear modulus. The sclera is mainly composed of types I and III collagen fibers and the Young's modulus is higher in the circumferential direction than the radial. In 1937 Friedenwald [59] introduced the "*ocular rigidity function*", equation 10, that describes the relationship between the changes in intraocular pressure and ocular volume in low strains. [46]

$$\ln\left[\frac{IOP}{IOP_0}\right] = \mathrm{K}(V - V_0) \tag{10}$$

Where IOP_0 and V_0 is the original intraocular pressure and volume respectively and K (in humans ~0.05 μl^{-1}) is the coefficient of ocular rigidity. At IOP of 15 mmHg, the change in volume is approximately 1 μl/mmHg. [46] If the corneoscleral shell is assumed as a sphere of 24 mm in diameter, 1 and 5 mmHg rise in the pressure would lead to 1.4 μm and 6.4 μm increase in diameter respectively, which is insignificant compared to the focal length of the lens system in the eye. The total optical power of the eye is 60 D [11], a 6.5-μm increase in the eye length is equivalent of 0.02 D decrease in optical power. Glasses are usually prescribed in steps of 0.25 D. The optical system is much more complicated than that suggests but it gives estimation of the order of magnitude. The sclera is stiffer than the cornea [46] and the lens system cannot be represented as one lens but the changes in intraocular pressure and its effect on the volume and refractive outcome can be left out of the simulations.

The collagen fibrils in the sclera are arranged more randomly than in the cornea. The thickness of the fibrils varies from 25 nm to 230 nm and the lamellar bundles they form, vary in thickness of 0.5 μm to 230 μm. Orientation is mainly parallel to the scleral surface and the fibrils are interwoven to each other as are in the stromal cornea. In the outermost layer of the sclera the bundles of collagen intersect at various angles, in the posterior layers orientation is either meridional or circumferential. The thickness and width also increases toward the posterior layers.

The cornea and the sclera are represented so far as an anisotropic nonlinear viscoelastic or elastic material but there is an elastic limit beyond which plastic deformation occurs. It is hypothesized that the plastic deformation of the sclera might contribute to the occurrence of myopia, when the volume of the eye increases from the plastic deformation. It might be caused by genetically associated decrease in the elastic limit, higher than normal stresses due accommodation (extended times of reading) or regular increases in the intraocular pressure due to squinting and rubbing of the eyes. [46]

Optical behavior of the cornea depends on the biomechanical equilibrium of the intraocular pressure and the intrinsic stiffness of the cornea [50]. Alterations to the balance lead to modification of vision. Removing a part of tissue modifies the shape of the cornea and the biomechanical properties are also changed.

Radial keratectomies severe the lamellae, which reduce the peripheral tension, leading to the peripheral expansion and central flattening [40], which is one way to correct myopia.

2.5 Measuring the biomechanical properties of the cornea

Piñero and Alcón [60] state that: "*Biomechanics is usually defined as 'mechanics applied to biology'. Due to the variety and complexity of the behavior of biological structures and materials, the term biomechanics is better defined as the development, extension and application of mechanics for the purposes of understanding better the physiology and physiopathology, as well as the diagnosis and treatment of disease and injury.*"

Biomechanical models aim to describe the response of a biological material to an applied load, which relates different input parameters with an output [60]. Biomechanical models try to predict the effects and results of different treatments and diseases, the accuracy of these models depend highly on the accuracy of the parameters used in the models. For finite element modeling, increasing the complexity of the model, increases the accuracy but also increases the amount of calculations needed for processing the analysis. Also when increasing the complexity of the model, the possible errors might multiply, leading to poor results.

In this and the following chapters Young's modulus is often mentioned even though it is misleading to describe nonlinear materials with linear material properties, but many of the sources used in this thesis have only provided linear material properties. The relative differences in linear material properties are transformed to match the relative differences in nonlinear material properties.

In the review of corneal biomechanics [60], Piñero and Alcón describe the modern methods, which use *in vivo, ex vivo* and predictive biomechanical models, to estimate the biomechanical properties of the cornea.

In vivo characterizations are non-invasive methods that give estimations of the biomechanical properties.

Applanation tonometry is a way to estimate the Young's modulus of the cornea. Intraocular pressure (IOP) is related to the Young's modulus (E) and the correction factor (k). k depends on the corneal thickness, anterior corneal radius, Poisson's ratio and the area of applanated cornea. Equation 11 shows the relation between the E, IOP and k. [60, 61]

$$E = k_2 IOP_{true} \tag{11}$$

where the true intraocular pressure (IOP_{true}) is calculated from the measured intraocular pressure (IOP_G) by using equation 12.

$$IOP_{true} = \frac{IOP_G}{k_1} \tag{12}$$

The Young's modulus, in MPa, for a cornea that is 520 μm thick and the IOP_{true} in mmHg is expressed by the equation 13. [60, 61]

$$E = 0.02291 * IOP_{true} \quad (13)$$

Other way around the intraocular pressure can be measured from the indentation depth of the eye, which can be derived from the Friedenwald's "ocular rigidity function" in equation 10, when the ocular rigidity is known. [46]

The ocular response analyzer (ORA) characterizes some biomechanical properties in a clinical setting. It analyzes the corneal behavior at a bidirectional applanation from a pulse of air that causes the cornea to flatten and reach concave state and return to normal state. Changes in the cornea are measured from a refracted infrared light that is emitted to the cornea. At first state the pulse creates the maximum concavity in the cornea and at the second state cornea returns to its original convex form. Figure 19 shows the diagram from the ocular response analyzer where the viscoelasticity of the cornea can be seen.

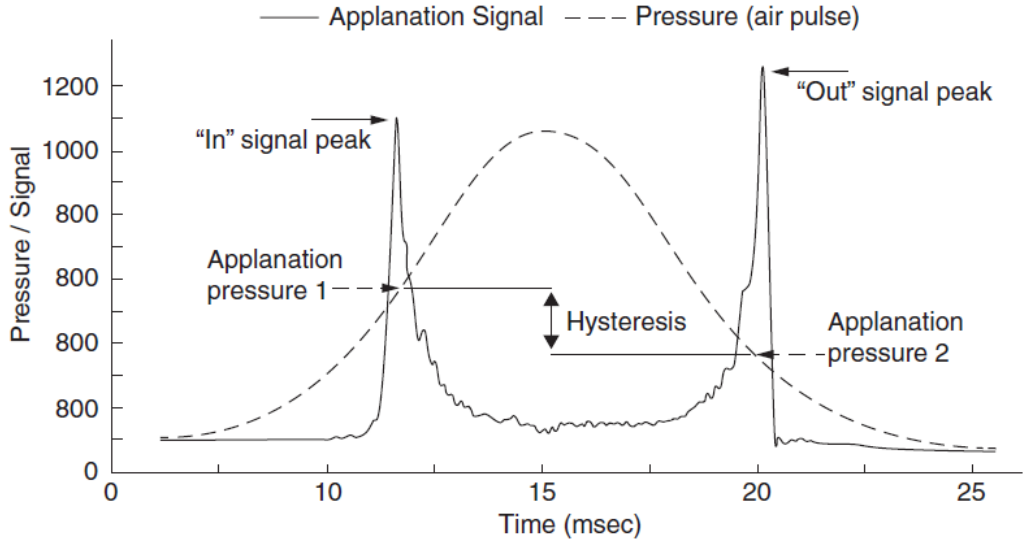

Figure 19. The diagram from the ocular response analyzer (ORA). The applanation signal visualizes the velocity of the corneal deformation. [60]

Mechanical testing of corneal samples is often used to determine the viscoelastic anisotropic properties of the cornea. Inflation tests are a way to measure regional properties in the cornea. The Young's modulus can be calculated from the distance of the markings under different pressures. The inflation tests have much more complicated methodology than the strip extensometry. Strip extensometry is mechanically much easier to produce but mathematically more complicated to get reliable measurements. In strip extensometry the errors originate from the spherical shape of the cornea and the variation of thickness. When the strip specimen is pulled, the strain is not uniformly distributed since the posterior surface is smaller than the anterior. The variation of thickness must be considered when determining the elastic moduli. [62]

Small incision lenticule extraction, SMILE, have made it possible to make mechanical testing to *in vivo* stromal cornea but no research of that subject was found while making this thesis.

2.6 Biomechanical properties of the cornea

Tensile testing for viscoelastic material can easily result in low values of Young's modulus. When the load is applied in some finite rate, there is time for viscous flow to occur in the material, which increases the total strain in the material. When the measurements, where the viscous flow have been possible, are used to determine Young's modulus, the results show significantly lower than the actual Young's modulus of the material. Increasing the loading rate decreases the viscous flow and eventually, at high enough loading rate, viscous flow is not detected anymore and the true Young's modulus can be determined. [63]

Cornea is an anisotropic, nonlinear viscoelastic material. In nonlinear elastic materials the stress-strain curve is not linear, meaning that the Young's modulus varies with the stresses. In cornea, with higher stresses, less deformation occurs. In viscoelastic materials the stress-strain curve vary with different strain rates. In the following review of biomechanical properties of the cornea, the determined Young's and shear moduli are highly dependent on the conditions of the measurements and thus not very consistent. In this thesis the focus is on the relative differences between the different layers and orientations. Based on the current research the absolute values of corneal biomechanical properties are extremely difficult to determine and since the variation between eyes is significant, it is not even necessary. As long as there are no reliable methods to determine the biomechanical properties of *in vivo* eyes, the biomechanical models remain to be estimations of average donor eyes.

Collagen type-I fibrils are the main load carrying structures in the cornea [45]. It is hypothesized that the collagen fibrils in a load-free state are crimped [64]. Liu et al [65] proposed the "crimping degree" to represent the ratio between straightened length the original crimped length of a collagen fibril. At a load-free state the crimping degree is assumed to follow a Gaussian function. When the load is applied, each collagen fibril undergoes an independent deformation, resulting an arrangement of collagen fibrils at different degrees of crimping, from fully extended to still crimped. Figure 20 shows different degrees of crimping in corneal collagen fibrils. Plastic deformation occurs when the individual collagen fibrils are broken even though no macroscopic rupture is present.[65]

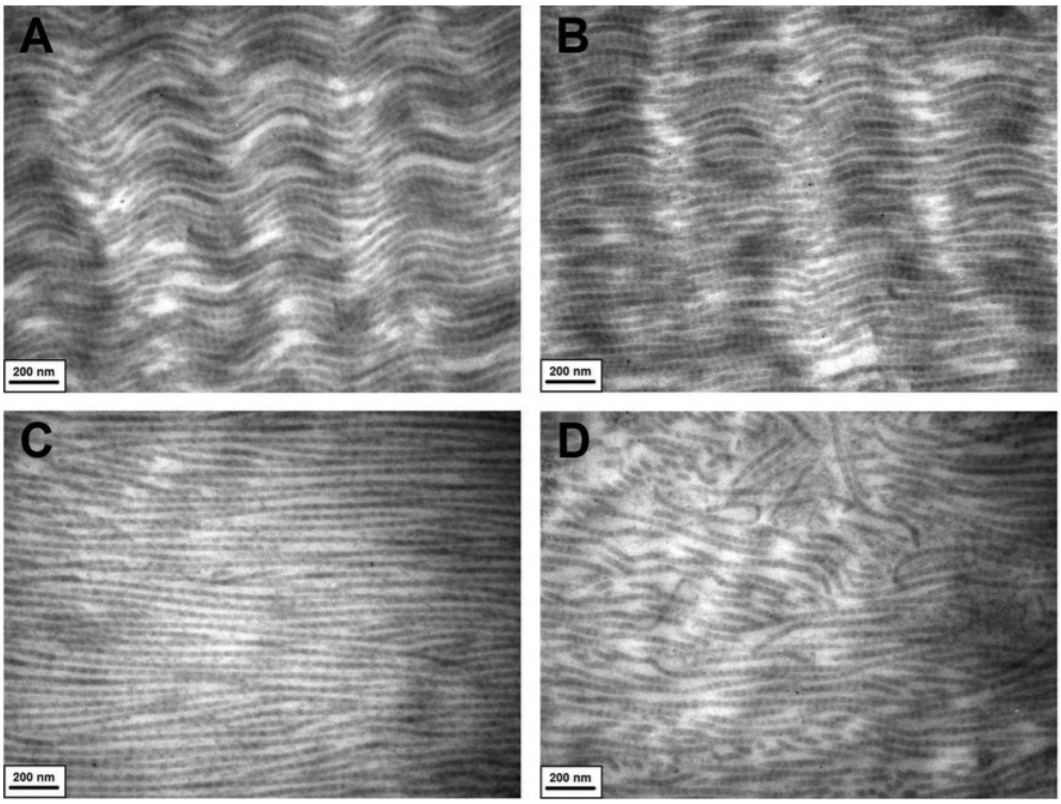

Figure 20. Crimping in collagen fibrils, (A) load-free condition, (B) under elongation, (C) fully straightened, (D) broken fibrils even though the sample strip had not ruptured [65]

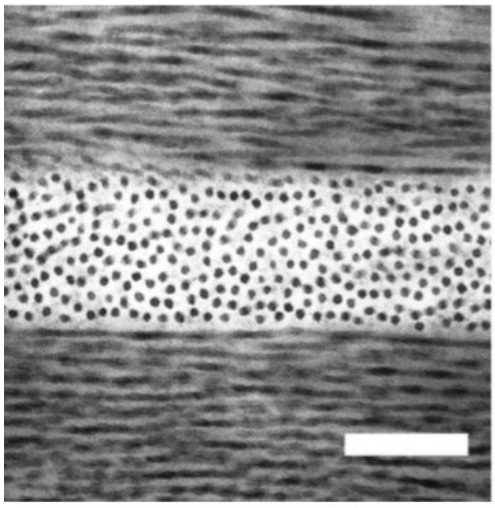

Figure 21. Three adjacent stromal lamellae. In the middle lamella, the collagen fibers are oriented towards the viewer and the adjacent top and bottom lamellae are approximately at a right angle compared to the middle lamella. All of the collagen fibrils are parallel to the surface of the cornea. [42]

Hjortdal [54], Randleman et al [55], Petsche et al [48], Elsheikh et al [52], Sloan et al [66] and Jayasuriya et al [51] studied the regional, directional and depth-dependent material properties of the cornea, mostly corneal stroma. All studies

showed significant anisotropic mechanical properties of the cornea, which is expected considering the heterogeneous nature of the collagen fibril orientation. Differences in the results were significant between the researchers.

Hjortdal [54] used 8 eyes from donors of 64 to 88 years of age. Four regions of cornea were defined: the central 3 mm region, para-central 1.5 – 3.5 mm from the corneal apex, peripheral 3.5 – 5.5 mm from the corneal apex and limbal region from 0.5 mm inside to 0.5 mm outside of the border of cornea and limbus. In the measurements all the layers of the cornea were included in the samples. The Young's moduli where derived from the nonlinear stress-strain data. Superior-inferior Yong's modulus was measured to be 8.6 MPa and circumferential Young's modulus was 13.0 MPa. Regional strains were derived from placing small mercury droplets on the epithelium and endothelium and measuring the distances between the droplets under different pressures, 2 – 100 mmHg.

Jayasuriya et al [51] studied the piezoelectric and mechanical anisotropies of 19 donor corneas. The study showed that the Young's modulus has a high correlation with the direction and hydration. The sample widths are not mentioned in the study. Superior-inferior cuts had a Young's modulus of ~1.3 MPa, when hydrated and after 35 minutes of drying, increased to ~4 MPa. Nasal-temporal cuts had Young's modulus of ~3 MPa, when hydrated and after 40 minutes of drying, increased to ~6 MPa. Diagonal cuts had initial Young's modulus of 0.3 MPa and after 35 minutes of drying, increased to ~1 MPa. Young's modulus was obtained from a dynamic stress applied to the samples at a steady frequency of 104 Hz. "*A dynamic stress, σ = 5 N, peak to peak"*. As the actual sample sizes are not mentioned it is not possible to say what is the actual stress in the measurements and was the variation of corneal thickness considered when determining the stress i.e. the force per unit area. Further on it was not mentioned how much the drying affects on the volume of the cornea and thus the area where the force is applied. Measurements made *in vivo* showed that the central corneal thickness decreased by 3 % in one minute when the subjects were not blinking [67].

Randleman et al [55]used 20 donor corneas to measure depth-dependent cohesive tensile strength from donors of age 20 to 78 years. Samples were 3 mm wide nasal-temporal cuts from limbus to limbus. Measurements showed the force needed to separate two layers of lamellae at different depths. At anterior stroma it started from ~50 g/mm and decreased toward the posterior stroma to ~5 g/mm. Donor age showed correlation to the cohesive tensile strength at central depth between 40 % to 60 %, it increased 38% from ages 20 to 78 years.

Petsche et al [48] studied depth-dependent transverse shear properties of corneal stroma. Torsional rheometry was used for eight 6 mm diameter buttons of donor human corneas, ages 82 – 86 years. From each donor, one cornea was cut into thirds through the thickness and other was measured with a full thickness stroma. Results showed that the shear moduli for axial strain were 7.71 kPa, 1.99 kPa, 1.31 kPa and 9.48 kPa for anterior, central, posterior and full thickness samples, respectively. The higher full thickness shear modulus was thought to be a result of the loss of interactions between different layers.

Jue & Maurice [68] measured the Young's modulus of Descemet's membrane to be 0.5 MPa

Last et al [33] examined human donor corneas unsuitable for transplantation, with atomic force microscopy. Donor ages ranged between 58 and 72 years. Samples were 3 x 3 mm pieces of central cornea, epithelium and endothelium was

removed, and orientation was not mentioned in the materials and methods section. They measured the Young's modulus for anterior and posterior (Descemet's) basement membranes. Descemet's membrane has a higher Young's modulus than anterior basement membrane, 50 ± 17.8 kPa and 7.5 ± 4.2 kPa respectively. It might be due the larger pore size in the anterior basement membrane, leading to more densely packed Descemet's membrane.

For incompressible material the shear modulus G is one third of the materials Young's modulus, equation 14.

$$\mathrm{G} = \frac{E}{3} \tag{14}$$

For polymers the shear modulus is related to the number of crosslinks in the material, equation 15

$$\mathrm{G} = \mathrm{nkT} \tag{15}$$

Where *n* is the number of crosslinks, *k* is a constant and T is the temperature. Combining the equations 14 and 15, it is seen that the number of crosslinks is directly proportional to the Young's modulus of the cornea, which is consistent with the measurements where more densely packed, and higher number of crosslinks, Descemet's membrane shows higher Young's modulus than the anterior basement membrane. Both of which have lower Young's modulus than the stroma. [33]

In a more recent study Last et al [69] investigated the Young's modulus for different layers of cornea, using atomic force microscopy. The values obtained are: 7.5 ± 4.2 kPa for anterior basement membrane, 109.8 ± 13.2 kPa for Bowman's membrane, 33.1 ± 6.1 kPa for anterior stroma and 50 ± 17.8 kPa for Descemet's membrane.

Lombardo et al [36] measured 4 fresh human corneas from donors aged 68.5 ± 6 years. Samples were corneal discs with a diameter of 8.0 mm and epithelium removed. In their literature review they found the variation of the Young's modulus of the total cornea to be between 0.5 – 57 MPa. The measurements gave Young's modulus of the anterior stroma to be 1.14 – 2.63 MPa.

Knox Cartwright et al [70] researched the stiffening effect of corneal crosslinking (CCL) to donor human corneas. The mean donor age was ~82 years and varied from 76 to 90 years. The Young's modulus was determined from the strain maps, where central displacements and thin shell theory was used to calculate the Young's modulus. The Young's modulus for 9 corneas before CCL treatments were 0.47±0.03 MPa. Two variations of CCL treatment increased the Young's modulus to 2.06±0.22 MPa and 3.48±0.41 MPa.

In another study by Knox Cartwright et al [71] the age-related increase of corneal stiffness was researched from 50 donor corneas between the ages of 24 and 102 years. They found that Young's modulus (E), in MPa, for the whole cornea depends on the age (y) of the cornea, as in equation 16.

$$\mathrm{E} = 0.0032\mathrm{y} + 0.20 \tag{16}$$

The Young's modulus for 20 year old would be 0.27 MPa and for a 100 year old 0.52 MPa. Age related increase in cohesive tensile strength measured by Randleman et al [55] is 38 % from 20 to 78 years, with equation 16 the increase in Young's modulus is 70 % from 20 to 78 years.

Sloan et al [66] researched the depth- and location-dependent mechanical response of shear loading from 14 human donor eyes, the age of the donors varied

from 54 to 74 years. Specimens were buttons of cornea, 3 mm in diameter, from central and superior region. A 300 mmHg initial compression and a shear strain to produce a 25-µm displacement were applied for the measurements. The measurements indicated that the maximum shear modulus of the cornea was at the depth of 25 % of the corneal thickness, unlike in other studies that state that the stiffest part is at the anterior stroma. Though the study says that the epithelium was intact for the measurements and no mention of the Bowman's membrane were in the article, it might be that the measurements showed the stiffest part to be at the anterior stroma, which comes close to the 25 % of depth, with the resolution of 50 µm, when the thickness of epithelium and Bowman's membrane are 52 µm and 15 µm respectively. Figure 22 shows the results of Sloan et al, NT means nasal-temporal and SI superior-inferior. One interesting discovery was that the NT shear modulus G in the anterior stroma was independent of location but in the posterior stroma the NT shear modulus was significantly higher in the superior region than central. It might be due the higher stresses induced by upper eyelid, which would lead to stiffening effect [66].

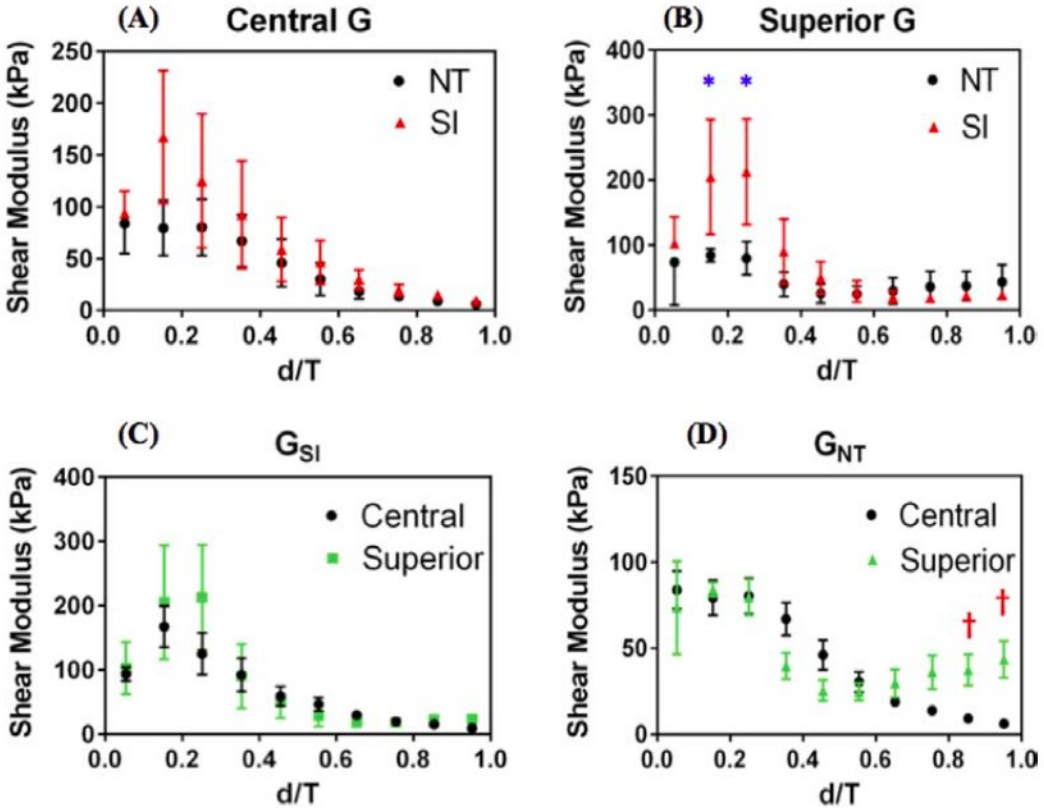

Figure 22. Shear moduli vs. fractional cornea depth [66]

Eilaghi et al [72] studied the mechanical properties of the sclera by biaxial testing. They measured 10 eyes of 5 human donors. The average age of donor was 55.4 years. They measured 6 x 6 mm samples of each quadrant of the sclera, the longitudal and latitudinal stress strain data was obtained to determine the Young's modulus in two directions. Results showed the sclera to be nearly isotropic, with longitudal and latitudinal Young's moduli of 2.8±1.9 MPa and 2.9±2.0 MPa, respectively. There were no statistically significant correlation between sample thickness and stiffness.

Seiler et al [37]studied the effect of Bowman's membrane to the overall mechanical stability of the cornea. With uniaxial stress strain analysis they found out that the corneas with Bowman's membrane intact had 4.75 % higher stress-strain ratio than the corneas without the Bowman's membrane, though the experimental error was about ±10 %. That shows that the Bowman's membrane's effect on the stress-strain ratio is higher than the proportion of the thickness of the overall cornea, i.e. the Young's modulus in the Bowman's membrane is higher than average Young's modulus of the cornea.

Elsheikh et al [73] studied the mechanical properties and thickness variation of the sclera from 36 donors aged 52-96 years. Uniaxial measurements were made for strip specimens. Average scleral thickness was 1062 μm at the posterior pole, 716 μm 18-20 mm away from the posterior pole and 767 μm at the limbal edge. They found larger differences in the elastic moduli in different directions than Eilaghi et al[72]. The tangential Young's modulus increased from posterior sclera to near limbus, with high strain rates the differences between different areas decreased. Viscoelasticity showed 30 % to 39 % increase in tangential Young's modulus with strain rate rise from 8 % to 200 %. Tangential Young's modulus for anterior scleral specimen was 14.4 MPa with a small strain.

Another study made by Elsheikh et al [52] measured the corneal anisotropy in porcine and human corneas. They found that for porcine cornea the best fit was achieved with an exponential function, equation 17.

$$\sigma = \mathrm{A}(e^{B\varepsilon} - 1) \tag{17}$$

Where σ and ε are the stress and the strain, respectively, and A and B are constants. Figure 23 shows the stress-strain behavior for multiple orientations in human cornea. With small strains the stiffness is similar with the nasal-temporal, superior-inferior and diagonal samples but as the strain gets higher the differences are more visible. From a small number of human donor corneas the superior-inferior stiffness was measured to be 20 % and 49 % higher than the nasal-temporal and diagonal samples, respectively. It was mentioned that the numerical values should be used cautiously since the number of samples was small. [52]

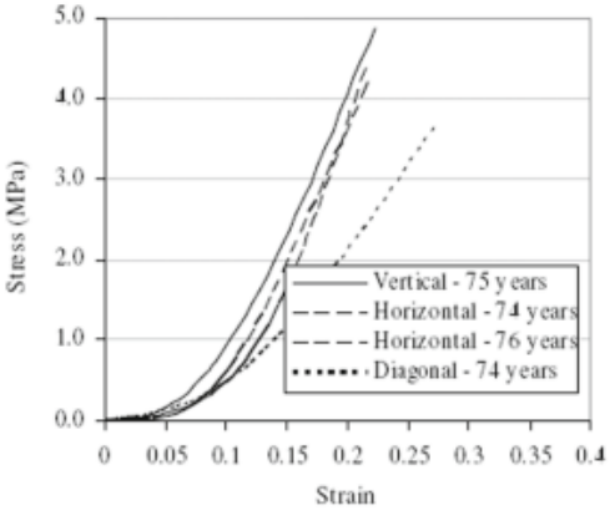

Figure 23. Human cornea stress-strain behavior [52]

Table 4 shows the different measurements of Young's modulus E and axial shear modulus G of cornea in different orientations and locations and the method used in the measurement.

Table 4. Mechanical properties of cornea and sclera

Layer		**Young's Modulus (E)**	**Shear modulus (G), A** axial, **T** transverse	**Method**	
				E	**G**
Anterior basement		7.5 ± 4.2 kPa [33]		AFM	
Bowman's		109.8±13.2 kPa [33]		AFM	
Stroma	Anterior	1.1 – 2.6 MPa [36]	**A** 7.71± 6.3 kPa [48]	AFM	TR
		33.1±6.1 kPa [33]	T 50-240 kPa [66]	AFM	SS
		1.39±0.28 kPa [74]		ARF	
	Central		**A** 1.99±0.5 kPa [48]		TR
			T 20-70 kPa [66]		SS
	Posterior	0.71±0.21 kPa [74]	**A** 1.31±1.0 kPa [48]	ARF	TR
			T 10 kPa [66]		SS
Descemet's		50±17.8 kPa [33]		AFM	
		0.5 MPa [68]		PL	
Whole cornea	Nasal-temporal	3 MPa [51]		PE	
		1 MPa [27]		N/A	
	Superior-inferior	8.6 MPa [54]		PL	
		1.1 MPa [51]		PE	
		3 MPa [27]		N/A	
	Circumferential	13 MPa [27]		N/A	
	Diagonal	0.4 MPa [51]		PE	
	Direction not mentioned	0.5 – 57 MPa [36]	38.7±8.6 kPa [27]	N/A	
		5.3±1.1 MPa [75]	**A** 1.8±0.4 MPa [75]	USS	USS
		2.0±1.0 MPa [75]	**A** 6.8±3.4 MPa [75]	USD	USD
		0.47±0.03 MPa [70]	**T** 9.38± 2.9 kPa [48]	RS	TR
		0.27-0.52 MPa [71]		RS	
		$3.2*10^{-3}y+0.2$ MPa [71]		RS	
		3.81±0.4 MPa [73]		UA	
Sclera	Meridional	2.9±2.0 MPa [72]		BA	
	Circumferential	2.8±1.9 MPa [72]		BA	
		14.44±2.51 MPa [73]		UA	

Table 5. Methods used for measuring mechanical properties of cornea and sclera

Abbreviation	**Explanation**
AFM	Atomic force microscopy [33, 36, 69]
ARF	Acoustic radiation force elastic microscopy [74]
BA	Biaxial mechanical testing [72]
N/A	Not available [27]
PE	Piezoelectric coefficient method [51]
PL	Pressure loading [54] & [68]
RS	Radial shearing speckle interferometer [70, 71]
SS	Shear strain measurement from displacement tracking [66]
TR	Torsional rheometry [48]
UA	Uniaxial stress strain measurement [73]
USD	Ultrasonic technique in dextran solution [75]
USS	Ultrasonic technique in saline solution [75]

Since the variation of the measurements is so large it is not possible to create a reliable model out of the direct numerical values. Instead comparing values measured in similar methods can be an effective way to create a consistent model.

2.7 Effects of the corneal surgeries

PRK only consumes the anterior layers of the cornea leaving larger part of the posterior layers untouched than other techniques. The epithelium is removed in the procedure and it takes time to regenerate, making the overall recovery and recovery of vision slower than other techniques.

The lamellae in the LASIK flaps do not adhere to the stroma, which makes it possible to have a corrective procedure afterwards without creating a new flap. The mechanical benefits of the Bowman's membrane and part of anterior stroma are lost since the mechanical stresses are not transmitted from the rest of the cornea to the flap.

The SMILE cap has a small opening (2 – 3 mm) where the lenticule can be removed. Otherwise the Bowman's membrane and anterior stroma remain intact. The area where the lenticule is created does not remain adhered, similarly as with LASIK flap but the cap diameter can be smaller than the LASIK flap diameter. The stresses are distributed with the remaining stroma and the cap, though there is a small difference in the arch lengths of the cap and stroma, leading to larger strains in the residual stroma than the cap.

After removing the lenticule the arc length of the anterior cap is longer than the profound stromal pocket [76]. It might affect the biomechanical response after SMILE since the tensile stress of the cornea is affecting the stromal cornea before the anterior cap. That is for the myopic procedures. For hyperopic procedures the profound stromal pocket arc length would be longer than the anterior cap length, assuming that the refractive correction is made to the stromal pocket and the cap thickness is uniform throughout the area. The hyperopic SMILE procedures are not commercially available at the moment.

Arc length of a circle can be determined using equation 18 to calculate the angle θ and with equation 19 to calculate the arc length.

$$\theta = \sin^{-1}\frac{C}{2r} \tag{18}$$

$$S = \frac{\theta}{2\pi} * 2\pi * r = \theta * r \tag{19}$$

Where C is the width of ablation area and r is radius of arc. Assuming that the ablation is an arc of a circle the radius of the ablation sphere can be calculated using equation 20, where x is the ablation depth and y is the optical zone of the ablation.

$$r = \frac{y^2}{8x} + \frac{x}{2} \tag{20}$$

With equations 18 19 & 20 the arc length of the ablation profile can be calculated, optical zone is then subtracted from the arch length of the ablation and that gives the difference of arc length of the ablated area from the arc length of the anterior cap at the same area. When subtracting the arch length of the anterior cap of the optical zone from the total arc length of the anterior cap and adding the arc length of the ablated area, it gives the arc length of the stromal pocket. Comparing that to the arc length of the anterior cap, it gives the total difference of the arc lengths of stromal pocket and anterior cap.

With optical zone of 6.5 mm, corneal radius 7.77 mm, lenticule thickness 100 μm (~5.5 diopters of refractive correction) and cap thickness 130 μm, the difference between the arc length of the cap and posterior stroma in the optical zone is approximately 0.06% and less when the total cap length is considered.

3 Finite element analysis of biomechanical properties of the cornea

Section 2.6 reviewed the current knowledge of the biomechanical properties of the human cornea, based on that information Section 3.2 defines the material properties on which the finite element model is built on. Section 3.1 reviews the previous research made by using finite element analysis. Section 3.3 provides a detailed description of each step in the finite element analysis of the human cornea and validation for the material properties and boundary conditions in the analysis.

3.1 Previous FEM models

Studer et al [39, 50, 77], Whitford et al [78], Sinha Roy et al [35, 79] Pandolfi et al [13, 80]and Ariza-Gracia et al [81, 82] have created models of the human cornea using finite element method. The models are based on the collagen distribution and orientation in the cornea. The models, except the one by Sinha Roy et al, do not consider the different layers or the depth-dependent properties of the cornea and since the anterior one third of the stroma has a higher resistance to deformation than the posterior two thirds combined, the stress distribution is not accurate. Also the lack of Bowman's membrane, which is the stiffest layer of the cornea, in the models affects the stress distribution. The models are non-linear i.e. hyperelastic, meaning that the non-linearity of the stress-strain curve is considered, but the viscoelasticity is not taken into account. That leads to underestimation of the resistance of deformation since the stress distribution is thought to remain the same after the modification to the cornea. The viscous flow occurs in the cornea and when considering the refractive surgery, the distribution of Von Mises stresses is smoother than the hyperelastic model predicts.

Sinha Roy et al also made an anisotropic, hyperelastic model that do not consider the viscous flow. In contrary to the models by Studer et al the depth-dependent mechanical properties of the stroma was considered. The depth-dependent properties were based on measurements of Randleman et al [55] and approximation of Reinstein et al [56]. The depth-dependent material properties were derived from the out of plane distribution of collagen fibrils and the model, which is discussed in the following section, only considers the collagen fibrils parallel to the surface. The Bowman's layer was also left out of the simulations. In the simulations that compared the Von Mises stresses in LASIK and SMILE procedures, the simulations were made with equal flap and cap thicknesses, which are not usually used in the clinical environment.

3.2 Determining the material properties of the model

In the central anterior region of the stroma 89% of the collagen fibrils are isotropically oriented, toward the posterior central region 58% are isotropically arranged, leaving 42% preferentially arranged to nasal-temporal and superior-inferior directions, 21% each [44]. Outside the central area the preferred collagen fibril orientation changes to circumferential. Abahussin et al [44] hypothesized that the higher stiffness of nasal-temporal and superior-inferior strips compared to diagonal strips of the cornea is a result of the orientation of the lamellae in the posterior stroma. Numerical data of preferential alignment in the periphery was not found. Since the main load carrying structures in the cornea are the lamellae, composed of collagen fibrils, the model itself is mainly based on the orientation and mechanical

properties of collagen fibrils, which will be discussed more thoroughly in the following sections.

Intertwining, branching and anastomosis varies through the depth of the cornea affecting the mechanical properties, also the size and form of the lamellae changes in different depths. The effect of intertwining, branching and anastomosis to the mechanical properties of the cornea is unclear in terms of numerical values.

No study was found where all the layers and directions were considered. To build a model based on the mechanical measurements, it is needed to combine the relative differences of different layers and orientations to get an estimation of all the layers and orientations. Since the stress strain curve of the cornea is most accurately represented with an exponential function, equation 17, the different measurements of Young's modulus, where the stresses are not equal, are not comparable.

As mentioned before, Young's modulus does not represent the nonlinear materials accurately, especially when it is not known whether the measured Young's modulus is tangential or secant, presumably when the type is not mentioned the secant Young's modulus is measured. Since most of the research measures the Young's modulus, the relative differences in Young's moduli are assumed to apply to the relative differences in non-linear stress-strain curves as well.

Table 6 shows the relative stiffness's of different layers and orientations, assuming that the Young's modulus is directly proportional to the shear modulus of the material. Superior-inferior (SI) direction was chosen to be the principal direction, meaning that the stiffness of all layers equals the stiffness of superior-inferior direction. The differences of the stiffness's between NT and ST directions are significant and the measurements showed variation of amount of collagen fibrils in those directions, thus it is reasonable to simplify the model by assuming the stiffness in both directions as equal. Assumption of equal stiffness in both NT and SI directions simplifies the modeling as will be seen in the following sections.

In Table 6 the relative stiffness's are averaged if multiple studies have measured the same layers, and since Sloan et al [66] was the only one to measure the depth- and direction-dependent properties the differences of anterior, central and posterior stroma was averaged over nasal-temporal and superior-inferior directions, the directional information was not used, since no experiments including all the layers were not made.

Table 6. Relative stiffness of different layers and orientations

Layer/orientation of cornea	Relative stiffness compared to anterior stroma	Sources
Anterior basement	23 %	[69]
Bowman's membrane	332 %	[69]
Anterior stroma	100 %	[48, 66, 69]
Central stroma	39 %	[48, 66]
Posterior stroma	11 %	[48, 66]
Descemet's membrane	151 %	[69]
All layers	123 %	[48]
Nasal-temporal direction	219 %	[51, 52]
Superior-inferior direction	123 %	[51, 52, 54]
Circumferential direction	115 %	[54]
Diagonal	64 %	[51, 52]

Figure 24 shows the relative Young's moduli from Table 6 in different layers of the cornea and the layers combined, excluding epithelium and endothelium. Anterior basement membrane and non-collagenous epithelium and endothelium are disregarded due to minimal overall effect on the mechanical properties of the cornea. Stroma is mainly responsible of the overall stability of the cornea but the Bowman's and Descemet's membranes are significantly stiffer than the adjacent stromal layers.

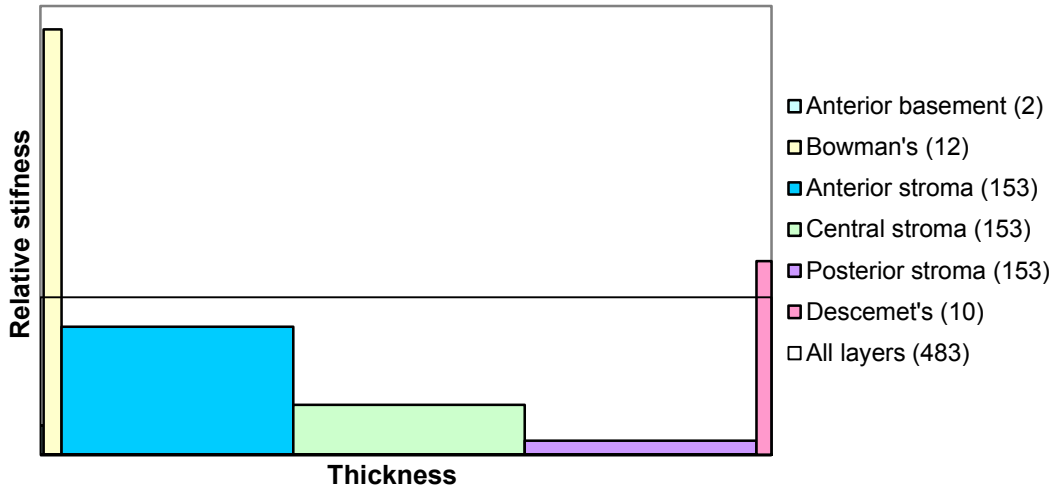

Figure 24. Corneal layer thickness vs. relative stiffness. When all the layers are intact the relative stiffness is higher than what would be if the layers were separated.

3.3 Creating the 3D model of the cornea

Instead of using actual measured corneal topography, a simplified model is created to eliminate the irregularities of the cornea. It is assumed that both the anterior and posterior surfaces are spherical, with a minimum thickness at the vertex. The model is rotationally symmetric in respect to the z-axis, nasal-temporal and superior-inferior dimensions are considered equal, since in most cases the refractive surgeries are made in circular area. Astigmatism corrections with excimer lasers ablate in elliptical surface but the flap or epithelial surface ablation is usually circular.

It is possible to use the conicoid surface (equation 1) from Liou-Brennan model or fitting suitable curves to a cross-sectional photo of a cornea and use a revolve-tool in the modeling program to create the model. In this case, since only the biomechanics are considered, the corneal surfaces are assumed to be spherical.

Pandolfi and Holzapfel [80] proposed a method to evaluate the stress free configuration of the human eye, which Elsheikh et al [83] used in their research to create a stress free model of the human eye. For that model, the first step is to create a stress free model of measured properties of the eye, after that the intraocular pressure (IOP) is applied, to see the deformed state of the eye and when the deformation is subtracted from the original configuration, it gives the stress free configuration. When the IOP is applied again it gives the approximately the physiological shape of the cornea with the load applied. After 8 iterations the model had good accuracy.

Combining the information from the x-ray diffraction studies and the electron microscopy studies, about the collagen fibril orientation and lamellar structure with the mechanical measurements, gives estimation about the typical corneal behavior of +60 year-old corneas.

From *en face* view the cornea can be divided to three concentric regions: central, paracentral and peripheral. Central region has the orthogonal arrangement of collagen fibrils with majority still randomly oriented, nasal-temporal and superior-inferior meridians are stiffer compared to diagonal. Peripheral region has circumferential arrangement of collagen, which leads to stiffer response in circumferential stresses than other directions. Paracentral region is a transition zone from orthogonal arrangement to circumferential arrangement. Refractive surgery is assumed to affect only the central and paracentral region.

Cross-sectional structure of the cornea from the anterior to the posterior surface is epithelium, anterior basement membrane, Bowman's membrane, stroma, Descemet's membrane and endothelium. Epithelium and endothelium can be disregarded from the mechanical modeling but the thickness of the epithelium must be considered when estimating the thickness of flap or cap. Anterior basement membrane is thin and has small Young's modulus compared to profound layers, thus the effect to mechanical properties is small. Bowman's membrane is the stiffest layer of the cornea but thin compared to the stroma, the collagen fibrils are randomly oriented radially, but parallel to the anterior surface.

The stroma is the thickest part of the cornea and the structure transforms through the thickness. Anterior stroma is mostly consisted of randomly oriented collagen fibrils, with only 11 % orthogonally. The lamellae are highly interwoven, flat, thin and tape-like structures. Toward the posterior regions the number of interconnections of lamellae decrease exponentially and the collagen fibrils are more orthogonally arranged, in posterior region approximately 42 % of collagen fibrils are oriented in nasal-temporal or superior-inferior directions. The structures of lamellae change to thicker and wider, a more broadsheet-like structure. The stiffness decreases through depth, it is not known if the decrease is linear, exponential or what kind of curve it follows. The intact stroma is stronger than the sum of its parts, which might be the result of the interconnections at different depths.

Descemet's membrane is stiffer than posterior stroma but also thin. The collagen fibrils are randomly oriented and the structure is similar to Bowman's membrane.

Collagen fibrils in rest are in crimped state. When the stress, in this case intraocular pressure (IOP), is applied collagen fibrils start to extend. In physiological state the proportion of crimped collagen fibrils follow the Gaussian curve where the peak is at slightly extended fibrils. There are always fully extended and fully crimped collagen fibrils while most remain in slightly extended state. When the applied force is increased the peak of the curve moves toward the fully extended state, while the proportion of fully crimped fibrils decreases. When the proportion of fully extended fibrils increase, the needed stress to extend the tissue increases, which might explain the exponential stress-strain curve of mechanical measurements. On the other hand, when the fully extended fibrils continue to extend, some individual fibrils break, leading to irreversible deformation of the tissue.

3.3.1 FEM modeling in Abaqus CAE 6.13-3

Units

Abaqus does not have a built in system of units. The user has to be consistent with the units when creating the model. In this thesis the unit of length is chosen to be in millimeters (mm). Table 7 shows the system of units chosen for this thesis.

Table 7. System of units

Length	mm
Force	N
Mass	tonne (10^3 kg)
Time	s
Stress	MPa
Energy	mJ
Density	tonne/mm^3
Young's modulus	MPa

To determine the suitable material properties, few simple models were created. First a model that simulates the strip extensometry was created. The model was a 3 mm wide and 11 mm long corneal strip that had varying thickness from the central 540 μm to peripheral 791 μm. A second model was made to simulate the inflation tests made to corneas.

Part

The mechanical testing made of cornea is usually strip extensometry, where strains from different stresses are measured, or inflation tests where the apical rise is measured for different intraocular pressures. In this thesis the two types of tests are simulated to verify the material properties that determined later in this section. The model cornea used in this thesis has the following geometrical properties: anterior radius 7.7 mm, posterior radius 6.4 mm, central thickness 540 μm, peripheral thickness 791 μm and width 11 mm. In addition a horizontal transition zone is included in the model for better control of boundary conditions and stresses. Figure 25 shows the parts for both extensometry and inflation simulations, the part for extensometry is a 1.5 mm wide strip cut from the part of inflation test. With boundary conditions the simulations are of 3 mm wide strip cut for extensometry and whole cornea for inflation test.

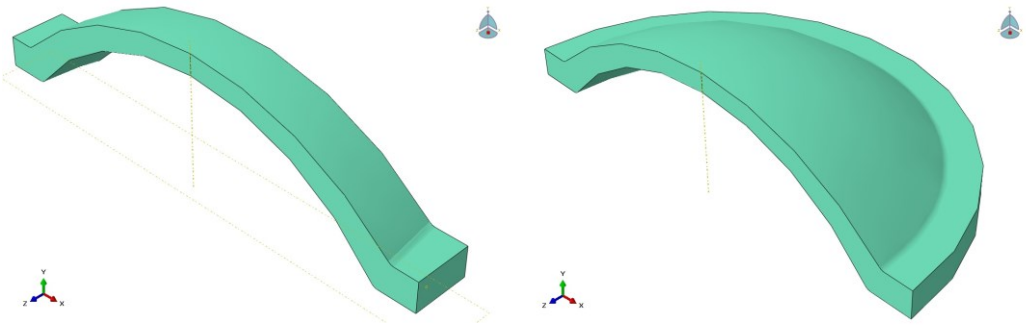

Figure 25. Parts for simulating extensometry and inflation tests

In Abaqus a part is first created from a sketch, with previous geometrical properties, that is revolved 180° to create half a cornea. The remaining face is then partitioned to divide the cornea to different layers, from anterior surface to posterior surface: epithelium, Bowman's membrane, anterior stroma, central stroma, posterior stroma and Descemet's membrane. After that the stroma is divided to central and peripheral regions at 4 mm from the apex.

Meshing

Meshing is done by manually assigning seeds to different sections for suitable amount of elements.

Boundary conditions

In extensometry simulation, the other end is encastred to represent the clamp in the other end and other end is locked in y- and z-directions to enable the pull to affect along the x-axis. The face along the x-, y-plane is assigned to act symmetrical along the z-axis, so the actual simulation represents actually a 3 mm wide strip cut.

In inflation simulation the face of the transition zone is encastred to represent the clamping of the sample and the face along the x-, y-plane is assigned to be symmetrical along the z-axis to simulate the circular corneal sample instead of half a circle.

Material properties

All the models were first tested with a uniform elastic material, to identify errors caused by the boundary conditions, meshing and forces affecting the model. When the simulation of a linear elastic model was consistent, the material properties were changed to hyperelastic. Anterior stroma was the first one to be defined. Using equation 17, an artificial test data was created to approximate the nonlinear stress-strain relationship of the cornea.

A hyperelastic isotropic material based on only one set of test data, uniaxial, was created. Since only uniaxial data was available the strain energy potential was chosen to be the Marlow form. In strip extensometry, the Marlow form showed consistent behavior, though when the strip extensometry was fitted to the experimental measurements the inflation test showed significantly stiffer response compared to the experimental measurements. For example the Neo Hooke form, without other test data, resulted in linear apical rise in inflation tests, and for Marlow form it was nonlinear.

Following the hyperelastic isotropic material properties, a hyperelastic anisotropic material properties were created using the Gasser-Ogden-Holzapfel

(GOH) [84] model to estimate the cornea with distributed collagen fibril orientation.

Gasser-Ogden-Holzapfel model

The GOH model was developed for modeling the arterial layers with distributed collagen fiber orientations [84]. Later on the model have been used for other collagenous soft tissues such as skin [85] and cornea [35, 79, 81, 82]. The model is suitable for incompressible solids with two preferred directions along the unit vectors a_1 and a_2 [85]. The strain energy density function Ψ is described in equation 21.

$$\Psi = \Psi(\mathrm{C}, H_1, H_2) \tag{21}$$

where C is the right Cauchy-Green strain tensor and H_1 and H_2 are structure tensors. Ψ depends on equation 22 as follows

$$\Psi = \frac{\mu}{2}(I_1 - 3) + \mu \sum_{i=1,2} \frac{k_{i1}}{2k_{i2}} \left\{ e^{k_{i2}[tr(H_i C)-1]^2} \right\} \tag{22}$$

where I_1 is a strain invariant and μ, k_{i1} and k_{i2} are material constants. μ would be the shear modulus (G) of the material without the fibers. k_{i1} and k_{i2} are material constants for the fibers in small and large strains, respectively. The dispersion of the fibers in GOH model is taken into account with a dispersion parameter κ ($0 \leq \kappa \leq$ ⅓) that describes the degree of anisotropy, 0 representing ideally aligned fibers and ⅓ representing isotropy. κ is determined from numerical integration of equation 23

$$\kappa = \frac{1}{4} \int_0^{\pi} \rho(\Theta) sin^3\Theta \, d\Theta \tag{23}$$

where ρ(Θ) is a density function from normalized π-periodic Von Mises Distribution. Figure 26 shows the von Mises distribution of collagen fibers with different values of κ.

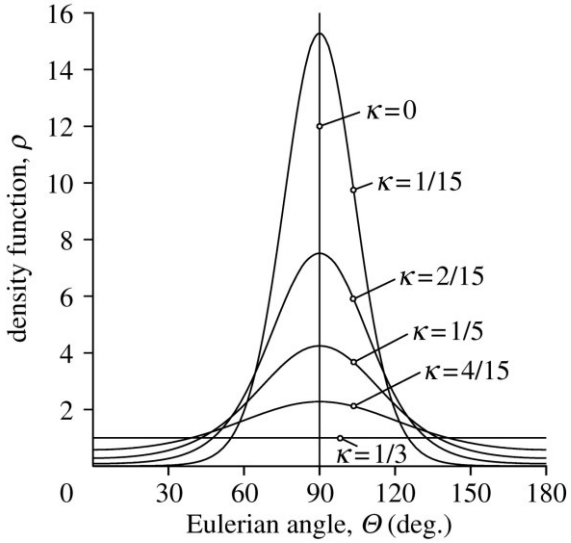

Figure 26. Von Mises distribution of collagen fibers with different values of the dispersion parameter κ [84].

The previous equations 21 to 23 are from Annaidh et al [85], more detailed description of GOH model can be found from [35, 79, 81, 82, 84-86]. The model

assumes that the fibers do not support compression and would buckle under compression [84].

In Abaqus the material parameters needed, for the hyperelastic, anisotropic material with Holzapfel strain energy potential, are *number of local directions*, C10, D, k_1, k_2 and κ. Number of local directions is set to 2 to create a model of two families of fibers in right angle parallel to the surface. $C10 = \mu/2$, $k1 = k_1\mu$, $k2 = k_2$ and $0 \leq \kappa \leq ⅓$ [85] D is the compressibility parameter where D = 0 represents incompressibility [81]. C10 and k1 are parameters related to the linear elastic properties of the material, which mainly affects in low strains and k2 is a stiffening parameter that mainly contributes at higher strains [85].

Finding good estimations for different parameters can be difficult since the experimental results show significant variation and no single research has assessed all the properties that are used in this modeling, which makes it extremely difficult to derive all the parameters directly from the experimental research. Other important issue is the dispersion parameter κ, which has a high effect on the strip extensometry simulations. The fibers only work under extension and in the model the fibers that are not parallel to the direction of the extension do not fully contribute to the stiffness until they are parallel to the direction of extension. The lower dispersion factor κ the stiffer the material appears to be to the direction of the preferentially oriented fibers. To compensate the effect of changes in κ, the stiffening parameter k2 can be decreased. The smaller stiffening parameter in the posterior stroma is consistent with the assumption that the intertwining and number of crosslinks between the collagen fibrils decreases through the depth of the stroma. Also the width and thickness of the lamellae in the anterior stroma is smaller than in the posterior stroma. Combination of lamellar structure, intertwining and collagen crosslinks may explain the depth-dependent mechanical properties of the cornea.

The material parameters were tested also in a model of 1 mm x 1 mm x 1 mm cube where the stress-strain curve can be determined for comparison of the experiments made by Elsheikh et al [52, 87]. The experimental stress-strain curve is assumed to be of engineering stress instead of true stress.

Pandolfi et al [80], Ariza-Gracia et al [81] and Lanchares et al [88] provided their parameters of the FEM model utilizing the Holzapfel strain energy potential. Table 8 shows the material parameters by Pandolfi et al and Ariza-Gracia et al. The material parameters have a high variation, up to 4 orders of magnitude. The parameters from Ariza-Gracia et al and Lanchares et al have been derived from experimental research using non-linear regression analysis and the parameters from Pandolfi et al have been determined through trial and error to fit the experimental data.

Table 8. Material parameters for the Holzapfel strain energy potential

	C10 (MPa)	D (MPa^{-1})	k1 (MPa)	k2 (-)	κ (-)
Pandolfi et al	0.06	-	0.02	400	0.1333
Ariza-Gracia et al	0.05	0.0	130.9	2490	0.33329
Lanchares et al	0.1	1e-5	0.234	29.917	-

The parameters used in this thesis are not derived from the experimental research directly but modified from the previous FEM models to fit the expected stress-strain curves. The problem with the trial and error method and regression

analysis from only one source, is that optimizing multiple parameters to one type of experiment increases the possibility to finding a local minimum, where the parameters fit to a certain type of experiment but not multiple [50].

The dispersion parameter κ in the Ariza-Gracia et al model signifies nearly isotropic distribution of collagen fibers and in the Pandolfi et al model that 60% of the fibers are aligned in the preferential (nasal-temporal and superior-inferior) directions and 40% isotropically.

To examine previous parameters the 1 x 1 x 1 mm cube was assigned with previous material parameters and extended by applying a 1 MPa surface traction. The simulation gives directly the stress-strain curve when the step time period is 1 s and the undeformed area defines the surface traction during the simulation i.e. the engineering stress is measured. Figure 27 shows the initial and deformed state of the simulation with the material parameters from Ariza-Gracia et al.

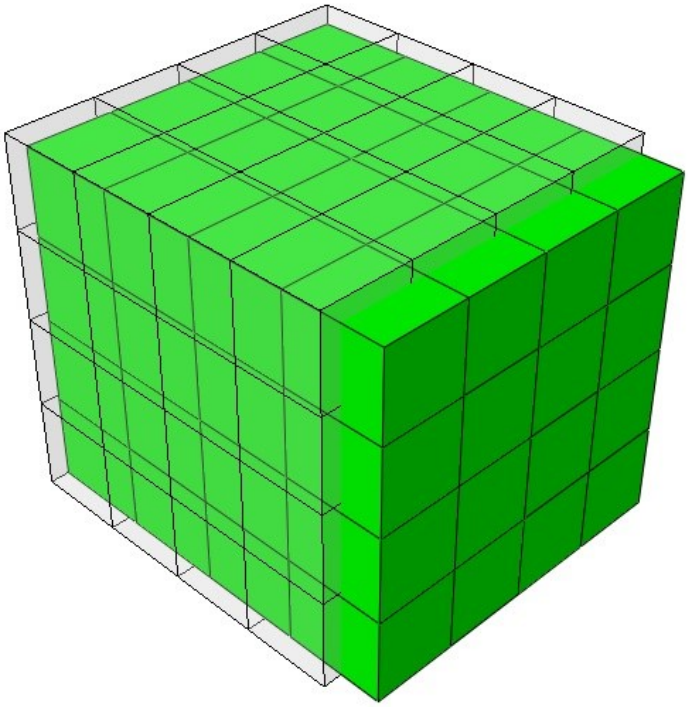

Figure 27. Initial and deformed state of the 1x1x1 mm simulation

Figure 28 shows the simulated stress-strain curves of the cornea where the material parameters are from [80, 81] with assumed superior-inferior (SI) and diagonal (D) samples. The simulations with the material parameters from Lanchares et al were left out from the graph due to strain levels of almost twice as large as diagonal from Pandolfi et al.

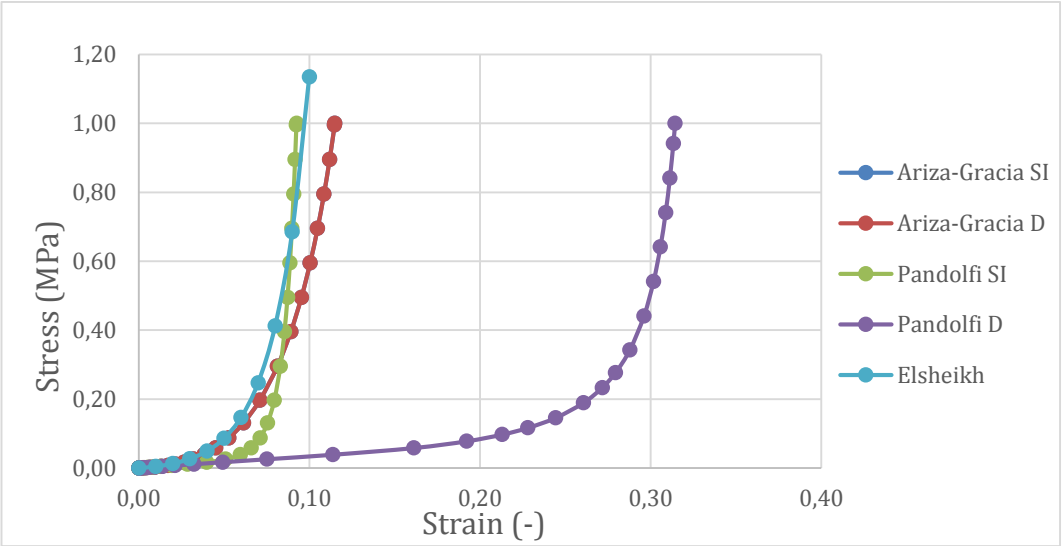

Figure 28. Stress-strain curves with different material parameters and orientations. SI simulates superior-inferior sample and D diagonal, Elsheikh is the experimental curve.

The experimental curve from [87] represents superior-inferior sample from 65 – 79 years old donors, fitted to equation 17 with constants A and B, 0.0077 and 59, respectively. The dispersion parameter κ is set to 0.33329 (nearly isotropic distribution) in the Ariza-Gracia model [81] that leads to equal stress-strain curve for diagonal and superior-inferior simulations. The difference in superior-inferior and diagonal simulations with the material parameters from Pandolfi et al [80] is significantly higher than expected.

As can be seen from Figure 28 neither of the models is not directly suitable for extensometry simulations. The stress-strain curve with material parameters from Ariza-Gracia et al is relatively close to the experimental results from Elsheikh et al.

The relative differences of the stiffness of layers and orientations, Table 6, are derived of series of experimental mechanical testing where the Young's modulus E or shear modulus G is determined. For nonlinear material the two moduli do not tell much about the overall response of stresses in a material. Since the current data is limited to the relative differences, in this thesis, they are assumed to apply to stresses that create a 10% strain level in the material. For extensometry simulations the 10% strain level is relatively high but not too close to the ultimate tensile strength of the cornea. In the model by Studer et al [50] at 12 % strain level the differences in superior-inferior and diagonal simulations are significant. Elsheikh et al [52] provided relative stiffness's for porcine corneal samples at 10%, 15% and 20% strain levels.

With the trial and error method the first parameters were determined, Table 9, that results to relatively close match with the Elsheikh et al [52], for NT and diagonal samples of 69-70 year old corneas.

Table 9. Initial material parameters

C10 (MPa)	D (MPa^{-1})	k1 (MPa)	k2 (-)	κ (-)
0.05	0.001	30	10	0.294

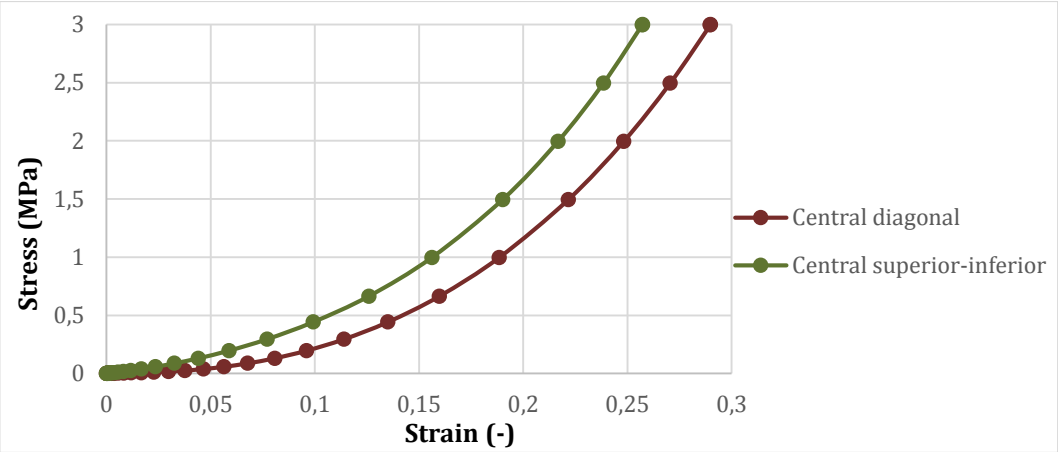

Figure 29. Stress-strain curves of central stroma in superior-inferior and diagonal directions

With material parameters from Table 9 a strip extensometry and inflation tests were made with uniform material parameters i.e. the layers were excluded from the simulations. The extensometry simulation showed too soft response to the stresses compared to the experimental results and inflation test showed too stiff response compared to the experimental results. The uniaxial extensometry is chosen to be the baseline where the material parameters are fitted. Inflation test is then adjusted by changing the pressure instead of the material parameters to create similar curve with only higher pressures than in the experiments.

Studer et al [50] wrote, "*A common problem during the identification of material properties for soft tissues is that the model's reaction is either too soft for bi-axial inflation or too stiff for uniaxial extensiometry experimental data.*" With the previous material parameters the opposite occurred. The extensometry simulation showed too soft response and the inflation simulation too stiff.

Since the extensometry simulations showed milder response to stresses than expected the first parameters were chosen to represent the central stroma. The parameters for different layers were defined by examining the stress-strain curves with different material parameters. The parameters that created the stress-strain curves that match the relative stiffness's of Table 6, were chosen as the material parameters. As previously the relative difference of stiffness is measured at 10% strain level.

Table 10 shows the final material parameters for all the layers of the cornea. Figure 30 shows the stress-strain curves for all the layers of the cornea and the stress strain curves at the diagonal direction for the stromal layers.

Table 10. Material parameters for all the layers of the cornea

Layer	C10 (MPa)	D (MPa^{-1})	k1 (MPa)	k2 (-)	κ (-)
Epithelium	0.05	0.001	1	1	0.33333
Bowman's	3	0.001	500	400	0.33333
Anterior stroma	0.7	0.001	100	30	0.31
Central stroma	0.05	0.001	30	10	0.294
Posterior stroma	0.05	0.001	3	10	0.25
Descemet's	3	0.001	200	400	0.33333

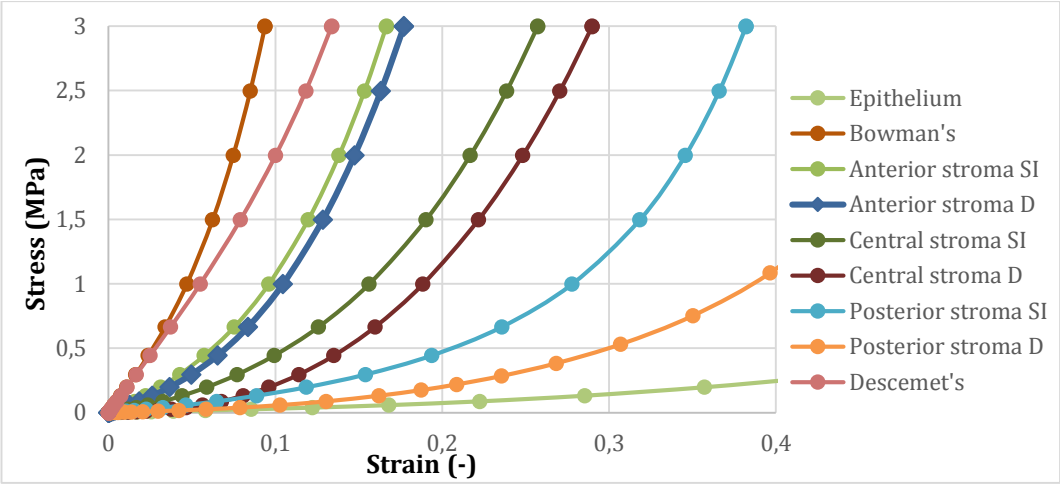

Figure 30. Stress-strain curves for different layers and orientations. SI=superior-inferior, D=diagonal.

Table 11 shows the relative differences of stiffness's for different layers of the cornea at 10% strain level when using the material parameters from Table 10.

Table 11. Relative differences of different layers in the simulations and the relative difference of stiffness in diagonal orientation

Layer	Relative stiffness with 10% strain	Relative stiffness in diagonal orientation	Dispersion parameter κ
Epithelium	-	-	-
Bowman's	280%	*100%*	0.33333
Anterior stroma	100%	*80%*	0.294
Central stroma	39%	*44%*	0.28
Posterior stroma	13%	*37%*	0.25
Descemets	168%	*100%*	0.33333

After the material properties for the layers were identified the two models for inflation and extensometry tests were modified to have all the layers and orientations, Figure 31 Figure 32 and Figure 33 show the top and cross-section views of the models with the preferred orientations. The model for the extensometry simulation is a 1.5 mm wide cut from the model of inflation test. With the boundary condition, that makes the model symmetric along the z-axis, the inflation model is simulating the whole cornea and the extensometry is simulating 3 mm wide strip cut. For the superior-inferior and diagonal extensometry simulations the preferred collagen fiber orientation is turned 45°.

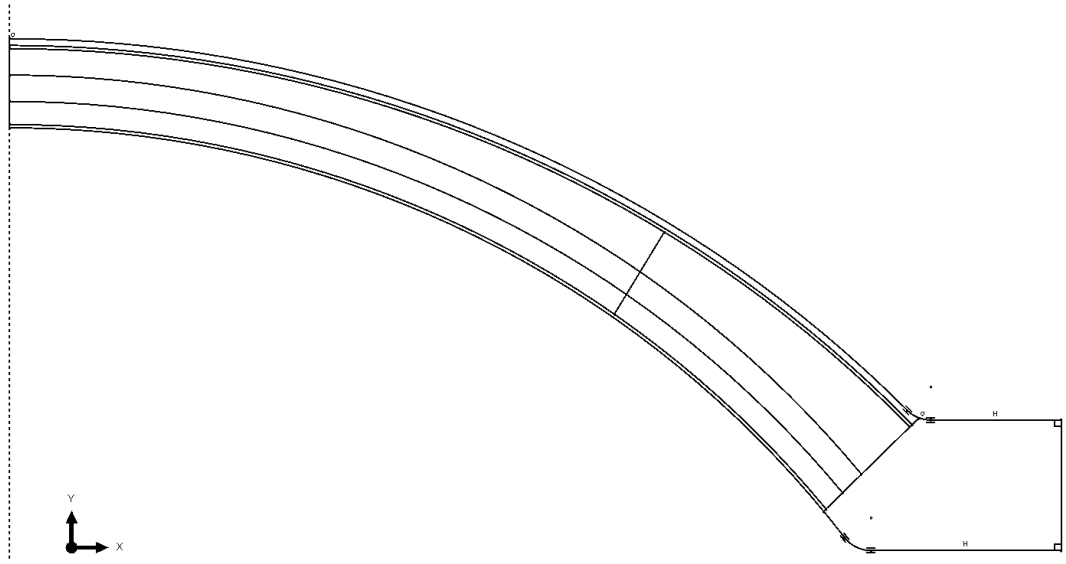

Figure 31. Final sketch with all the layers. The anterior stroma is assumed to be the only layer with increasing thickness towards the periphery.

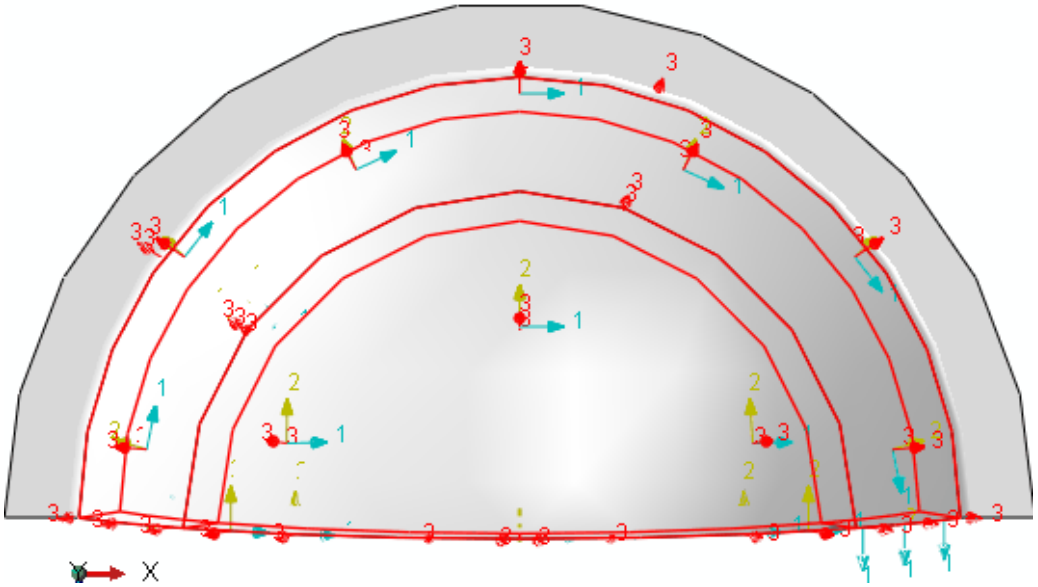

Figure 32. Top view of the model with the preferred orientations of the central and paracentral region of the cornea. The primary axes 1 and 2 are the preferred orientations for the collagen fibrils and axis 3 is normal of the anterior surface.

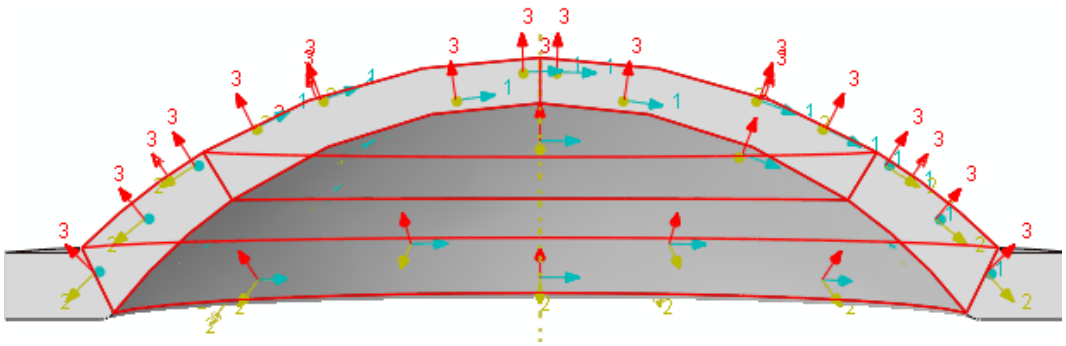

Figure 33. Cross-section view of the model with the orientations of the central and paracentral regions of the cornea.

Figure 34 and Figure 35 show the initial and deformed states of the inflation simulation. In the simulation the apical rise is measured both from the anterior and posterior surfaces. From those measurements the remaining corneal central thickness (CCT) can be determined. The pressure that simulates the intraocular pressure (IOP) is applied to the posterior surface of the model. The model showed stiffer response than expected and to see the differences of the surgical procedures the pressure was chosen to be higher than in actual inflation tests. The intraocular pressure was 2 MPa, which is approximately two orders of magnitudes higher than the pressures used in inflation tests (150 mmHg or 0.02 MPa). Intraocular pressure that rises up to 2 MPa would lead to rupture well before that level is reached.

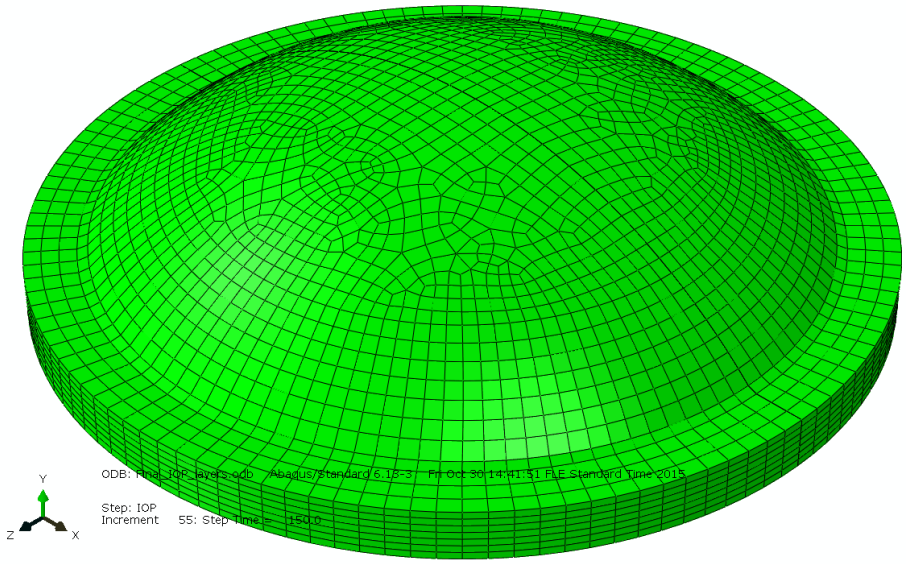

Figure 34. Initial state for the inflation simulation

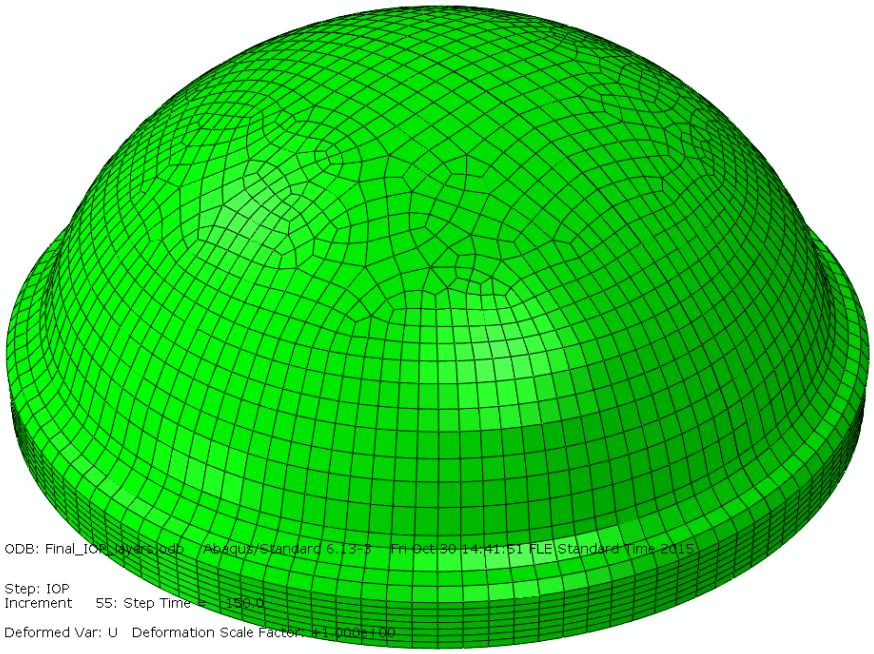

Figure 35. Deformed state in the inflation simulation

Figure 36 and Figure 37 show the initial and deformed states of the extensometry simulations. The surface traction that simulates the extensometry test is applied to the right end surface of the model and the other end is locked to simulate the clamping. The surface traction is defined per unit of undeformed area to maintain equal force throughout the simulation and the rotation is not followed. The surface traction is 0.8426 MPa which is equal to 2 N force along the x-axis.

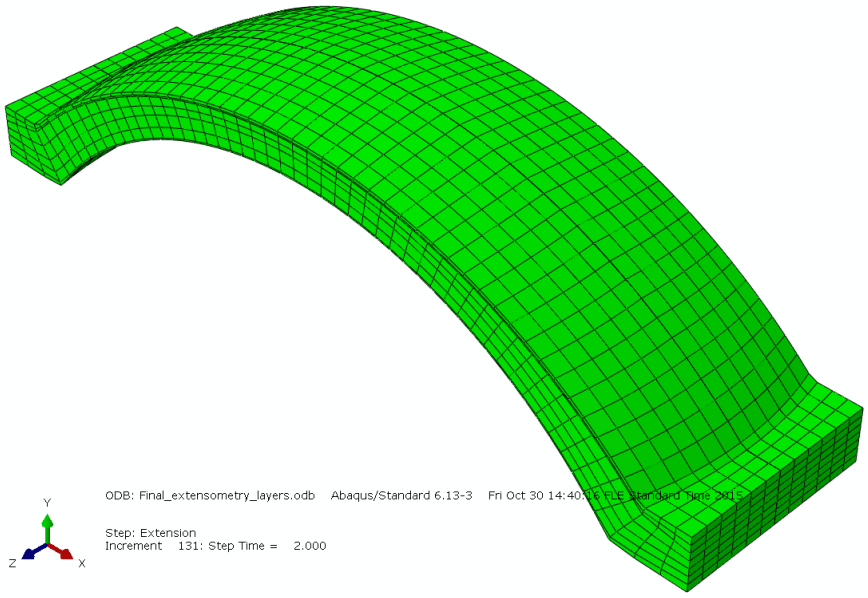

Figure 36. Initial state in the extensometry simulation

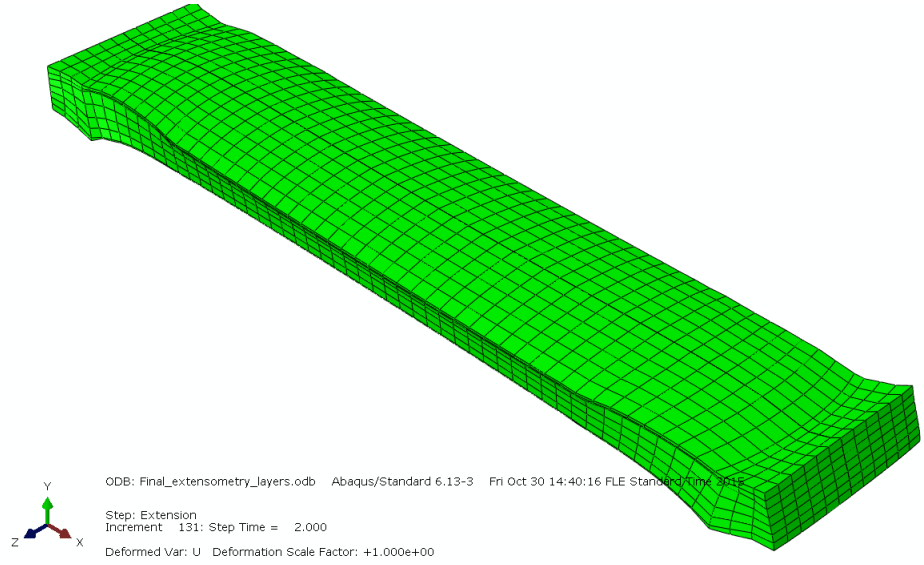

Figure 37. Deformed state in the extensometry simulation

Figure 38 shows the deformed state in extensometry simulation, with different visualization to show the von Mises stresses (MPa) in the model.

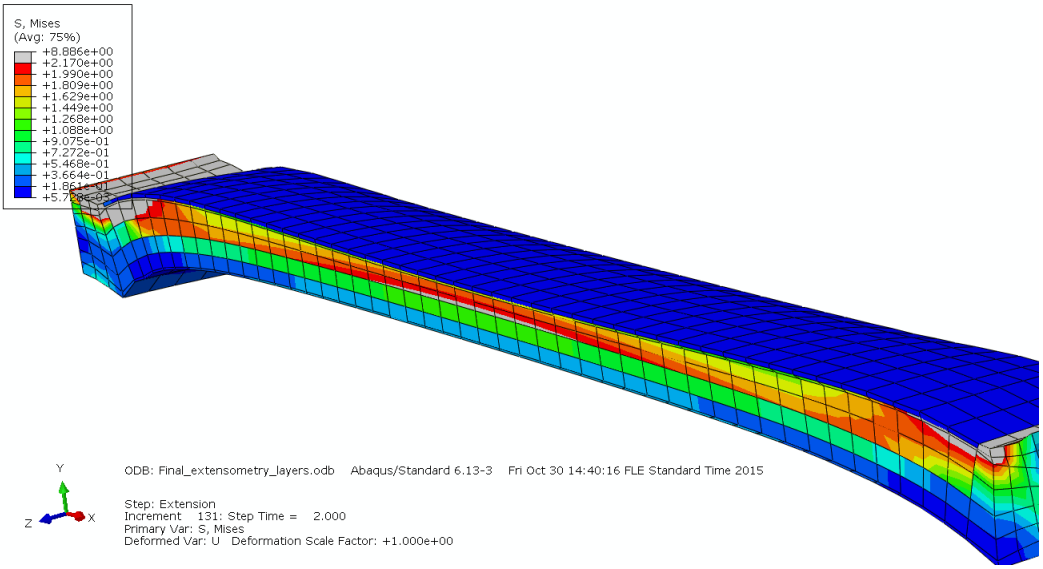

Figure 38. Deformed state in the extensometry simulation. Different colors are representing the von Mises stresses (MPa) in the model. For visualization purposes the Bowman's and Descemet's membranes are assigned to have the material properties of anterior and posterior stroma, respectively.

3.4 Simulation of refractive surgery

In this thesis the two types of refractive surgery techniques for comparison are LASIK and SMILE. The refractive correction was chosen to be a myopic correction with central ablation of 100 µm and optical zone of 6.5 mm. That is equivalent of approximately -7 diopters, according to the Munnerlyn equation, equation 7. Figure 39 shows the profiles of the lenticule in SMILE procedure and ablation + flap in LASIK. For the simulations there is an additional 20 µm (compared to the clinical 15 µm) of removed tissue in SMILE procedure. The flap 100 µm, in LASIK simulations, is removed completely. Two cap thicknesses were chosen for SMILE simulations 140 µm and 200 µm to see the difference in mechanical behavior with removal of tissue from the deeper layers of the stroma. In practice the cap width is larger (7.9 mm) than the optical zone but in this model the cap would not have an effect on the mechanical properties, therefore it was left out of the model. Table 12 shows the dimensions of the tissue removed for the simulations and Figure 39 shows half of the profile of the tissue removed.

Table 12. Properties of the tissue removed in the simulations

	SMILE	**FemtoLASIK**
Cap/flap thickness (µm)	140/200	100
Cap/flap width (mm)	6.5	9
Optical zone (mm)	6.5	6.5
Minimum lenticule/ablation thickness (µm)	20	0
Maximum lenticule/ablation thickness (µm)	120	100

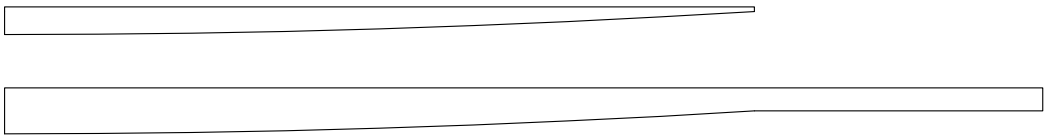

Figure 39. Profiles of the tissue removed in SMILE (above) and LASIK (below)

Figure 40 and Figure 41 show the models for extensometry and inflation tests for LASIK. The flap is completely removed from the simulation since the optical properties are not considered in the simulations and the effect of the flap to the overall properties of the cornea is negligible.

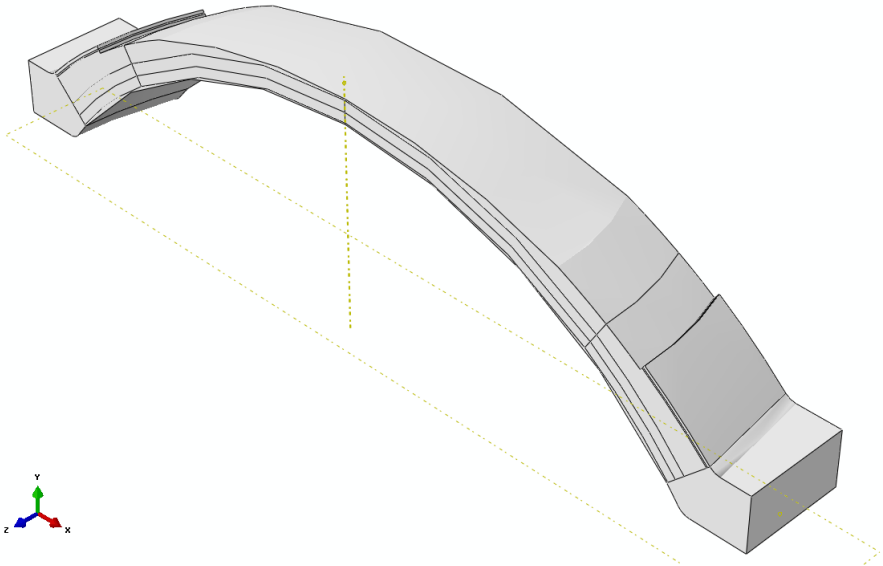

Figure 40. The model for the LASIK extensometry simulation

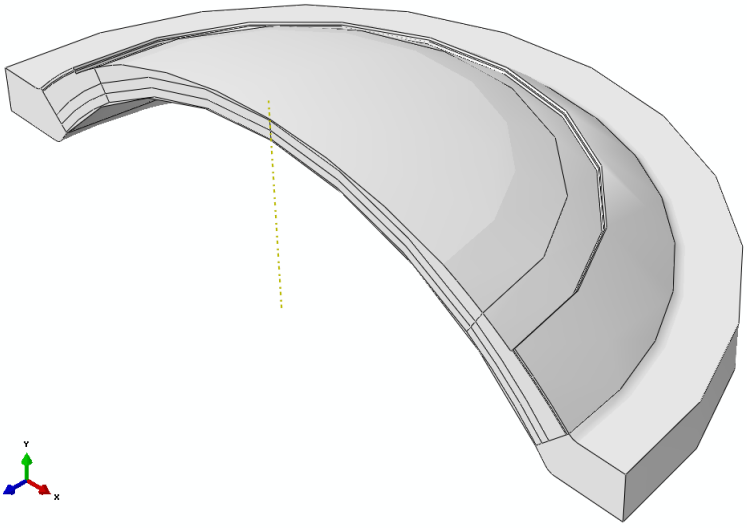

Figure 41. The model for the LASIK Inflation simulation

Figure 42 and Figure 43 show the models for the SMILE extensometry and inflation simulations. The models for SMILE with a thicker cap are otherwise the same but the tissue is removed from more posterior section of the stroma.

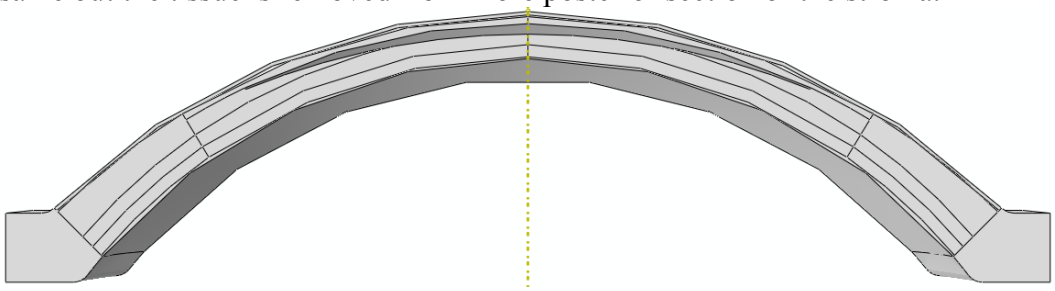

Figure 42. The model for SMILE extensometry simulation

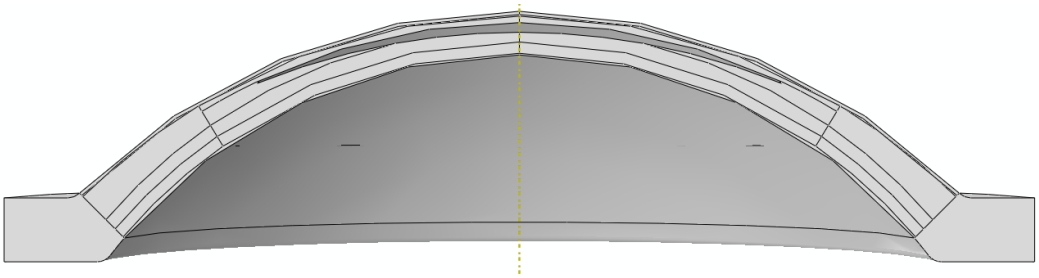

Figure 43. The model for SMILE inflation simulation

4 Results

The theoretical framework for the corneal biomechanics is based on many assumptions and wide range of results for similar mechanical testing. To build a model that considers nonlinearity, anisotropy, viscoelasticity and regional variations, is an extremely difficult task with the current knowledge of corneal biomechanics. For the simulations, in this thesis, the main assumptions are that the Young's and shear moduli are directly proportional, the degree of anisotropy in the cornea is similar in nasal-temporal and superior-inferior directions, anterior layers of the cornea are stiffer than the posterior layers, collagen fibers are the main load carrying structures in the cornea, the epithelium and the flap in the cornea do not contribute to the mechanical behavior of the cornea, and viscoelasticity is negligible in static explicit, non-dynamic simulations. And since the optical properties are not considered in the simulations, the structure of the cornea is a simplified version of its physical counterpart. Initial stresses and strains are not considered i.e. the configuration of the cornea is stress-free and the simulations presents a state where the tissue removal is made at stress-free state and the intraocular pressure is added after the procedure.

When the material properties for different layers and orientations were assigned by trial and error, the complete model would represent the relative response of the cornea accurately but not the cornea in the physiological conditions. That affects the interpretation of the results in a way that the stresses and strains in the model should not be considered as representing the actual values in real corneas but as relative differences in theoretical conditions. The stress free configuration of the cornea is unknown and the stresses and strains, in physiological conditions, cannot be accurately determined with current models and measurements. Instead of giving numerical results when comparing different surgical procedures, broader terms are used to describe the relative differences in the biomechanical properties of the cornea after different types of refractive surgery. Finding the correct material properties, to fit the relative differences, the inflation and extensometry testing, would require either user subroutines in Abaqus, to have more control over the material properties, or almost endless cycle of repetition when trying to fit all the properties with trial and error. In this thesis only one iteration cycle, of all the layers and orientations, was performed.

Following section describes briefly the results of the simulations and what that would indicate in the clinical situation. Following the results, an analysis is presented of how suitable the model is to predict the response of the cornea in physiological conditions.

4.1 Extensometry simulations

Extensometry simulations were made with a 0.8426 MPa surface traction along the x-axis, which is equal to 2 N pull along the x-axis. Extending the strip cut with 2 N force was chosen to make the comparison to actual extensometry testing [87] easy. Since the numerical data was not easily accessible the curve from [50] was used for the comparison of previous extensometry simulation and testing. Figure 44 shows the curve from extensometry simulation, which represents a superior-

inferior strip from the cornea, and the curve from [50] which represent the extensometry simulation and experiment of corneas from 69-70 year-olds. The origin of the curve was chosen to be in the state of the simulation where the model was already extended with a small force i.e. 0.8 mm was subtracted from the x-axis values to account for the initial straightening of the model, which is not seen in the extensometry testing.

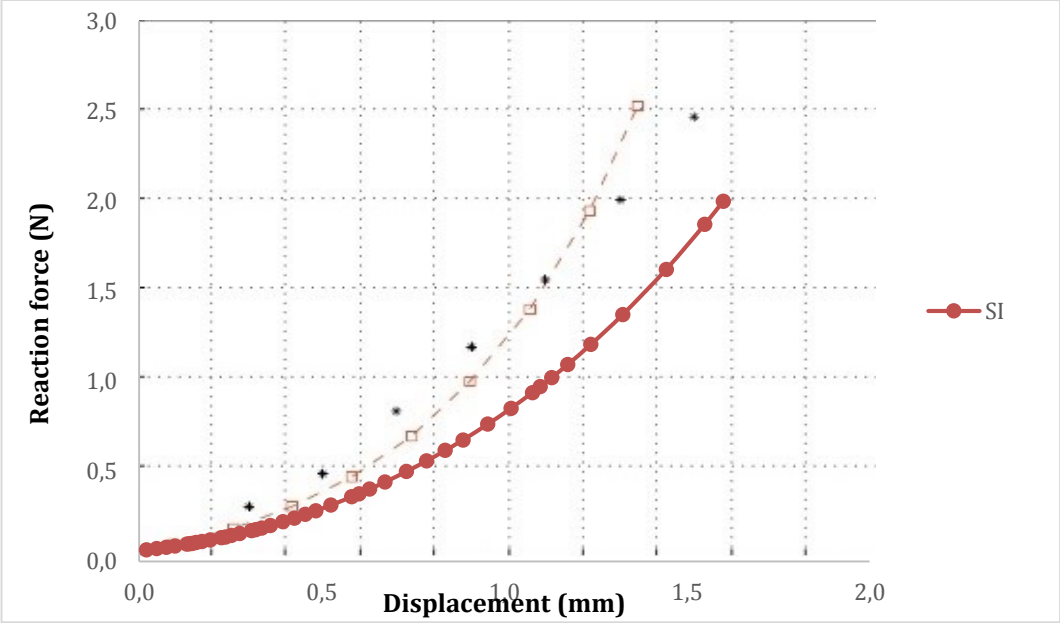

Figure 44. Results of the superior-inferior extensometry (red circles) simulation compared to the extensometry simulation of Studer et al [50] (red dashed line) and extensometry testing by Elsheikh et al [87] (*).

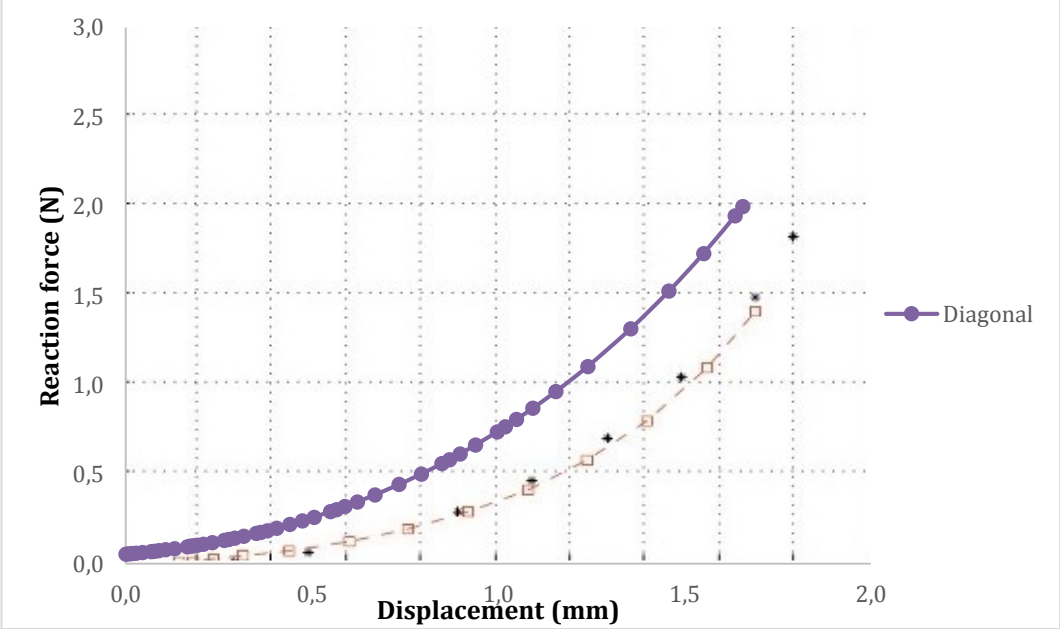

Figure 45. Results of the diagonal extensometry (purple circles) simulation compared to the extensometry simulation of Studer et al [50] (red dashed line) and extensometry testing by Elsheikh et al [87] (*).

Figure 44 and Figure 45 shows that the response to the stresses is too soft for the superior-inferior sample and too stiff for the diagonal sample. The SI and diagonal sample simulations show very little anisotropy, Figure 46, which means that the dispersion parameter κ should have had a lower value than the assigned ones. The anterior stroma is thicker and stiffer than the other stromal layers and thus contributes to the overall mechanical behavior more than the other layers. The anterior stroma is assumed to be the only layer to increase in thickness towards the periphery and that also contributes more to the overall biomechanical properties of the cornea.

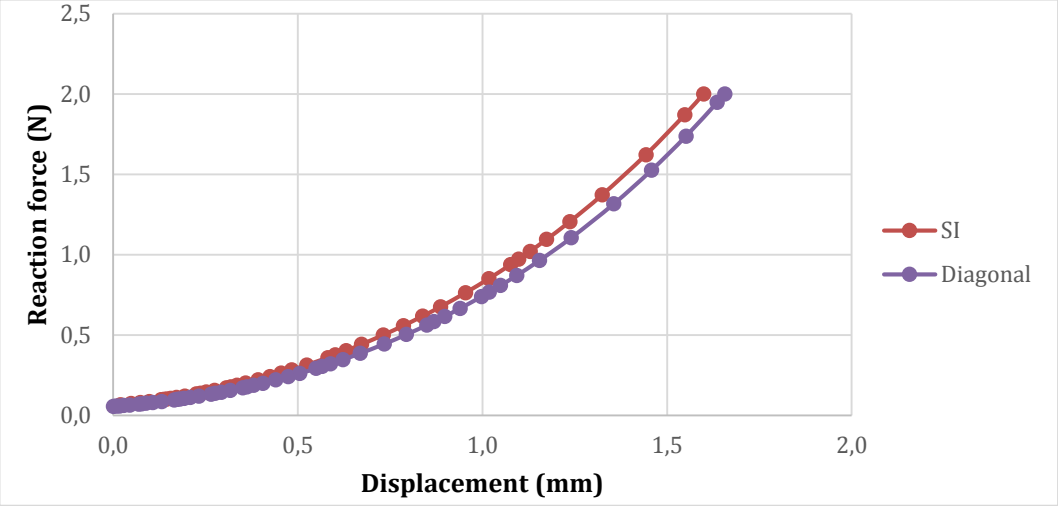

Figure 46. Strip extensometry simulation for superior-inferior (SI) and diagonal cuts of the cornea

Figure 47 shows the results of the superior-inferior extensometry simulations. LASIK has the softest response to the extension and SMILE with 140 µm cap and deep SMILE with 200 µm cap are relatively close to the untreated eye, with deep SMILE showing slightly stiffer response than the SMILE with 140 µm cap. In Figure 47 the initial straightening of the model is seen, where with little force the model is extended by 0.8 mm. The simulations for diagonal extensometry showed similar response for extension.

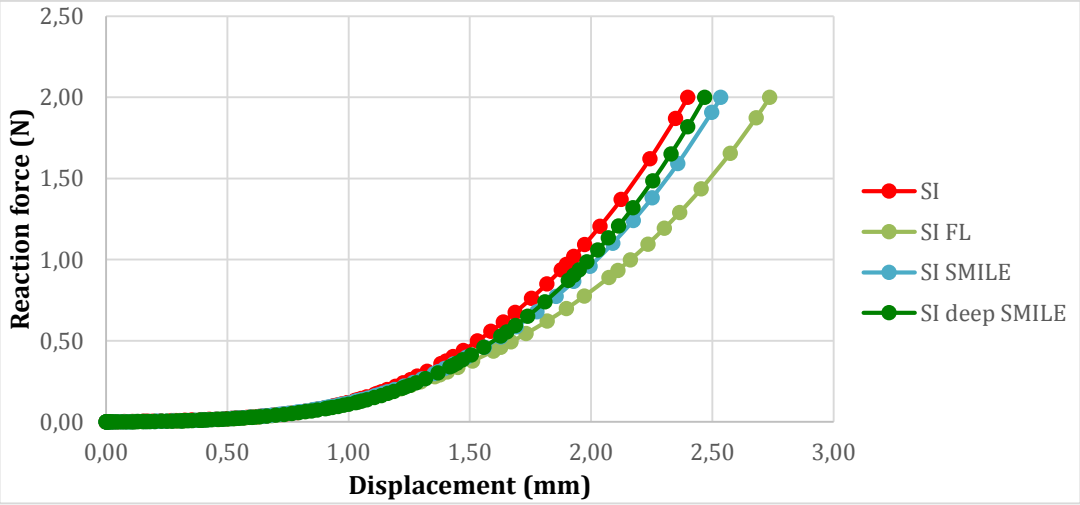

Figure 47. Comparison of superior-inferior (SI) extensometry simulations of different surgical techniques. FL=femtoLASIK with 100 µm flap, SMILE with 140 µm cap and deep SMILE with 200 µm cap.

4.2 Inflation simulations

Inflation simulations were made with an intraocular pressure (IOP) of 2 MPa which is ~15 000 mmHg. The apical rise was measured from the anterior and posterior surfaces. Figure 48 shows the apical rise from the apex. In inflation tests the pressure rises up to 150 mmHg (~0.02 MPa) and the apical rise is approximately 0.35 mm. In the simulations the apical rise up to 0.02 MPa, Figure 49, creates almost linear curve and that is much stiffer than the experimental tests and previous simulations.

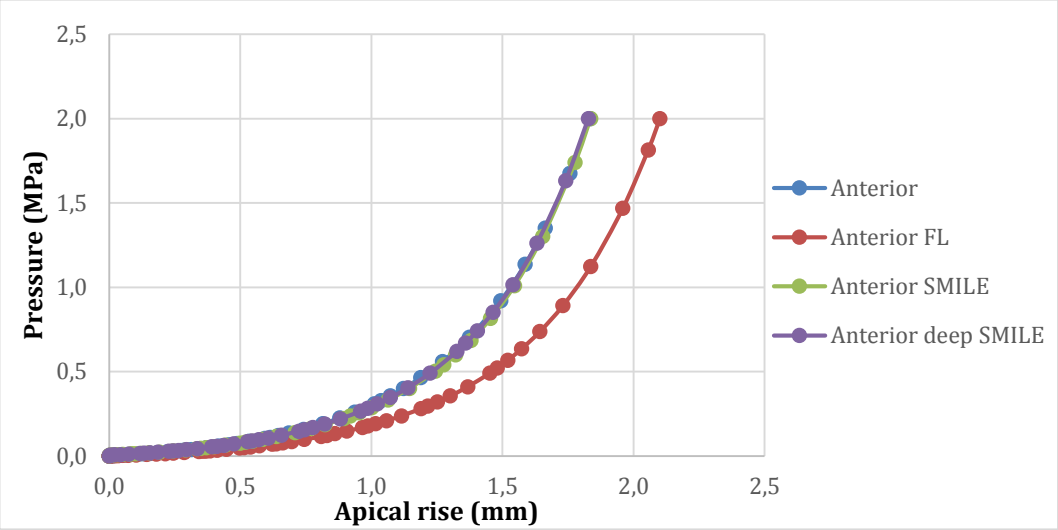

Figure 48. The apical rise from the apex of the anterior surface

Figure 49 shows the beginning of the increase in IOP. The lenticule is removed in stress-free state in the simulation. The cavity disappears due to the deformation of the softer posterior layers of the stroma and the IOP that is applied to the posterior surface. The anterior surface has a small negative apical rise in the beginning until the posterior layers of the stroma reaches the cap.

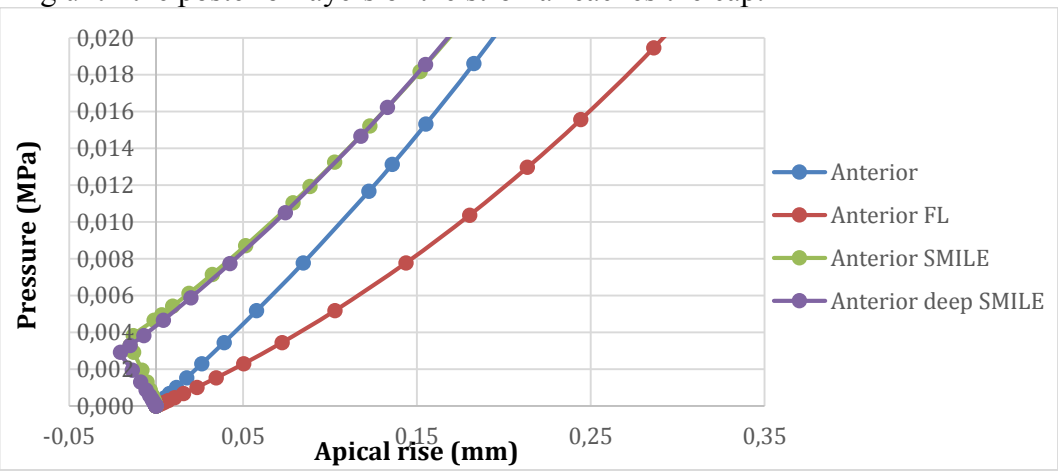

Figure 49. Apical rise with low pressure from the apex of the anterior surface

Figure 50 shows the initial deformation of the posterior stroma. The highest stresses are in the Descemet's membrane, which is much stiffer layer than the posterior stroma in the simulations.

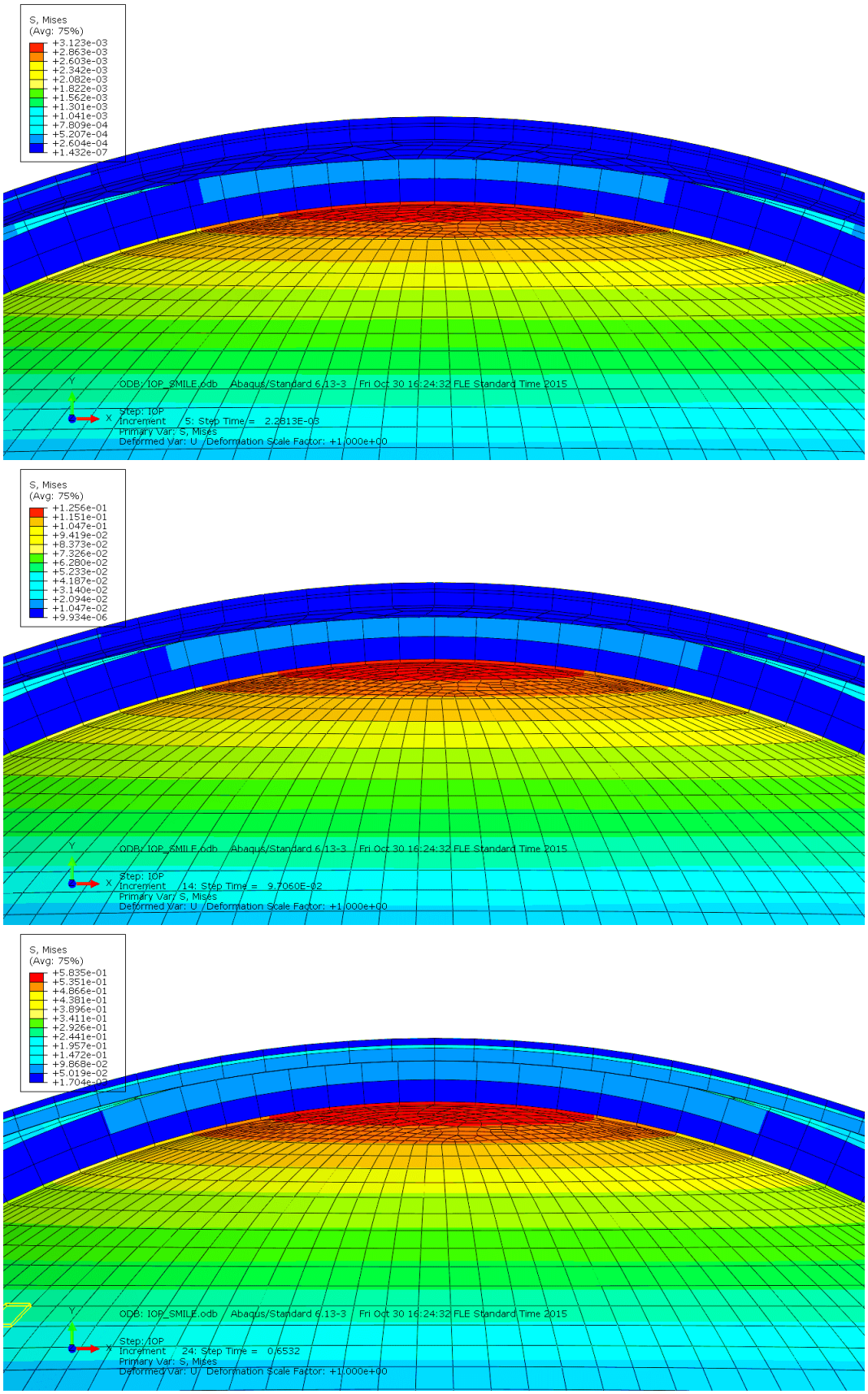

Figure 50. Inflation simulation of SMILE procedure: the posterior stroma reaches the cap before the apex of the anterior surface rises

The apex in the posterior surface acts different than the anterior surface in the simulation, Figure 51 and Figure 52. SMILE curve follows the curve of untreated cornea subtracted with the thickness of lenticule removed. Overall the femtoLASIK seems to have the highest impact to the biomechanical properties as in the other simulations, however the early part of the curve of the anterior surface apical rise, the femtoLASIK appears to show stiffer behavior than the SMILE, which is caused by the thicker residual stroma in femtoLASIK than in SMILE.

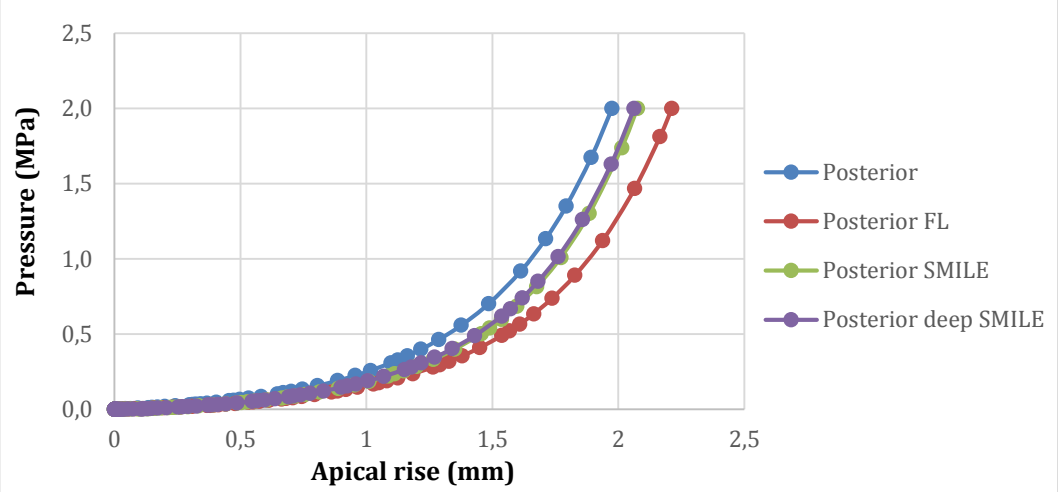

Figure 51. Inflation simulation of the apical rise of the apex of the posterior surface

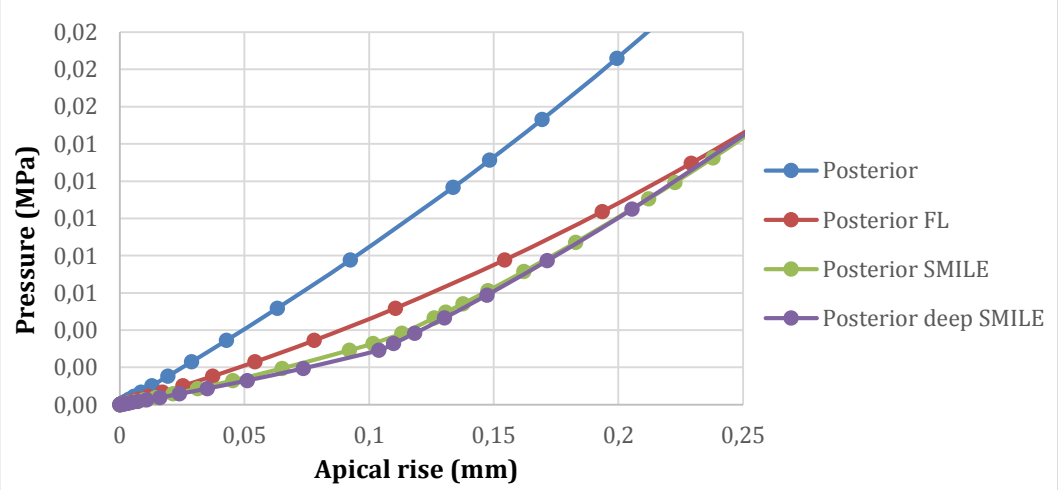

Figure 52. Initial apical rise of the posterior surface

5 Discussion

The simulations show similar results as previous theoretical studies that have compared the effect of SMILE and LASIK surgeries [35, 56]. The stiffer anterior stroma remains intact in SMILE and thus contributes more to the overall biomechanical stability of the cornea. The collagen fibers in LASIK flap are not adhered to the stroma and do not contribute to the stability of the cornea, which leads to a softer overall response of the cornea, compared to SMILE. The differences in the simulations of SMILE and non-treated eyes are relatively small and would indicate that even for high refractive corrections the changes in corneal biomechanics would be small compared to LASIK.

5.1 Applicability to the corneas *in vivo*

The simulations cannot be compared directly to the physiological conditions of the cornea but if the findings from the simulations are true, the LASIK procedure should cause more deformation in the anterior surface and depending on position of the curve of the apical rise and IOP, Figure 52, either less or more deformation in the posterior surface. The aim of refractive surgery is to modify the curvature of the anterior surface in order to move the focal point of the eye to the correct position in the fovea. The anterior layers of the cornea are theoretically stiffer than the posterior layers, which indicates that the SMILE procedure should have less effect on the curvature of the anterior surface and more to the curvature of the posterior surface and vice versa in LASIK, Figure 53. However if the curvature of the posterior surface were changed the change in optical power would be small, the refractive indices of cornea and *aqueous humour* are 1.376 and 1.336, respectively. If refractive surgery changes the curvature of the posterior surface, it is considered as a complication, *ectasia*, which is similar condition as *keratoconus.* Bulging of the posterior surface is transmitted to the anterior surface, which leads to a poorer vision and may require additional treatments.

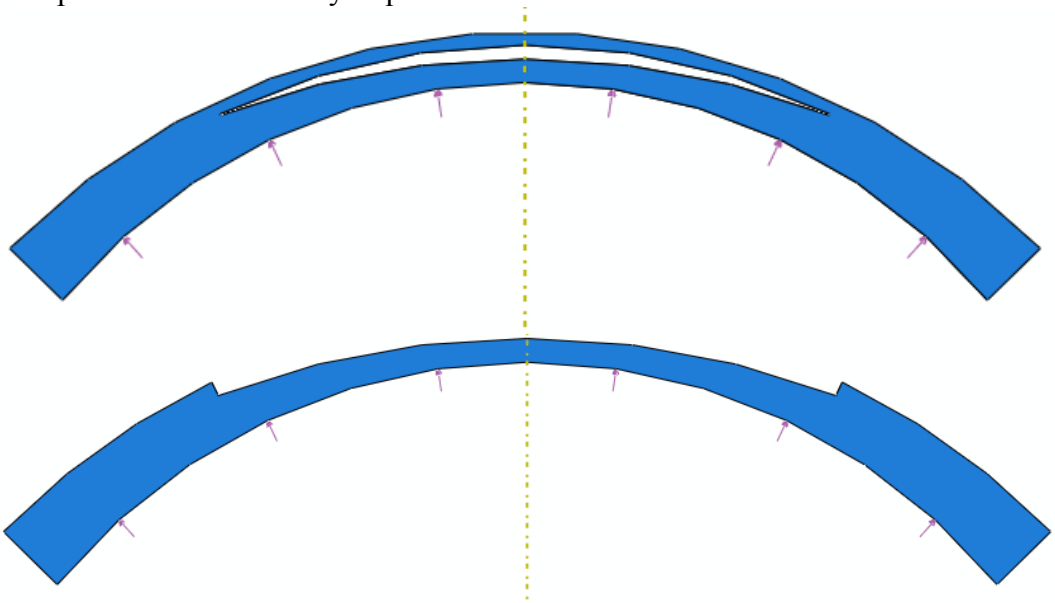

Figure 53. Cornea in stress-free state after SMILE and LASIK

Even if the *ectasia* is not diagnosed, some signs of deformation after high myopia SMILE and LASIK should occur in the posterior surface in physiological

conditions. In LASIK over 50% of tissue can be removed from the apex of the cornea and if the anterior layers are significantly stiffer the posterior stroma should experience some kind of deformation. Figure 54 shows the difference in tangential curvature in pre and post operational corneas. Both of the patients underwent approximately -8 diopters of refractive correction. The residual central stromal thickness of the femtoLASIK patient is above 250 µm and the residual stromal thickness of the SMILE patient is above 300 µm and cap thickness of 130 µm, which adds up to over 430 µm of intact cornea in SMILE. The figure shows that there is a minimal difference in the curvature of the posterior surface, especially in the central zone, which is more accurately measured. Peripheral changes may be explained with measurement errors. Comparisons of other patients with different high myopia corrections showed similar behavior regardless of the type of the procedure. Figure 55 shows the difference of the tangential curvature of the anterior surface of the cornea. The difference in sagittal curvature of the posterior surface is smaller than the difference in tangential curvature, Figure 56.

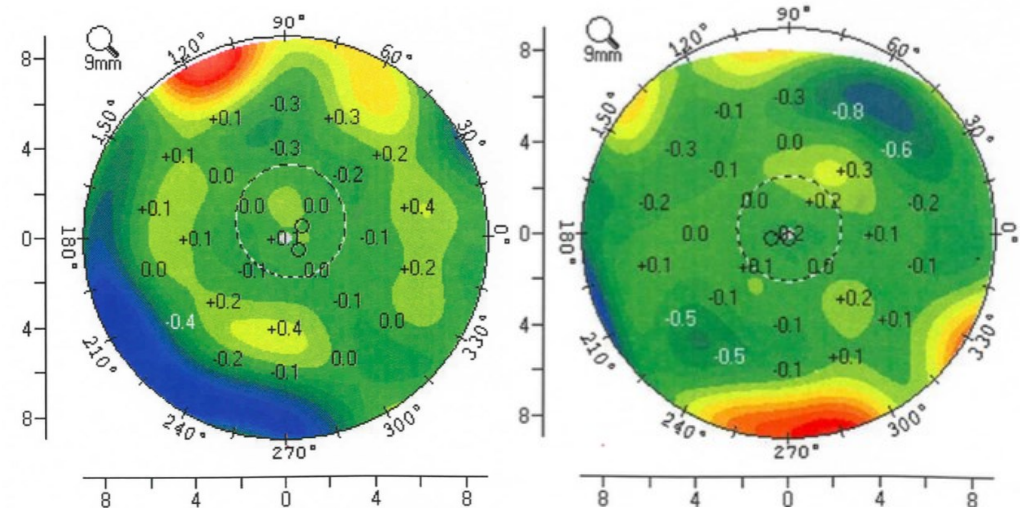

Figure 54. The difference in tangential curvature (diopters) of the posterior surface pre and post operation of femtoLASIK (left) and SMILE (right)

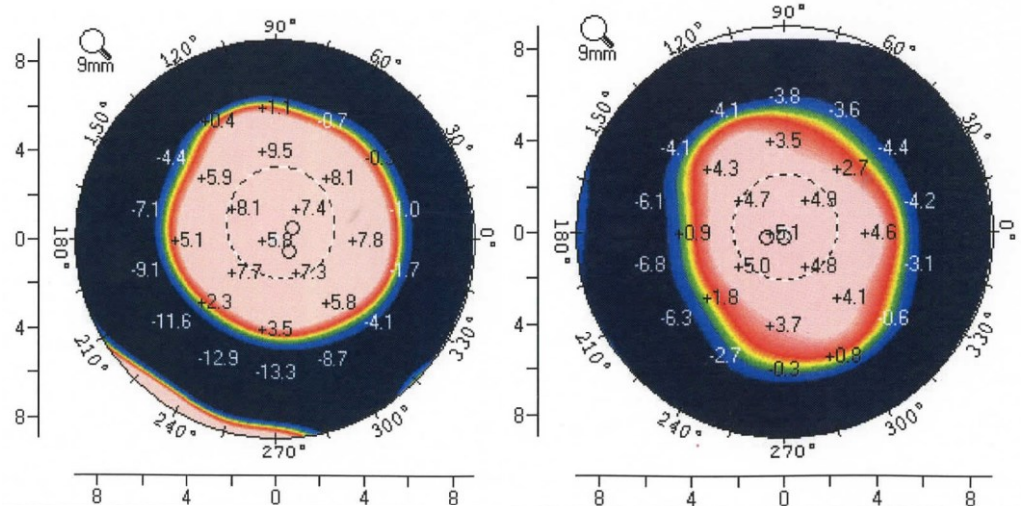

Figure 55. The difference of tangential curvature (diopters) of the anterior surface pre and post operation of femtoLASIK (left) and SMILE (right)

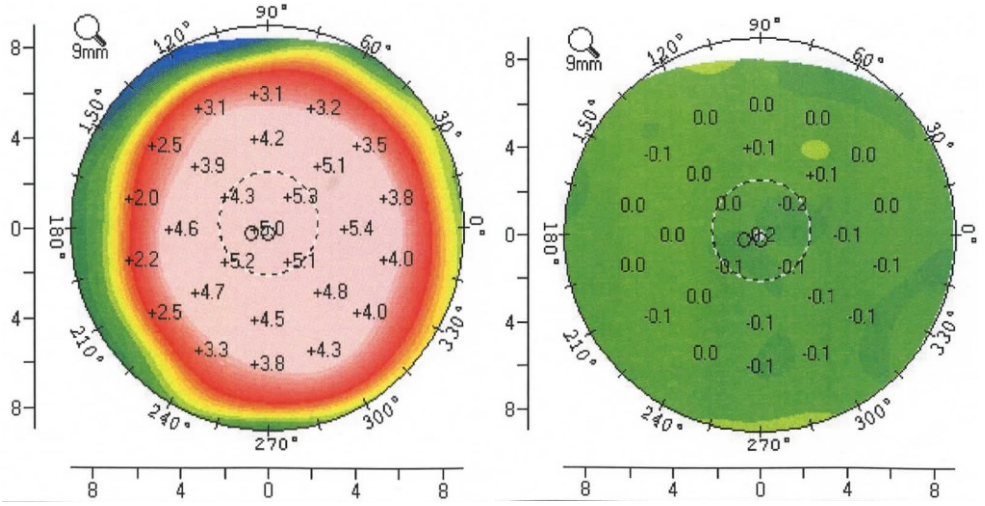

Figure 56. The difference of sagittal curvature after SMILE of the anterior (left) and posterior (right) surfaces of the cornea

All the change in curvature of the cornea is visible in the anterior surface, not in the posterior surface. That is significantly different than what the theoretical biomechanical models would predict. That may be explained by the error in the models that considers the stiffness of different layers. Posterior layers appear to be much stiffer than the anterior layers in physiological conditions. That is not directly contradictory with the measurements that state that the anterior layers are stiffer than the posterior layers. The posterior stroma may support all the stresses of the cornea while the anterior layers are stress free i.e. the anterior layers are stress-free or experience only small strains and the posterior layers experience high stresses and strains, which explains the stiffer response of the posterior layers in physiological conditions. Other way to express the previous sentence is to say that the tangential Young's modulus is significantly higher in posterior layers of the cornea than the anterior. The overall stiffness in experimental extensometry and inflation tests, which creates much higher stresses than physiological conditions, can still be higher in anterior layers compared to posterior layers.

A study by Vestergaard et al [89] found no significant biomechanical difference from paired eye study where other eye was treated with SMILE and other eye with FLEX, which is otherwise the same procedure than SMILE but instead of small incision where the lenticule is removed, a flap is created below of which the lenticule is removed. The results were explained with the small number of patients who had SMILE in the other eye and FLEX in the other and that the differences are so small that those might be visible after higher number of patients. If the anterior layers of the stroma do not have a significant effect on the biomechanical equilibrium of the cornea the flapless surgical technique would not differ from the techniques that creates the flap in the anterior cornea.

Pedersen et al [76] found no significant difference between the flap-based and flapless techniques when comparing eyes *in vivo* with ocular response analyzer. Other studies [90, 91] also found no significant difference between eyes treated with SMILE and LASIK though some similar studies [92, 93] found changes between the LASIK and SMILE groups.

The similar biomechanical response *in vivo* after SMILE and LASIK may be a result of the low impact of the anterior layers of the stroma to the corneal biomechanics in physiological conditions. The changes between pre and post operation may be explained with only the removal of tissue i.e. the flap cut does not induce more stresses in the cornea than the lenticule extraction, only changes in the posterior layers causes changes in the overall biomechanics. The flap cut and SMILE cut do not alter the viscoelastic behavior significantly but the lenticule extraction and laser ablation have significant effect on the viscoelastic properties.

In conclusion, the stresses and strains are not known in the cornea in physiological conditions but the cornea behaves in a way that would suggest that the posterior layers are stiffer (tangential Young's modulus is higher) than the anterior layers and that the anterior layers might be stress-free. 250 μm of residual central stromal thickness is thought to be the safe limit of LASIK and PRK but it has been suggested [56] that in SMILE the residual stromal thickness could be even less than 250 μm without increasing the risk of *ectasia*. The previous findings suggest that the limits of SMILE should not differ from other types of treatments.

5.2 Additional research

Additional research is required of corneas in physiological conditions. The previous models, such as the one in this thesis, overestimates the contribution of anterior layers and underestimates the contribution of posterior layers to the equilibrium of the cornea in physiological conditions. Tonometry and other clinical measurements could benefit from more accurate models of the cornea *in vivo*. Diagnostics and treatment of corneal diseases that involve biomechanical changes could become more accurate when the stresses and strains in the cornea are known. Theoretical models that predict the patient-specific behavior of the cornea usually have uniform material properties through the depth of the cornea and if the stress-free or pre-loading conditions are considered the distribution of the stresses in the analysis is not similar to the stresses in the cornea in physiological conditions.

Current models can predict corneal behavior in experimental conditions where the intraocular pressure can be high enough to cause loss of vision in live eyes or where the extensometry tests create stresses that are significantly higher than in physiological conditions. To improve the theoretical models of the cornea and the eye, the heterogeneous, viscoelastic, hyperelastic and anisotropic material properties should be determined more accurately. The stresses of the cornea in physiological conditions should be known before expecting that the patient specific modeling would provide more accurate results than a statistical analysis or an evaluation from an experienced physician.

References

[1] P. Palttala, "Silmien laserleikkaukset yleistyvät - "Kaupallinen peli" huolestuttaa lääkäriä," *Helsingin Sanomat,* pp. 1/20/2015, 2014.

[2] J. F. Doane, "Refractive Corneal Surgery Without an Excimer Laser. Are LASIK's days numbered?" *Cataract and Refractive Surgery Today (CRST),* pp. 97, 7.2014, 2014.

[3] M. Sacks, A. D'Amore and C. Hobson, "Chapter I.1.4 - finite element analysis in biomechanics," in *Biomaterials Science (Third Edition)*, Lemons,Buddy D.RatnerAllan S.HoffmanFrederick J.SchoenJack E., Ed. Academic Press, 2013, pp. 21-34.

[4] H. L. Liou and N. A. Brennan, "Anatomically accurate, finite model eye for optical modeling." *Journal of the Optical Society of America.A, Optics, Image Science, and Vision,* vol. 14, pp. 1684, 1997.

[5] F. L. Pedrotti and L. S. Pedrotti, "Optics of the eye," in *Introduction to Optics*, 2nd ed.Anonymous Englewood Cliffs NJ: Prentice Hall, 1993, pp. 152-155.

[6] A. Alarcón, R. Anera, L. del Barco and J. Jiménez, "Designing multifocal corneal models to correct presbyopia by laser ablation." *J. Biomed. Opt.,* vol. 17, pp. 018001, 2012.

[7] T. Eppig and A. Langenbucher, "Simulation of stray light with a phakic intraocular lens with a central hole," *Acta Ophthalmol.,* vol. 92, 2014.

[8] L. Nan, X. Tang and Y. Liu, "[Depth of focus in spherical and aspheric intraocular lenses]." *中华眼科杂志,* vol. 48, pp. 137, 2012.

[9] E. Rank, L. Traxler, N. Bayer, B. Reutterer, K. Lux, A. Drauschke, R. Raghavachari, R. Liang and S. SPIE INT, "Reproducibility analysis of measurements with a mechanical semiautomatic eye model for evaluation of intraocular lenses," *Proceedings of SPIE--the International Society for Optical Engineering,* vol. 8936, 2014.

[10] J. Pietila, "Laser-assisted in situ keratomileusis flap creation with the three-dimensional, transportable Ziemer FEMTO LDV model Z6 I femtosecond laser," *Acta Ophthalmologica, 2014 Nov, Vol. 92(7), Pp. 650-655,* vol. 92, pp. 650-655, 2014.

[11] J. W. Ruberti, A. Sinha Roy and C. J. Roberts, "Corneal biomechanics and biomaterials," *Annu. Rev. Biomed. Eng.,* vol. 13, pp. 269-295, 2011.

[12] A. SORSBY, M. SHERIDAN, G. LEARY and B. BENJAMIN, "Vision, Visual Acuity, and Ocular Refraction of Young Men - Findings in a Sample of 1,033 Subjects," *Br. Med. J.,* vol. 1, pp. 1394-1398, 1960.

[13] A. Pandolfi and F. Manganiello, "A model for the human cornea: constitutive formulation and numerical analysis," *Biomechanics and Modeling in Mechanobiology,* vol. 5, pp. 237, 2006.

[14] B. Moffat, D. Atchison and J. Pope, "Explanation of the lens paradox," *Optometry Vision Sci.,* vol. 79, pp. 148-150, 2002.

[15] J. Schwiegerling, "Ocular function," in *Field Guide to Visual and Ophthalmic Optics*Anonymous Bellingham, WA: SPIE, 2004, pp. 1-25.

[16] H. Zhao and M. Mainster, "The effect of romatic dispersion on pseudophakic optical performance," *Br. J. Ophthalmol.,* vol. 91, pp. 1225, 2007.

[17] F. L. Pedrotti and L. S. Pedrotti, "Optics of the eye," in *Introduction to Optics*, 2nd ed.Anonymous Englewood Cliffs NJ: Prentice Hall, 1993, pp. 120.

[18] E. Hecht, "More on geometrical optics: Aberrations," in *Optics*, 4th ed.Anonymous San Francisco: Addison Wesley, 2002, pp. 254.

[19] R. Vidal Olarte, "Entendiendo e interpretando las aberraciones ópticas," *Cien. Tecnol. Salud. Vis. Ocul Issn: 1692-8415,* vol. 9, pp. 105, 2011.

[20] H. Tran and S. Zagai. Näkemisen laatu monitehotekomykiöllä : Tarkastelun kohteena alcon AcrySof ReSTOR. 2012.

[21] L. THIBOS, "Theory and measurement of ocular chromatic aberration," *Vision Res.,* vol. 30, pp. 33-49, 1990.

[22] W. Li, S. Du, M. Li, M. Chen and C. Sun, "Fuzzy classification of orchard pest posture based on zernike moments," in *Fuzzy Systems (FUZZ-IEEE), 2014 IEEE International Conference On,* 2014, pp. 1096-1103.

[23] L. Buratto, S. Slade and M. Tavolato, *LASIK the Evolution of Refractive Surgery.* Thorofare, NJ, USA: SLACK incorporated, 2012.

[24] R. Paschotta, "Gas lasers: Excimer lasers," in *Field Guide to Lasers*, R. Paschotta, Ed. Bellingham, WA: SPIE, 2008, pp. 87.

[25] C. R. Munnerlyn, S. J. Koons and J. Marshall, "Photorefractive keratectomy: a technique for laser refractive surgery," *Journal of Cataract & Refractive Surgery,* vol. 14, pp. 46-52, 1988.

[26] D. Z. Reinstein, T. J. Archer and M. Gobbe, "Small incision lenticule extraction (SMILE) history, fundamentals of a new refractive surgery technique and clinical outcomes," *Eye and Vision,* vol. 1, pp. 3, 2014.

[27] J. W. Ruberti and J. D. Zieske, "Prelude to corneal tissue engineering – Gaining control of collagen organization," *Prog. Retin. Eye Res.,* vol. 27, pp. 549-577, 9, 2008.

[28] S. Jonuscheit, M. J. Doughty, R. Martin, A. Río-Cristóbal, V. Cruikshank and S. Lang, "Peripheral nasal-temporal corneal asymmetry in relation to corneal thickness: a Scheimpflug imaging study," *Ophthalmic and Physiological Optics,* vol. 35, pp. 45-51, 2015.

[29] J. Jester, C. Murphy, M. Winkler, J. P. G. Bergmanson, D. Brown, R. Steinert and M. Mannis, "Lessons in corneal structure and mechanics to guide the corneal surgeon," *Ophthalmology,* vol. 120, pp. 1715-7, 2013.

[30] H. Dua, L. Faraj, M. Branch, A. Yeung, M. Elalfy, D. Said, T. Gray and J. Lowe, "The collagen matrix of the human trabecular meshwork is an extension of the novel pre-Descemet's layer (Dua's layer)." *Br. J. Ophthalmol.,* vol. 98, pp. 691, 2014.

[31] H. Dua, L. Faraj, D. Said, T. Gray and J. Lowe, "Human Corneal Anatomy Redefined A Novel Pre-Descemet's Layer (Dua's Layer)," *Ophthalmology,* vol. 120, pp. 1778-1785, 2013.

[32] H. Mckee, L. Irion, F. Carley, A. Brahma, M. Jafarinasab, M. Rahmati Kamel, M. Kanavi and S. Feizi, "Re: Dua et al.: Human corneal anatomy redefined: a novel pre-Descemet layer (Dua's layer) (Ophthalmology 2013;120:1778-85)," *Ophthalmology,* vol. 121, pp. E24-E25, 2014.

[33] J. A. Last, S. J. Liliensiek, P. F. Nealey and C. J. Murphy, "Determining the mechanical properties of human corneal basement membranes with atomic force microscopy," *J. Struct. Biol.,* vol. 167, pp. 19-24, 7, 2009.

[34] D. Reinstein, T. Archer, M. Gobbe, R. Silverman, J. Coleman and I. SLACK, "Epithelial thickness in the normal cornea: Three-dimensional display with artemis very high-frequency digital ultrasound," *Journal of Refractive Surgery,* vol. 24, pp. 571-581, 2008.

[35] A. Sinha Roy, W. Dupps and C. Roberts, "Comparison of biomechanical effects of small-incision lenticule extraction and laser in situ keratomileusis: finite-element analysis." *J. Cataract Refract. Surg.,* vol. 40, pp. 971, 2014.

[36] M. Lombardo, G. Lombardo, G. Carbone, M. P. De Santo, R. Barberi and S. Serrao, "Biomechanics of the anterior human corneal tissue investigated with atomic force microscopy," *Invest. Ophthalmol. Vis. Sci.,* vol. 53, pp. 1050-1057, Feb 29, 2012.

[37] T. Seiler, M. Matallana, S. Sendler and T. Bende, "Does Bowman's layer determine the biomechanical properties of the cornea?" *Refract. Corneal Surg.,* vol. 8, pp. 139, 1992.

[38] Y. Komai and T. Ushiki, "The three-dimensional organization of collagen fibrils in the human cornea and sclera," *Invest. Ophthalmol. Vis. Sci.,* vol. 32, pp. 2244-2258, Jul, 1991.

[39] H. Studer, H. Riedwyl, C. Amstutz, J. V. M. Hanson and P. Buchler, "Patient-specific finite-element simulation of the human cornea: A clinical validation study on cataract surgery." *J. Biomech.,* vol. 46, pp. 751-758, 2013.

[40] A. Kilic, "Femtosecond laser flap complications," in *Femtosecond Laser Techniques & Technology*, 1st ed., A. Garg, J. L. Alió and E. D. Donnenfield, Eds. New Delhi, India: Jaypee Brothers Medical Publishers, 2012, pp. 130-135.

[41] H. Aghamohammadzadeh, R. Newton and K. Meek, "X-ray scattering used to map the preferred collagen orientation in the human cornea and limbus," *Structure,* vol. 12, pp. 249-256, 2004.

[42] N. J. Fullwood, "Collagen Fibril Orientation and Corneal Curvature," *Structure,* vol. 12, pp. 169-170, 2, 2004.

[43] W. J. Dupps Jr. and S. E. Wilson, "Biomechanics and wound healing in the cornea," *Exp. Eye Res.,* vol. 83, pp. 709-720, 10, 2006.

[44] M. Abahussin, S. Hayes, N. E. Knox Cartwright, C. S. Kamma-Lorger, Y. Khan, J. Marshall and K. M. Meek, "3D collagen orientation study of the human cornea using X-ray diffraction and femtosecond laser technology," *Invest. Ophthalmol. Vis. Sci.,* vol. 50, pp. 5159-5164, Nov, 2009.

[45] S. J. Petsche and P. M. Pinsky, "The role of 3-D collagen organization in stromal elasticity: a model based on X-ray diffraction data and second harmonic-

generated images," *Biomechanics and Modeling in Mechanobiology,* vol. 12, pp. 1101-1113, 2013.

[46] C. R. Ethier, M. Johnson and J. Ruberti, "Ocular biomechanics and biotransport," *Annu. Rev. Biomed. Eng.,* vol. 6, pp. 249-273, 2004.

[47] R. H. Newton and K. M. Meek, "The Integration of the Corneal and Limbal Fibrils in the Human Eye," *Biophys. J.,* vol. 75, pp. 2508-2512, 11, 1998.

[48] S. Petsche, D. Chernyak, J. Martiz, M. Levenston and P. Pinsky, "Depth-dependent transverse shear properties of the human corneal stroma." *Invest. Ophthalmol. Vis. Sci.,* vol. 53, pp. 873, 2012.

[49] P. M. Pinsky, D. van der Heide and D. Chernyak, "Computational modeling of mechanical anisotropy in the cornea and sclera," *Journal of Cataract & Refractive Surgery,* vol. 31, pp. 136-145, 1, 2005.

[50] H. Studer, X. Larrea, H. Riedwyl and P. Büchler, "Biomechanical model of human cornea based on stromal microstructure," *J. Biomech.,* vol. 43, pp. 836-842, 3/22, 2010.

[51] A. Jayasuriya, S. Ghosh, J. Scheinbeim, V. Lubkin, G. Bennett and P. Kramer, "A study of piezoelectric and mechanical anisotropies of the human cornea," *Biosens. Bioelectron.,* vol. 18, pp. 381-387, 2003.

[52] A. Elsheikh, M. Brown, D. Alhasso, P. Rama, M. Campanelli and D. Garway-Heath, "Experimental assessment of corneal anisotropy," *J. Refract. Surg.,* vol. 24, pp. 178-187, Feb, 2008.

[53] K. M. Meek and C. Boote, "The organization of collagen in the corneal stroma," *Exp. Eye Res.,* vol. 78, pp. 503-512, 3, 2004.

[54] J. Ø Hjortdal, "Regional elastic performance of the human cornea," *J. Biomech.,* vol. 29, pp. 931-942, 7, 1996.

[55] J. B. Randleman, D. Dawson, H. Grossniklaus, B. McCarey and H. Edelhauser, "Depth-dependent cohesive tensile strength in human donor corneas: implications for refractive surgery." *Journal of Refractive Surgery,* vol. 24, 2008.

[56] D. Reinstein, T. Archer and J. Randleman, "Mathematical Model to Compare the Relative Tensile Strength of the Cornea After PRK, LASIK, and Small Incision Lenticule Extraction," *Journal of Refractive Surgery,* vol. 29, pp. 454-460, 2013.

[57] M. Winkler, D. Chai, S. Kriling, C. Nien, D. Brown, B. Jester, T. Juhasz and J. Jester, "Nonlinear optical macroscopic assessment of 3-D corneal collagen organization and axial biomechanics," *Invest. Ophthalmol. Vis. Sci.,* vol. 52, pp. 8818-27, 2011.

[58] H. Hatami-Marbini and A. Rahimi, "Stiffening Effects of riboflavin/UVA corneal collagen crosslinking is hydration dependent," *J. Biomech.,* .

[59] J. S. Friedenwald, "Contribution to the Theory and Practice of Tonometry*," *Am. J. Ophthalmol.,* vol. 20, pp. 985-1024, 10, 1937.

[60] D. Piñero and N. Alcón, "Corneal biomechanics: a review." *Clinical and Experimental Optometry,* 2014.

[61] G. Orssengo and D. Pye, "Determination of the true intraocular pressure and modulus of elasticity of the human cornea in vivo," *Bull. Math. Biol.,* vol. 61, pp. 551-572, 1999.

[62] A. Elsheikh and K. Anderson, "Comparative study of corneal strip extensometry and inflation tests." *J R Soc Interface,* vol. 2, pp. 177-85, 2005.

[63] F. W. Cooke, "1.2 bulk properties of materials," in *Biomaterials Science: An Introduction to Materials in Medicine*, 2nd ed., B. D. Ratner, Ed. Academic press, 2004, pp. 31.

[64] R. Grytz and G. Meschke, "A computational remodeling approach to predict the physiological architecture of the collagen fibril network in corneo-scleral shells," *Biomechanics and Modeling in Mechanobiology,* vol. 9, pp. 225, 2010.

[65] X. Liu, L. Wang, J. Ji, W. Yao, W. Wei, J. Fan, S. Joshi, D. Li and Y. Fan, "A Mechanical Model of the Cornea Considering the Crimping Morphology of Collagen Fibrils," *Investigative Ophthalmology & Visual Science,* vol. 55, pp. 2739-2746, April 01, 2014.

[66] S. Sloan, Y. Khalifa and M. Buckley, "The Location- and Depth-Dependent Mechanical Response of the Human Cornea Under Shear Loading," *Invest. Ophthalmol. Vis. Sci.,* vol. 55, pp. 7919-7924, 2014.

[67] V. Dayanir, R. Sakarya, F. Özcura, E. Kir, T. Aktunç, B. S. Özkan and P. Okyay, "Effect of corneal drying on central corneal thickness," *J. Glaucoma,* vol. 13, pp. 6-8, 2004.

[68] B. Jue and D. M. Maurice, "The mechanical properties of the rabbit and human cornea," *J. Biomech.,* vol. 19, pp. 847-853, 1986.

[69] J. A. Last, S. M. Thomasy, C. R. Croasdale, P. Russell and C. J. Murphy, "Compliance profile of the human cornea as measured by atomic force microscopy," *Micron,* vol. 43, pp. 1293-1298, 12, 2012.

[70] Knox Cartwright, Nathaniel E MA, J. R. P. Tyrer and J. Marshall, "In Vitro Quantification of the Stiffening Effect of Corneal Cross-linking in the Human Cornea Using Radial Shearing Speckle Pattern Interferometry," *Journal of Refractive Surgery,* vol. 28, pp. 503, 2012.

[71] N. E. Knox Cartwright, J. R. Tyrer and J. Marshall, "Age-related differences in the elasticity of the human cornea," *Invest. Ophthalmol. Vis. Sci.,* vol. 52, pp. 4324-4329, Jun 17, 2011.

[72] A. Eilaghi, J. G. Flanagan, I. Tertinegg, C. A. Simmons, G. Wayne Brodland and C. Ross Ethier, "Biaxial mechanical testing of human sclera," *J. Biomech.,* vol. 43, pp. 1696-1701, 6/18, 2010.

[73] A. Elsheikh, B. Geraghty, D. Alhasso, J. Knappett, M. Campanelli and P. Rama, "Regional variation in the biomechanical properties of the human sclera," *Exp. Eye Res.,* vol. 90, pp. 624-633, 5, 2010.

[74] E. Mikula, K. Hollman, D. Chai, J. V. Jester and T. Juhasz, "Measurement of Corneal Elasticity with an Acoustic Radiation Force Elasticity Microscope," *Ultrasound Med. Biol.,* vol. 40, pp. 1671-1679, 7, 2014.

[75] H. Wang, P. L. Prendiville, P. J. McDonnell and W. V. Chang, "An ultrasonic technique for the measurement of the elastic moduli of human cornea," *J. Biomech.,* vol. 29, pp. 1633-1636, 12, 1996.

[76] I. Pedersen, S. Bak Nielsen, A. Vestergaard, A. Ivarsen and J. Hjortdal, "Corneal biomechanical properties after LASIK, ReLEx flex, and ReLEx smile by Scheimpflug-based dynamic tonometry." *Graefe's Archive for Clinical and Experimental Ophthalmology = Albrecht Von Graefes Archiv Für Klinische Und Experimentelle Ophthalmologie,* vol. 252, pp. 1329, 2014.

[77] H. Studer, H. Riedwyl and P. Büchler, "Importance of multiple loading scenarios for the identification of material coefficients of the human cornea," *Comput. Methods Biomech. Biomed. Engin.,* pp. 1-7, 2011.

[78] W. Charles and M. M. CharlesWhitfordHaraldStuderCraigBooteKeith, "Biomechanical model of the human cornea: Considering shear stiffness and regional variation of collagen anisotropy and density," *Journal of the Mechanical Behavior of Biomedical Materials,* pp. 76-87, 2015.

[79] A. S. Roy and W. J. Dupps, "Patient-specific modeling of corneal refractive surgery outcomes and inverse estimation of elastic property changes," *J. Biomech. Eng.,* vol. 133, pp. 011002, 2011.

[80] A. Pandolfi and G. Holzapfel, "Three-Dimensional Modeling and Computational Analysis of the Human Cornea Considering Distributed Collagen Fibril Orientations." *J. Biomech. Eng.,* vol. 130, pp. 6-6, 2008.

[81] M. Ariza-Gracia, J. Zurita, D. Piñero, B. Calvo and J. Rodríguez-Matas, "Automatized Patient-Specific Methodology for Numerical Determination of Biomechanical Corneal Response," *Ann. Biomed. Eng.,* pp. 1-20, 2015.

[82] M. Á Ariza-Gracia, J. F. Zurita, D. P. Piñero, J. F. Rodriguez-Matas and B. Calvo, "Coupled biomechanical response of the cornea assessed by non-contact tonometry. A simulation study," 2015.

[83] A. Elsheikh, C. Whitford, R. Hamarashid, W. Kassem, A. Joda and P. Büchler, "Stress free configuration of the human eye," *Med. Eng. Phys.,* vol. 35, pp. 211-216, 2013.

[84] T. C. Gasser, R. W. Ogden and G. A. Holzapfel, "Hyperelastic modelling of arterial layers with distributed collagen fibre orientations," *J. R. Soc. Interface,* vol. 3, pp. 15-35, Feb 22, 2006.

[85] A. N. Annaidh, K. Bruyere, M. Destrade, M. D. Gilchrist, C. Maurini, M. Otténio and G. Saccomandi, "Automated estimation of collagen fibre dispersion in the dermis and its contribution to the anisotropic behaviour of skin," *Ann. Biomed. Eng.,* vol. 40, pp. 1666-1678, 2012.

[86] A. Pandolfi and M. Vasta, "Fiber distributed hyperelastic modeling of biological tissues," *Mech. Mater.,* vol. 44, pp. 151-162, 1, 2012.

[87] A. Elsheikh, D. Alhasso and P. Rama, "Biomechanical properties of human and porcine corneas," *Exp. Eye Res.,* vol. 86, pp. 783-790, 5, 2008.

[88] E. Lanchares, B. Calvo, J. A. Cristóbal and M. Doblaré, "Finite element simulation of arcuates for astigmatism correction," *J. Biomech.,* vol. 41, pp. 797-805, 2008.

[89] A. H. M. Vestergaard, J. Grauslund, A. R. M. Ivarsen and J. Ø M. Hjortdal, "Central Corneal Sublayer Pachymetry and Biomechanical Properties After Refractive Femtosecond Lenticule Extraction," *Journal of Refractive Surgery,* vol. 30, pp. 102, 2014.

[90] Y. Shen, Z. Chen, M. C. Knorz, M. Li, J. Zhao and X. Zhou, "Comparison of corneal deformation parameters after SMILE, LASEK, and femtosecond laser-assisted LASIK," *Journal of Refractive Surgery,* vol. 30, pp. 310, 2014.

[91] A. Agca, E. B. Ozgurhan, A. Demirok, E. Bozkurt, U. Celik, A. Ozkaya, I. Cankaya and O. F. Yilmaz, "Comparison of corneal hysteresis and corneal resistance factor after small incision lenticule extraction and femtosecond laser-assisted LASIK: A prospective fellow eye study," *Contact Lens and Anterior Eye,* vol. 37, pp. 77-80, 4, 2014.

[92] D. Wu, Y. Wang, L. Zhang, S. Wei and X. Tang, "Corneal biomechanical effects: Small-incision lenticule extraction versus femtosecond laser–assisted laser in situ keratomileusis," *Journal of Cataract & Refractive Surgery,* vol. 40, pp. 954-962, 6, 2014.

[93] D. Wang, M. Liu, Y. Chen, X. Zhang, Y. Xu, J. Wang, C. To and Q. Liu, "Differences in the corneal biomechanical changes after SMILE and LASIK," *Journal of Refractive Surgery,* vol. 30, pp. 702, 2014.